NACA RM L50J18

NACA

RESEARCH MEMORANDUM

INVESTIGATION AT SUPERSONIC SPEEDS OF SOME OF THE FACTORS AFFECTING THE FLOW OVER A RECTANGULAR WING WITH SYMMETRICAL CIRCULAR-ARC SECTION AND 30-PERCENT-CHORD TRAILING-EDGE FLAP

By K. R. Czarnecki and James N. Mueller

Langley Aeronautical Laboratory
Langley Field, Va.

NATIONAL ADVISORY COMMITTEE FOR AERONAUTICS

WASHINGTON

January 2, 1951
Declassified August 31, 1954

NATIONAL ADVISORY COMMITTEE FOR AERONAUTICS

RESEARCH MEMORANDUM

INVESTIGATION AT SUPERSONIC SPEEDS OF SOME OF THE FACTORS AFFECTING THE FLOW OVER A RECTANGULAR WING WITH SYMMETRICAL CIRCULAR-ARC SECTION AND 30-PERCENT-CHORD TRAILING-EDGE FLAP

By K. R. Czarnecki and James N. Mueller

SUMMARY

An investigation has been made at supersonic speeds of some of the factors affecting the flow over a rectangular wing having a symmetrical circular-arc section and a 30-percent-chord trailing-edge flap. Results obtained over a Mach number range from 1.62 to 2.40 and at a Reynolds number of 1.07×10^6 indicated that the laminar-flow separations and the breaks or shifts in the section force and moment curves previously encountered experimentally at $M = 1.62$ also occurred at the higher test Mach numbers. When the boundary layer was made turbulent by fixing transition, the flow separations were eliminated or reduced and the agreement between the experimental and theoretical pressure distributions and aerodynamic coefficients was generally greatly improved. A decrease in the wing thickness from 9 percent to 6 percent not only improved the drag and the lift-drag characteristics of the wing but also slightly increased the flap effectiveness.

INTRODUCTION

As a result of the large number of airplanes and missiles being designed for the supersonic speed range, a great need has arisen for information on which to base the design of supersonic controls. In order to meet this need, a number of theoretical and experimental investigations of the aerodynamic characteristics of controls at supersonic speeds have been made (for example, references 1 through 12). Theoretical flap characteristics alone are inadequate, however, because of the existence of shock-boundary-layer interaction effects not considered in the theory. Most of the experimental investigations so far reported, on the other hand, have been limited to the transonic or low supersonic

Mach number range and to three-dimensional control surfaces. In addition, the investigations were confined to techniques that determine only the over-all characteristics of the control and give little or no insight into the reasons for the discrepancies between the theoretical and experimental results.

An investigation in the Langley 9-inch supersonic tunnel of the interaction effects by means of pressure distributions and by schlieren, shadowgraph, and liquid-film-flow observations was, therefore, undertaken to determine the nature and magnitude of the interaction effects for a three-dimensional rectangular wing with a trailing-edge flap. In the initial phase of the test program, which is presented in reference 13, Reynolds number effects in the range from 0.55×10^6 to 1.07×10^6 on the flow phenomena in an essentially two-dimensional-flow region and in a region influenced by the wing tip were investigated at a Mach number of 1.62 on a 9-percent-thick wing having a symmetrical circular-arc section and 30-percent-chord trailing-edge flap. Laminar separation was found to occur on the low-pressure side of the flap near the trailing edge and on the high-pressure side of the flap near the hinge line for the range of Reynolds number tested. In the present paper, the effects on separation and on the aerodynamic characteristics of the wing of varying the wing thickness from 9 percent to 6 percent and the Mach number from 1.62 to 2.40 at a Reynolds number of 1.07×10^6 are presented. The effects of fixing boundary-layer transition, of flap-gap leakage, and surface condition and model asymmetry are also covered.

The results of an analytical investigation for the development of an approximate method of accurately predicting the pressure distributions over the test wing in the regions influenced by the wing tip were reported in reference 14.

SYMBOLS

p_L	local static pressure on airfoil
p	stream static pressure
M	stream Mach number
M_L	local Mach number
γ	ratio of specific heats for air (1.4)
q	dynamic pressure $\left(\frac{\gamma}{2} pM^2\right)$

P	pressure coefficient $\left(\frac{p_L - p}{q}\right)$
$\frac{p_2}{p_1}$	pressure-rise ratio across shock
c	chord of airfoil
c_f	chord of flap
d	section drag force (positive rearward)
l	section lift force (positive upward)
n	section normal force (positive upward)
m	section pitching moment about midchord (positive when it tends to rotate the leading edge of airfoil upward)
h	flap section hinge moment (positive when it tends to deflect the flap downward)
l/d	section lift-drag ratio
c_d	section drag-force coefficient (d/qc)
c_n	section normal-force coefficient (n/qc)
c_m	section pitching-moment coefficient (m/qc^2)
c_h	flap section hinge-moment coefficient (h/qc_f^2)
ρ	mass density of free stream
μ	stream coefficient of viscosity
V	free-stream velocity
R	Reynolds number $(\rho Vc/\mu)$
R_L	local Reynolds number
α	airfoil angle of attack, degrees
δ	deflection of flap chord with respect to airfoil chord (positive in downward direction), degrees

t/c ratio of maximum thickness of airfoil section to airfoil chord length

x/c chordwise distance from wing leading edge in terms of airfoil chord length (positive rearward)

z/c vertical distance from plane of wing chord in terms of airfoil chord length (positive upward)

Slope parameters:

c_{n_α} rate of change of section normal-force coefficient with angle of attack $\left(\frac{\partial c_n}{\partial \alpha}\right)_\delta$

c_{m_α} rate of change of section pitching-moment coefficient with angle of attack $\left(\frac{\partial c_m}{\partial \alpha}\right)_\delta$

c_{h_α} rate of change of flap-section hinge-moment coefficient with angle of attack $\left(\frac{\partial c_h}{\partial \alpha}\right)_\delta$

c_{n_δ} rate of change of section normal-force coefficient with flap deflection $\left(\frac{\partial c_n}{\partial \delta}\right)_\alpha$

c_{m_δ} rate of change of section pitching-moment coefficient with flap deflection $\left(\frac{\partial c_m}{\partial \delta}\right)_\alpha$

c_{h_δ} rate of change of flap section hinge-moment coefficient with flap deflection $\left(\frac{\partial c_h}{\partial \delta}\right)_\alpha$

$\frac{\partial \alpha}{\partial \sigma}$ section-flap effectiveness parameter $\left(\frac{\partial c_n}{\partial \delta} \Big/ \frac{\partial c_n}{\partial \alpha}\right)$

$\frac{\partial c_n}{\partial c_h}$ section-flap effectiveness parameter $\left(\frac{\partial c_n}{\partial \delta} \Big/ \frac{\partial c_h}{\partial \delta}\right)$

Subscripts outside the parentheses around the partial derivatives indicate the variables held constant when the derivatives are taken.

APPARATUS AND METHODS

Wind Tunnel

The investigation was conducted in the Langley 9-inch supersonic tunnel, which is a continuous-operation closed-return tunnel with provisions for the control of the humidity and pressure of the enclosed air. Changes in test Mach number are provided by interchangeable two-dimensional nozzle blocks forming test sections approximately 9 inches square. Eleven fine-mesh screens in the settling chamber ahead of the nozzles aid in keeping the turbulence in the tunnel test section at a low level. For qualitative visual-flow observations, a schlieren optical system is provided. During the tests, the quantity of water vapor in the tunnel air was kept sufficiently low so that the effects of water condensation in the supersonic nozzle were negligible. The pressure in the tunnel was adjusted to provide the desired Reynolds number for the tests.

Models

Three models were used in the investigation: two pressure distribution models of 9- and 6-percent thickness for pressure measurements and shadowgraph studies and a schlieren model of 9-percent thickness for visual-flow observations. All models had 3-inch chords and rectangular plan forms and were equipped with 30-percent-chord full-span plain trailing-edge flaps. The airfoil sections in streamwise planes were symmetrical circular arcs having included angles between the wing upper and lower surfaces at the leading and trailing edges of 20.6° and 13.7° for the case of the 9- and 6-percent-thick wings, respectively. All wing tips were cut off in planes parallel to the free-stream direction and perpendicular to the airfoil span.

The models were machined from steel with the leading and trailing edges ground to a thickness of less than 0.002 inch. The wing contours were cut to within 0.002 inch of the specified values, and the wing surfaces were free of scratches and highly polished. There was, however, a very slight spanwise twist over the length of the 9-percent-thick pressure-distribution model. Also, the upper-flap surface did not fair smoothly into the wing surface at all points by an amount smaller than the tolerance of 0.002 inch but great enough to be noticeable in the pressure distributions. On the 6-percent-thick wing there was a slight irregularity on the lower-flap surface arising from difficulty in fairing over tube ducting that apparently also affected the pressure distributions slightly. The gap between the flap and fixed portion of the airfoil was 0.005 inch or about 0.0017 chord on all models. This gap was not sealed during the tests, except when noted.

A dimensional sketch of the pressure-distribution models is shown in figure 1. For convenience in carrying pressure leads from the wings to the outside of the tunnel and in setting angles of attack and flap-deflection angles, the models were mounted in the tunnel directly from the tunnel wall, as illustrated in figures 2 and 3. The models were so proportioned as to provide a reasonable spanwise length of essentially two-dimensional flow and freedom from interference from shock waves reflected from the tunnel walls. (See fig. 3 and reference 13.)

The pressure-distribution models were equipped with static-pressure orifices on both the upper and lower surfaces at two spanwise stations. One of the stations was located in the essentially two-dimensional-flow region of the wing between the disturbance waves originating at the wing leading-edge tunnel-wall juncture and wing-tip leading edge. At high angles of attack and large flap deflections these disturbances actually merge on the high-pressure side of the wing or flap because of the higher local Mach angles, and the flow at the station is no longer strictly two dimensional. For the range of α and δ investigated, however, the effects of the tip disturbances were negligible and the flow remained essentially two dimensional even at the largest angles of the tests and at the lowest free-stream Mach number. The other orifice station was located partially within the Mach cone from the wing tip but outside the Mach cone from the leading edge of the flap. (See fig. 3.)

At each station on the 9-percent-thick wing, each wing surface contained 16 pressure orifices of 0.014-inch diameter drilled perpendicular to the surface. Twelve of the orifices were on the main airfoil and four on the flap. On the 6-percent-thick wing, each surface at each station contained 14 orifices of which 5 were on the flap. The locations of the orifices and orifice stations are given in figure 1. Except for the leading- and trailing-edge orifices on the thinner wing, all orifices were drilled directly in line with one another. In order to establish some orifices as close to the leading and trailing edges as possible, these particular orifices were slightly staggered spanwise so as to eliminate the necessity of installing the orifices in the upper and lower surfaces directly over one another.

All pressure leads from the orifices were ducted to the outside of the tunnel internally through the models and through the steel supporting plate. The design of the mechanism for actuating the flap of the 6-percent-thick wing necessitated leaving a $\frac{1}{16}$-inch depression in the contour of the tunnel wall adjacent to the flap, the edges of which were beveled to reduce flow disturbances during testing (fig. 2(b)). In a series of tests in which the depression was filled in, the depression did not influence the pressures at the survey stations for the angle-of-attack and flap-deflection range of the investigation. No discontinuities in tunnel-wall contours were necessary for the thicker model.

Figure 4 shows the schlieren model and illustrates the method used to mount the model in the tunnel for schlieren observations. For these tests, the model was mounted horizontally from the lower nozzle block by means of a single, vertical, sweptback strut. In order to avoid any shock-wave - boundary-layer interaction at an airfoil tunnel-wall juncture and to eliminate any interference from the wall reflections of the tip Mach cones, the model was designed to span only the middle 60 percent of the tunnel width.

Pressure Measurements and Reduction of Data

The pressures on the wing surfaces and the total pressure in the tunnel settling chamber were recorded simultaneously by photographing a multiple-tube mercury manometer on which the pressures were indicated. Subsequently, the pressures were read directly from the film as pressure coefficients through the use of a film reader.

Section aerodynamic coefficients of normal force, pitching moment, and hinge moment were obtained by plotting the pressures normal to the wing or flap chord and mechanically integrating the area between the faired curves for the upper and lower surfaces. The effects of the chordwise components of the pressure forces on the aerodynamic characteristics were generally neglected because of the great labor required to reduce these pressures to coefficients and because it was found that the contribution of these components to the above aerodynamic coefficients was relatively small and in no way affected any of the comparisons. For pressure-drag and lift-drag ratio comparisons, however, a limited number of chordwise pressure-force coefficients were computed by plotting the pressures normal to a line perpendicular to the wing chord and mechanically integrating the areas between the faired curves. No attempt was made to include friction forces in any of the aerodynamic coefficients.

Test Methods and Range of Tests

During the investigation most pressure distributions, schlierens, and shadowgraphs were obtained by setting and holding constant the angle of attack of the airfoil and by varying the flap deflection in sequence from 0° to the limit of the positive or negative flap deflections. In order to provide a check on possible hysteretic effects, this procedure was modified for some of the pressure-distribution tests to running through the flap angle range from the most negative desired deflection to the maximum positive angle. Both the angles of attack and flap-deflection angles of the pressure-distribution models could be changed from outside the tunnel while the tunnel was in operation. Angles of attack and flap angles on the schlieren model, on the other hand, had

to be set while the tunnel was shut down and checked with the cathetometer while the tunnel was operating.

All schlieren photographs were obtained with the model in profile with the knife edges in the schlieren system generally both horizontal and vertical.

Pressure-distribution tests with smooth models were made at Mach numbers of 1.62, 1.93, and 2.40 over an angle-of-attack range which varied with Mach number and particular model within the maximum limits of -1.00° and 11.35°. At the two lower Mach numbers the upper limit was usually determined by tunnel choking. The flap-deflection range usually extended from at least -16° to 18° although the positive limit was not always reached because of tunnel choking at the higher angles of attack. With transition fixed near the leading edge on both wing surfaces, pressure distributions were obtained over the range of α and δ on the 9-percent-thick wing at $M = 1.93$ and the 6-percent-thick wing at $M = 1.62$. These tests on the thicker wing also included a limited study of various methods of fixing transition. (See fig. 5.) The transition or roughness strips were prepared by sprinkling common table salt, ground to an average grain size of slightly less than 0.01 inch, onto a thin layer of dope that had been sprayed on the wing just prior to the application of the salt grains.

Flap-gap leakage checks were made at $M = 1.62$ with the 6-percent-thick model and model asymmetry checks were made on the 9-percent-thick model at $M = 2.40$.

Schlieren photographs were obtained over approximately the same range of δ and model condition as in the pressure-distribution investigation but were limited to Mach numbers of 1.62 and 1.93. The angle-of-attack range, however, was extended to include negative angles in order to study the flow characteristics on both the low- and high-pressure sides of the wing without interference effects from the supporting strut. A study of the schlieren photographs indicated that such interference effects did exist. At $M = 2.40$ the schlieren-flow investigation was replaced by wall-shadowgraph studies. For this series of tests, the 9-percent-thick pressure-distribution model was used with the window insert which supported the model coated with a matte white finish to provide a satisfactory background against which to view changes in light intensity. A few additional shadowgraphs were also made at $M = 1.62$.

The tests including pressure distributions, schlierens, and shadowgraphs were made at a Reynolds number of 1.07×10^6 based on the airfoil chord of 3 inches.

Precision of Data

Stream surveys obtained with empty test section indicate that the mean values of the Mach number in the region occupied by the test models in the test nozzles were 1.62, 1.93, and 2.40 and that the variation about these means was less than 1 percent. Large irregularities in stream-flow direction in these regions were not evident.

The angle-of-attack and flap-deflection settings of the pressure-distribution and schlieren models are believed to be generally accurate to nearly $\pm 0.05^\circ$ and $\pm 0.1^\circ$, respectively, except for station 2 on the thicker pressure-distribution wing. At this station, the angle of attack was greater than that indicated by the clinometer by about 0.15° to 0.20° owing to the twist in the model resulting from wing-fabrication difficulties. In order to simplify comparisons and to reduce the number of required theoretical calculations, however, corrections for the twist were applied only in cases of special interest.

Individual pressure coefficients are usually accurate to ± 0.01, and discrepancies of greater magnitude are not due to errors in reading pressures but due to local surface irregularities which were usually deliberately neglected in fairing the experimental curves. The pressure-coefficient increments resulting from the slight misalinement of the upper-flap surface with the wing on the 9-percent-thick model and from surface waviness on the lower-flap surface of the thinner wing were not neglected.

The uncertainty in aerodynamic coefficients is believed to be about ± 0.005 in c_n, ± 0.002 in c_m, ± 0.01 in c_h, and ± 0.003 in c_d with the greatest error resulting from inaccuracies in fairing the pressure curves in the region of the flap hinge line and near the flap trailing edges. Installations of pressure orifices close to these points would have been very difficult owing to physical limitations imposed by the method of model construction and tube installation.

Theoretical Calculations

The theoretical two-dimensional chordwise pressure distributions included in this report were calculated from oblique-shock theory and the Prandtl-Meyer equations for the expansion of a two-dimensional supersonic flow. The theoretical calculations neglect the fact that, on circular-arc airfoils, the shocks at the wing leading edge and at the flap hinge line are curved and the flow behind the shocks is rotational.

The theoretical aerodynamic coefficients were obtained by mechanical integration with the use of the same procedures employed in obtaining the

experimental coefficients. Hence, the effects of chordwise forces on the aerodynamic characteristics exclusive of drag were neglected and the theoretical and experimental results are directly comparable.

RESULTS AND DISCUSSION

The presentation and discussion of the results of this investigation of the flow over a rectangular wing with trailing-edge flap have been divided into the following sections: effect of Mach number, effect of wing thickness, effect of fixing transition, effect of flap leakage, effect of model surface condition and asymmetry, and shock-boundary-layer interaction. Because of the small number of pressure orifices near the flap hinge line and trailing edge where some of the most rapid pressure changes occurred, a large number of pressure distributions were necessary to establish trends. Space limitations, however, have made it necessary to restrict the data presented in this paper to only that actually needed for typical illustrations of the effects under discussion. Consequently, when the fairing of some of the curves is not obvious it should be understood that the trends have been established from analyses of a considerably larger body of data, much of which is intermediate to that shown. Data presented have also been restricted to the two-dimensional station, but the effects at the three-dimensional station were similar unless specified otherwise.

Most of the data included in this report pertaining to the 9-percent-thick wing at $M = 1.62$ have been extracted from the test results previously described in reference 13.

Effect of Mach Number

Pressure distributions.- Some typical experimental pressure distributions obtained at the two-dimensional-flow stations of both the 9-percent- and 6-percent-thick wings are shown in figures 6 and 7 for the Mach numbers of 1.62, 1.93, and 2.40. The corresponding theoretical pressure distributions, where they could be obtained, are included with the experimental plots. Except for the regions affected by shock-boundary-layer interaction (see reference 13 for detailed discussion) and by local surface irregularities, the agreement between the theoretical and experimental pressures over the main wing for both wing thicknesses and all Mach numbers was excellent. (See figs. 6 and 7.) In the regions affected by the flow separations, the disagreement between the theoretical and experimental distributions was very large. At the higher flap angles and particularly at the higher Mach numbers, the discrepancy in pressures covered most of the flap surface and, in addition, an appreciable part

of the main wing. The data also show that, for corresponding α,δ configurations, the tendency toward separation increases with Mach number at constant Reynolds number.

The excellent agreement between theory and experiment for the parts of the wing unaffected by flow separation shows that, for the range of angles of attack and flap deflections covered in this investigation, the effects of shock curvature, which were neglected in theoretical calculations, are negligible over the Mach number range of 1.62 to 2.40. This conclusion was corroborated by theoretical calculations made by the method of reference 15 which revealed that the changes in pressure gradient just behind the shocks at the wing leading edge and flap hinge line would be within the experimental accuracy of the tests.

Another interesting feature of the pressure distributions over the wing is deduced from a study of the relation of the pressure distributions to the limiting-pressure coefficients. The negative limiting-pressure coefficients which correspond to absolute zero or vacuum pressure are indicated in the lower right-hand graphs of figures 6 and 7. The positive limiting-pressure coefficients which correspond to stagnation pressure are greater than 1 and hence have been omitted. As the free-stream Mach number is increased, the negative limiting pressures rapidly decrease toward 0, whereas the positive limiting-pressure coefficients increase. Obviously, then, at high positive α and δ the upper-flap surface contributes progressively less lift as the Mach number is increased until, at higher Mach numbers (calculations show these Mach numbers to be of the order of 4 or 5), the aerodynamic characteristics of the flap in this angle range are almost solely determined by the high-pressure side of the flap even when no flow separation is present.

Section force and moment characteristics.- The effect of Mach number on the section aerodynamic characteristics obtained by integrating the theoretical and experimental pressure distributions is shown in the typical plots of figures 8 - 13. Inspection of figures 8 and 9, which show the variation of the section normal-force, pitching-moment, and hinge-moment characteristics with flap deflection at constant α, indicates that the experimental absolute increments in coefficients due to flap deflection were smaller than the theoretical increments and were actually nearly zero for a small δ range near a total flap deflection $(\alpha + \delta)$ of 0°. Most of the discrepancy between the theoretical and experimental increments occurs as a result of the flow separations discussed in the previous sections. The remainder, which is almost negligibly small, derives from the fact that the flow does not expand the required angle around the hinge line on the flap low-pressure side because of the influence of the boundary layer. These "breaks" or regions of flap ineffectiveness were noted in the tests reported in reference 13 and are traceable to flow separation from the rear flap surfaces. The extent of

the breaks in terms of flap-deflection angles is seen to increase with Mach number for all the coefficient curves. The decreased slopes of the curves at the higher free-stream velocities make it comparatively more difficult to identify the breaks and, in general, the percentage change in the coefficients due to separation is greater at the higher Mach numbers.

The same considerations as to the effect of Mach number apply to the variation of the section normal-force characteristics with α at constant δ (figs. 10 and 11). In this case, however, the changes due to flow separations are relatively small compared to the changes produced by varying the angle of attack. For the 9-percent-thick wing, the regions where the force breaks occur are shown by a dotted line. Inasmuch as the lift on the main part of the wing is changing even in the critical α range when the trailing-edge flow separations are rapidly changing sides, the lifting effectiveness of the wing-flap combination is not entirely lost but is only changed. In the case of the 6-percent-thick wing, the breaks could be identified only at the lower angles of attack; hence, the identification of the region of flap ineffectiveness is omitted.

The variation of the theoretical and experimental section drag coefficients with α at the different test Mach numbers is shown in figures 12 and 13 for the two-dimensional station with $\delta = 0^\circ$. As anticipated from the study of the pressure distributions, the experimental drag coefficients were lower than the theoretical values and the magnitude of the discrepancy increased with Mach number.

Schlieren and shadowgraph flow observations.- A group of schlieren and shadowgraph flow pictures, covering most of the flow conditions of interest, is presented in figure 14. The flow on the strut side of the model in the schlieren pictures must be discounted because of interference effects from the supporting member. All flow phenomena of interest, however, such as flow separations at the flap hinge line and at the flap trailing edge, may be observed in detail on the strut-free wing surface.

A correlation of the schlieren and shadowgraph flow pictures with the corresponding pressure distributions shows that the flow separations at the flap hinge line and trailing edge are accompanied by a double or forked-shock phenomenon which was discussed in the results of the 9-percent-thick wing at $M = 1.62$. (See reference 13.) This phenomenon is a characteristic of laminar separation and its distinguishing features, clearly seen in figures 14(a) $\alpha = -5^\circ$ and $\delta = -18^\circ$, figure 14(b) $\alpha = 2^\circ$ and $\delta = 20^\circ$, are: (1) a weak, or separation, shock springing from the point of initial-flow separation; (2) a strong, or "main," shock just rearward of the hinge axis or flap trailing edge; (3) a clearly defined, dark line which seems to join both shocks at their points of

origination and which is in reality a mixing line between the separated flow above the line and the dead-air space below the line.

A number of pressure distributions were calculated for the separated regions at the various Mach numbers on the basis of the observed angles of flow separation and the assumption that the pressure at the surface would be equal to that of the flow outside the separation line. These calculated pressure distributions proved to be in good agreement with the experimental pressure distributions.

Near the trailing edge with the flap deflected, the flow pictures show the presence of shocks slightly behind and both above and below the trailing edge even at the highest flap angles. (See fig. 14(c), $\alpha = 4^\circ$, $\delta = 19^\circ$.) Moreover, no instance could be found where only one shock was present at the trailing edge no matter what the angle of attack or flap deflection, although, at these high flap angles, nonviscid airfoil theory predicts the occurrence of a shock at the trailing edge on the suction side of the flap but only an expansion on the high-pressure side. (See reference 13.)

Effect of Wing Thickness

Decreasing the wing thickness from 9 percent to 6 percent had little effect on the location of the points of initial flow separation when test conditions were held constant. (Compare figure 6(a) with figure 7(a), and figure 6(c) with figure 7(b)). The pressure increases at the separation point also appeared to be on the same order of magnitude. Outside the regions affected by separation, the agreement between theory and experiment was equally good on both models. Because the chordwise pressure gradients for the 6-percent-thick wing were smaller than those for the 9-percent-thick wing, the integrated losses in pressure behind the point of separation were usually less. Accordingly, the losses in force- and moment-coefficient increments due to changes in α or δ were usually proportionately smaller. (Compare figs. 8 and 9, figs. 10 and 11, and figs. 12 and 13.) The magnitudes of the force breaks or discontinuities in terms of α or δ also decreased.

In general, the theoretical and experimental slopes of the normal-force and moment-coefficient curves for the thinner wing were slightly greater, but the drag coefficient, as expected, was considerably less than that for the thicker wing. The experimental values of the effectiveness parameter $\frac{\partial \alpha}{\partial \delta}$ computed from the slopes of the normal-force-coefficient curves for the two-dimensional station at α and δ at or near 0° were about 0.19 and 0.23 for the 9- and 6-percent-thick wings, respectively, at all Mach numbers. The average experimental values of the parameter $\frac{\partial c_n}{\partial c_h}$ for station 1 were -0.56 and -0.59, in the same order. At

the three-dimensional station the differences in these parameters for the two models were usually slightly greater because of somewhat smaller tip losses on the thinner wing. These results appear to indicate that not only are the drag and lift-drag ratio characteristics of the thinner wing considerably better but also the effectiveness of the flap is slightly superior to that of the thicker wing.

Effect of Fixing Transition

The maximum Reynolds number and the Reynolds number range that could be covered in the investigation of reference 13 were very small and yet, as was shown, the effects of scale were relatively large. Therefore, in order to gain an idea of the probable aerodynamic characteristics of the flapped wings at very high Reynolds numbers, such as those corresponding to supersonic flight of full-scale airplanes and missiles at relatively low altitudes, an investigation was made of the pressure distributions over the models with transition fixed. Since little was known about the practicability of and the proper techniques for the fixing of boundary-layer transition at supersonic speeds, a short study was also made on the 9-percent-thick model at $M = 1.93$ of some of the various methods of fixing transition.

Pressure distributions.- The effect on the pressure distribution of fixing transition by means of $\frac{1}{8}$-inch-wide roughness strips near the leading edge on the upper and lower wing surfaces, both singly and in combination, is illustrated in figure 15. The results show that, whenever transition was fixed on a surface, the flow separation on that surface was eliminated or reduced. At high flap deflections, the effects of shock-boundary-layer interaction at the trailing edge were still felt some distance upstream on the low-pressure side of the flap even though the boundary layer was no longer laminar. The discrepancies between the results for the smooth surfaces for the various configurations are ascribed to irregularities in surface condition and not to the influence of one surface upon the other.

Increasing the width of the transition strip on the upper wing surface from 1/8 to 3/4 inch (configuration (b) and configuration (g), respectively, fig. 5) had no effect, and replacing the strip by a thin partial-span ridge of dope with a rather sharp leading edge (configuration (f), fig. 5) likewise produced no change in the pressure distributions relative to those for configuration (b), (fig. 5). Consequently, no data for these conditions are shown. Increasing the width of the transition strip to 2 inches (configuration (h), fig. 5), however, caused the boundary layer to become so thick that the pressure rises across the shocks at the flap hinge line and trailing edge were transmitted forward

through the turbulent boundary layer an appreciable distance. (Compare configurations (b) and (h) in fig. 16.) The location of the roughness strips close to the hinge line (configuration (e), fig. 5) proved undesirable because at large δ's, flow separation occurred ahead of the strip on the flap high-pressure side of the wing and the strip lost its effectiveness completely. (See configuration (e), fig. 16.) These results indicate, therefore, that the roughness-strip technique is a simple and efficient method of fixing transition and allows a considerable leeway in the size of strips that may be used.

As a result of the elimination of the flow separations by fixing transition, the agreement between the theoretical and experimental pressures was greatly improved (fig. 17). A plot of the effect of fixing transition on the chordwise pressure forces is included in figure 18. The results denote a decrease in the effectiveness of the transition strip in eliminating flow separation at the trailing edge at the high α's similar to the loss in effectiveness of the strip usually suffered on the flap low-pressure surface at very high flap deflections (fig. 15). As the flap was not deflected in the case under discussion, the phenomenon is apparently dependent upon the characteristics of the interaction between the trailing-edge shock and the turbulent boundary layer. These characteristics will be discussed subsequently.

Section force and moment characteristics.- An analysis of the results obtained with the configurations having roughness strips reveals that fixing transition was quite effective in eliminating the breaks or discontinuities in the force and moment-coefficient curves (figs. 19 and 20). In order to eliminate the discontinuities completely, transition generally had to be fixed on both the upper and lower surfaces simultaneously. The addition of the roughness strips often caused a small reduction in the linear range of the coefficient curves as compared to those for the smooth model. This trend is not apparent in figures 19 and 20 except for the configuration with the 2-inch roughness strip (configuration (h), fig. 20).

The section pressure-drag coefficient was also increased and the agreement between theory and experiment improved when transition was fixed on the wing (fig. 21). No changes of consequence in pressure lift-drag ratio occurred, nevertheless, because the increase in drag was compensated for by a corresponding increase in lift (see fig. 22). If the increased friction drag for the configurations with the roughness strips is accounted for, however, the over-all lift-drag ratio obviously will be decreased somewhat by fixing transition. The discrepancy between theoretical and experimental pressure lift-drag ratios for the 6-percent-thick model results from the tendency of the experimental pressures to be more positive than the theoretical pressures on the lower surface of the flap near the trailing edge. This trend is ascribed primarily to a rough surface condition on that side of the flap resulting from a difficulty in

fairing over tube ducting. Because of this effect the experimental absolute values of lift-drag ratio for the 6-percent-thick airfoil may not be too reliable although satisfactory for comparative purposes. Additional curves showing typical effects of fixing transition, including comparisons with theory, are presented in figures 23 and 24.

Schlieren flow observations.- The schlieren photographs of figure 25 indicate that, whenever the boundary layer was made turbulent by artificially inducing transition, the double shock, characteristic of laminar separation, was eliminated. At high flap angles, some separation was still evident at the trailing edge. A condition where flow separation was eliminated naturally on the smooth model is shown in figure 14(a), $\alpha = 10.8^\circ$, $\delta = -16^\circ$. As α was increased, the bow wave detached and the subsonic flow behind the shock separated from the sharp leading edge, overexpanded to a supersonic velocity, and reattached to the wing surface; a shock was thereby formed. When this shock became strong enough, it evidently caused the boundary layer to become turbulent and the flow separation ahead of the hinge line was eliminated.

Effect of Sealing the Hinge Gap

The main effect of sealing the wing-flap gap on the 6-percent model was to increase the extent of the laminar-separated flow regions on both wing surfaces (see fig. 26). The trend probably can be ascribed to the fact that, at high angles of attack and flap angles with the gap open, there was a small amount of air leakage through the gap from the high-pressure to the low-pressure side of the wing. The leakage or jet issuing normal to the wing surface caused a breaking up of the laminar boundary-layer flow on the low-pressure side and resulted in a turbulent type of flow with separation farther rearward on the wing. On the high-pressure side of the wing the leakage afforded a relief for the pressures in the dead-air region. These effects died out with decreasing angle of attack and/or flap deflection as the pressure differential across the gap decreased.

A comparison of the integrated aerodynamic coefficients for the sealed and unsealed gap showed a negligible difference.

Although the air leakage was small because the gap was made as small as possible, sealing produced noticeable objectionable changes in pressure distributions. These relatively large changes indicated that the wing-flap gap size may be of considerable importance when it is larger than that used on the configurations of this investigation. A larger gap could possibly influence the pressure distributions sufficiently to eliminate the breaks or flat spots in the curves of the integrated aerodynamic force and moment coefficients.

Effects of Model Surface Condition and Asymmetry

During the first part of this investigation of flapped airfoils some tests were made to determine whether the pressure distributions obtained at one time could be satisfactorily duplicated at a later date and whether there was any hysteresis in the pressure distributions due to approaching the angle setting from opposite directions. The results indicate generally excellent repeatability and no hysteresis even in the regions where the control effectiveness was very low such as when the control was nearly in the center of the wake. Some discrepancies in pressures were found, however, during the investigation of fixing transition. (See upper surfaces for configurations (a) and (c) at $\delta = 4^\circ$ or 8° in fig. 15.) These discrepancies are ascribed to differences in surface conditions. Numerous applications and removals of the roughness strips during this series of tests are believed to have made it extremely difficult always to return the model to its customary clean condition when strips were removed. The results thus stress the importance of surface condition if tests are made in the critical Reynolds number range.

In figure 27 are presented some typical data obtained from tests to determine the effect of model asymmetry and possible tunnel effects. The data for the model in the normal and inverted attitudes are in fairly good agreement except at $\delta = 16^\circ$. The integrated aerodynamic characteristics showed no important change even at this flap angle except in the flap hinge moment. Other pressure irregularities, such as the tendency for the pressures to be high on the lower surface of the 9-percent-thick wing between the 10- to 20-percent-chord stations (fig. 6), showed no disposition to change surfaces with model inversion and thus prove the discontinuities were caused by local-surface irregularities and not by variations in the tunnel stream.

Shock Boundary-Layer Interaction

The nature of the shock boundary-layer interaction phenomena as deduced from the results of this investigation is illustrated in the exaggerated diagrammatic sketches of figures 28 and 29. The reasons for the differences in interaction characteristics for the laminar and turbulent boundary layers become apparent in the analysis that follows.

First, the pressure increase across the shock at the flap hinge line or trailing edge was not communicated any appreciable distance upstream through the subsonic part of the boundary layer unless flow separation was present regardless of whether the boundary layer was laminar or turbulent. When the pressure rise across the shock exceeded a certain critical value the flow separated from the surface causing the

appearance of a weak shock at the point of separation. Any further increase in pressure-rise ratio simply propelled the point of separation forward accompanied by a small but abrupt pressure increase, whereas the main shock and main pressure rise occurred some distance behind the hinge line or flap trailing edge. (See figs. 28(a), 29(a), and 30.) Experimentally, the pressure-rise ratio across a shock is taken as the ratio of the most positive surface pressure immediately behind the main shock to the most negative pressure immediately preceding the separation shock unless otherwise specified. Behind the trailing-edge shocks, the static pressure was assumed equal to that of the free stream. For the laminar boundary layer, the value of the critical pressure-rise ratio as deduced from a study of critical pressure distributions similar to those presented in figure 6(c) ($\alpha = 8.35^\circ$ and $\delta = -8^\circ$) for the flow at the hinge line and figure 7(a) ($\alpha = 8.35^\circ$ and $\delta = 8^\circ$) for the flow at the trailing edge usually ranged between about 1.05 to 1.20 with most of the values approaching the upper limit. For the case of the turbulent boundary layer (transition fixed), the value of the critical ratio was in the neighborhood of 2 (from analysis of data similar to that presented in figs. 15 and 17) but could not be very accurately determined because turbulent separation was difficult to identify. In these tests the pressure-rise ratio of 2 was exceeded only at the trailing edge of the flap and usually only at the higher flap deflections. The results for transition fixed with the 2-inch strip are discounted because of the probably abnormal thickness of the boundary layer generated by the strip.

For the case of the laminar boundary layer and pressure-rise ratio above the critical, the flow on the flap high-pressure side of the wing (fig. 28(a)), after separating or detaching, continued along a straight path until it intersected the flap surface some distance downstream of the hinge line. The main shock occurred at this intersection and the transition from a laminar to a turbulent boundary layer took place under the foot of the shock. Under the foot of each shock, also, the pressure increased rather abruptly; elsewhere between the two shocks, the surface pressure remained constant. As the Reynolds number was decreased the distance under the shocks over which the rapid changes in pressure occurred generally increased. (Compare the pressure distributions on the lower wing surface at $\delta = 12^\circ$ or 16°, fig. 15 (configuration (b)).) The pressure-rise ratio across the main shock was apparently fixed by the angle the reattaching flow must turn through to parallel the surface at the point of intersection; hence, the geometry of the wing-flap combination has an important effect on the location of the separation point. Up to the present time no satisfactory method of determining the separation point has been developed, but improved versions of the modified Pohlhausen technique proposed in reference 16, used in conjunction with the flow conditions described above, appear to hold some promise.

Downstream of the flap trailing edge, the flow pattern was the same as that described in reference 13 and had shocks forming at the intersection of the flows from the upper and lower surfaces. Some calculations based on the flow conditions just described and on flow-separation points and angles determined from pressure distributions led to trailing-edge shock locations and angles which were in good agreement with those of the schlieren pictures for corresponding wing-flap configurations. Another interesting observation is that the pressure-rise ratios for laminar separation were so small that, at $\alpha = \delta = 0^\circ$, the flow probably will separate from both flap surfaces simultaneously on wings having trailing-edge included angles considerably less than the 13.7° angle of the 6-percent-thick wing if the boundary layer remains laminar.

When the boundary layer was turbulent, separation was no longer present and the flow at the hinge line followed the contour of the wing-flap combination as indicated in figure 28(b). As a result of the fact that there was no flow separation, the pressure rise across the hinge shock was communicated upstream only a negligibly short distance. At the flap trailing edge the same general considerations held as for the flow at the hinge line with turbulent boundary layer when the flap angles relative to the free stream ($\alpha + \delta$) were small. At higher flap deflections, however, the pressure-rise ratio across the trailing-edge shock appeared to be sufficiently high to cause separation of the turbulent boundary layer as shown to a small extent in figure 29(b). Consequently, at the higher flap angles, the pressure rise across the trailing-edge shock was propagated a relatively long distance upstream but still usually less than that in the case of the laminar boundary layer. (See fig. 17.)

CONCLUSIONS

An investigation has been made over a Mach number range from 1.62 to 2.40 at a Reynolds number of 1.07×10^6 of some of the factors affecting the flow over rectangular wings having 9- and 6-percent-thick symmetrical circular-arc sections and 30-percent-chord trailing-edge flaps. An analysis of the results indicated that:

1. The laminar-flow separations on the low-pressure side of the flap near the trailing edge and on the high-pressure side of the flap and wing at the hinge line that were found previously at $M = 1.62$ also were present at the higher test Mach numbers.

2. As a result of the boundary-layer separations, the breaks or shifts in the experimental section force and moment curves encountered at $M = 1.62$ also existed at the higher test Mach numbers.

3. For similar wing-flap configurations, increasing the Mach number at constant Reynolds number caused the separation points to move forward, the magnitudes of the breaks in the force and moment coefficient curves in terms of angle of attack or flap deflection to increase, and, as predicted by theory, the slopes of the curves to decrease.

4. Decreasing the wing thickness from 9 percent to 6 percent not only greatly improved the drag and lift-drag characteristics of the wing but also slightly improved the flap effectiveness.

5. The effects of fixing transition to simulate high Reynolds numbers were to eliminate or greatly decrease flow separation, to do away with the breaks or shifts in the force and moment curves, and to improve generally the agreement between the theoretical and experimental pressure distributions and force and moment curves.

6. Sealing the hinge gap to eliminate leakage caused the separation points to move forward, but, for the range of leakage investigated, had little effect on the integrated force and moment characteristics.

7. The distances that the pressure rises across the hinge and trailing-edge shocks were communicated upstream through the boundary layer were primarily dependent upon whether the boundary layer was laminar or turbulent and whether the critical pressure-rise ratio for flow separation was exceeded. In general, this distance was considerably greater when the boundary layer was laminar.

Langley Aeronautical Laboratory
National Advisory Committee for Aeronautics
Langley Field, Va.

REFERENCES

1. Lagerstrom, P. A., and Graham, Martha E.: Linearized Theory of Supersonic Control Surfaces. Jour. Aero. Sci., vol. 16, no. 1, Jan. 1949, pp. 31-34.

2. Frick, Charles W., Jr.: Application of the Linearized Theory of Supersonic Flow to the Estimation of Control-Surface Characteristics. NACA TN 1554, 1948.

3. Tucker, Warren A., and Nelson, Robert L.: Theoretical Characteristics in Supersonic Flow of Constant-Chord Partial-Span Control Surfaces on Rectangular Wings Having Finite Thickness. NACA TN 1708, 1948.

4. Ivey, H. Reese: Notes on the Theoretical Characteristics of Two-Dimensional Supersonic Airfoils. NACA TN 1179, 1947.

5. Sandahl, Carl A.: Free-Flight Investigation of Control Effectiveness of Full-Span, 0.2-Chord Plain Ailerons at High Subsonic, Transonic, and Supersonic Speeds to Determine Some Effects of Wing Sweepback, Taper, Aspect Ratio, and Section Thickness Ratio. NACA RM L7F30, 1947.

6. Strass, H. Kurt: The Effect of Spanwise Aileron Location on the Rolling Effectiveness of Wings with 0° and 45° Sweep at Subsonic, Transonic, and Supersonic Speeds. NACA RM L50A27, 1950.

7. Thompson, Robert F.: Lateral-Control Investigation of Flap-Type Controls on a Wing with Quarter-Chord Line Swept Back 35°, Aspect Ratio 4, Taper Ratio 0.6, and NACA 65A006 Airfoil Section. Transonic-Bump Method. NACA RM L9L12a, 1950.

8. Hammond, Alexander D.: Lateral-Control Investigation of Flap-Type Controls on a Wing with Unswept Quarter-Chord Line, Aspect Ratio 4, Taper Ratio 0.6, and NACA 65A006 Airfoil Section. Transonic-Bump Method. NACA RM L50A03, 1950.

9. Johnson, Harold I.: Measurements of Aerodynamic Characteristics of a 35° Sweptback NACA 65-009 Airfoil Model with $\frac{1}{4}$-Chord Plain Flap by the NACA Wing-Flow Method. NACA RM L7F13, 1947.

10. Johnson, Harold I., and Brown, B. Porter: Measurements of Aerodynamic Characteristics of a 35° Sweptback NACA 65-009 Airfoil Model with $\frac{1}{4}$-Chord Horn-Balanced Flap by the NACA Wing-Flow Method. NACA RM L9B23a, 1949.

11. Conner, D. William, and Mitchell, Meade H., Jr.: Control Effectiveness and Hinge-Moment Measurements at a Mach Number of 1.9 of a Nose Flap and Trailing-Edge Flap on a Highly Tapered Low-Aspect-Ratio Wing. NACA RM L8K17a, 1949.

12. Sivells, James C., and Conner, D. William: Preliminary Investigation at a Mach Number of 1.9 and a Reynolds Number of 2,200,000 of Three Ailerons Applicable to the Bell XS-2 Airplane Design. NACA RM L8D02, 1948.

13. Czarnecki, K. R., and Mueller, James N.: Investigation at Mach Number 1.62 of the Pressure Distribution over a Rectangular Wing with Symmetrical Circular-Arc Section and 30-Percent-Chord Trailing-Edge Flap. NACA RM L9J05, 1950.

14. Czarnecki, K. R., and Mueller, James N.: An Approximate Method of Calculating Pressures in the Tip Region of a Rectangular Wing of Circular-Arc Section at Supersonic Speeds. NACA RM L9J10, 1950.

15. Munk, M. M., and Prim, R. C.: Surface-Pressure Gradient and Shock-Front Curvature at the Edge of a Plane Ogive with Attached Shock Front. Jour. Aero. Sci., vol. 15, no. 11, Nov. 1948, pp. 691-695.

16. Lees, Lester: Interaction between the Laminar Boundary Layer over a Plane Surface and an Incident Oblique Shock Wave. Rep. No. 143, Princeton Univ., Aero. Eng. Lab., Jan. 24, 1949.

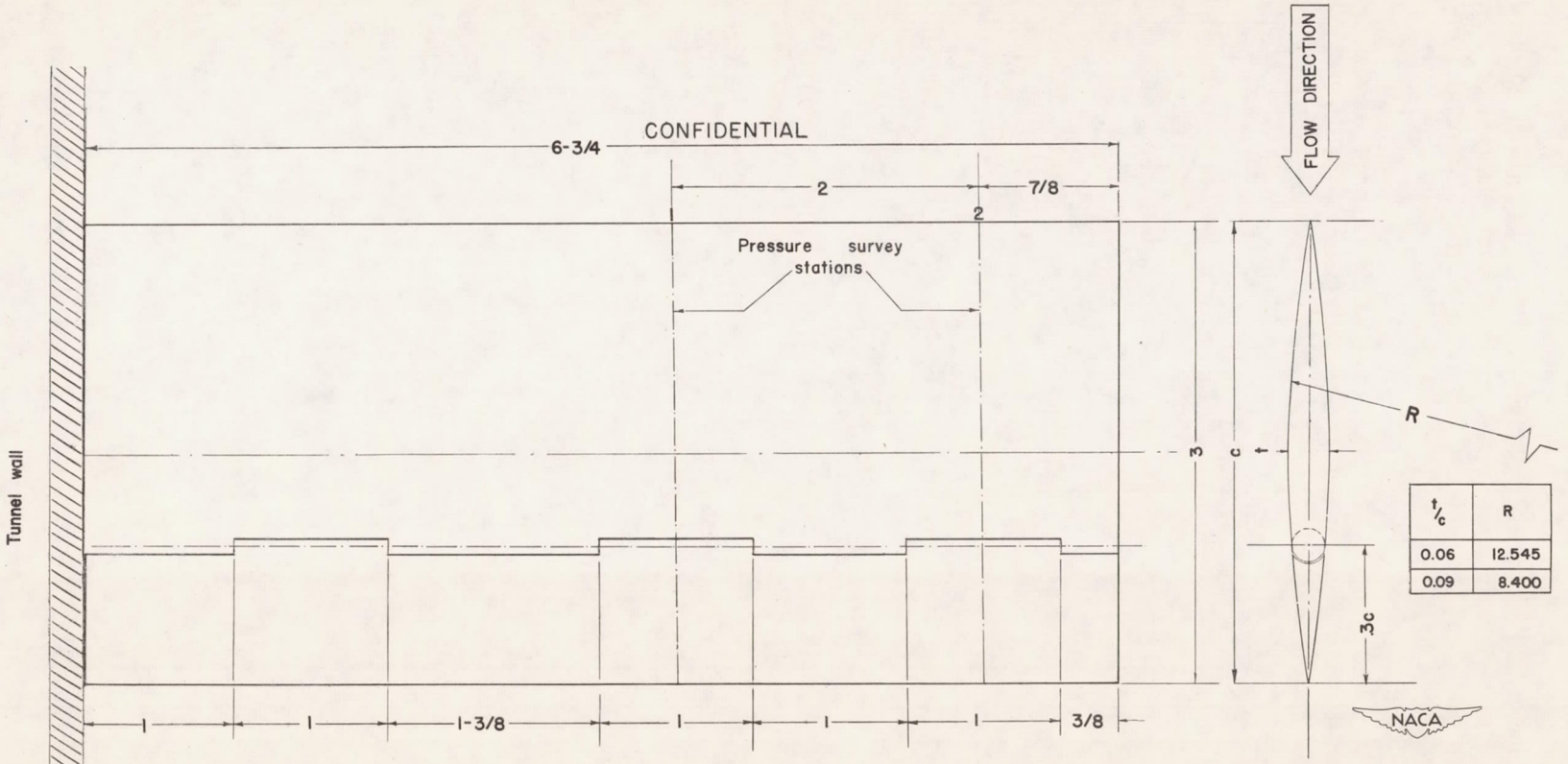

t/c	R
0.06	12.545
0.09	8.400

ORIFICE LOCATIONS

Orifice number		1	2	3	4	5	6	7	8	9	10	11	12	13	14	15	16
Distance from wing L.E., x/c	t/c = 0.09	.067	.112	.157	.202	.267	.332	.397	.462	.511	.555	.602	.624	.733	.790	.863	.933
	t/c = 0.06	.050	.125	.200	.275	.350	.425	.500	.575	.675	.750	.800	.850	.900	.950	—	—

Clearance between wing and flap .005 inch throughout.

Leading edge radius of flap is equal to one-half the thickness of the section at the hinge line.

All dimensions in inches.

Figure 1.- Sketch showing pertinent dimensions of test models.

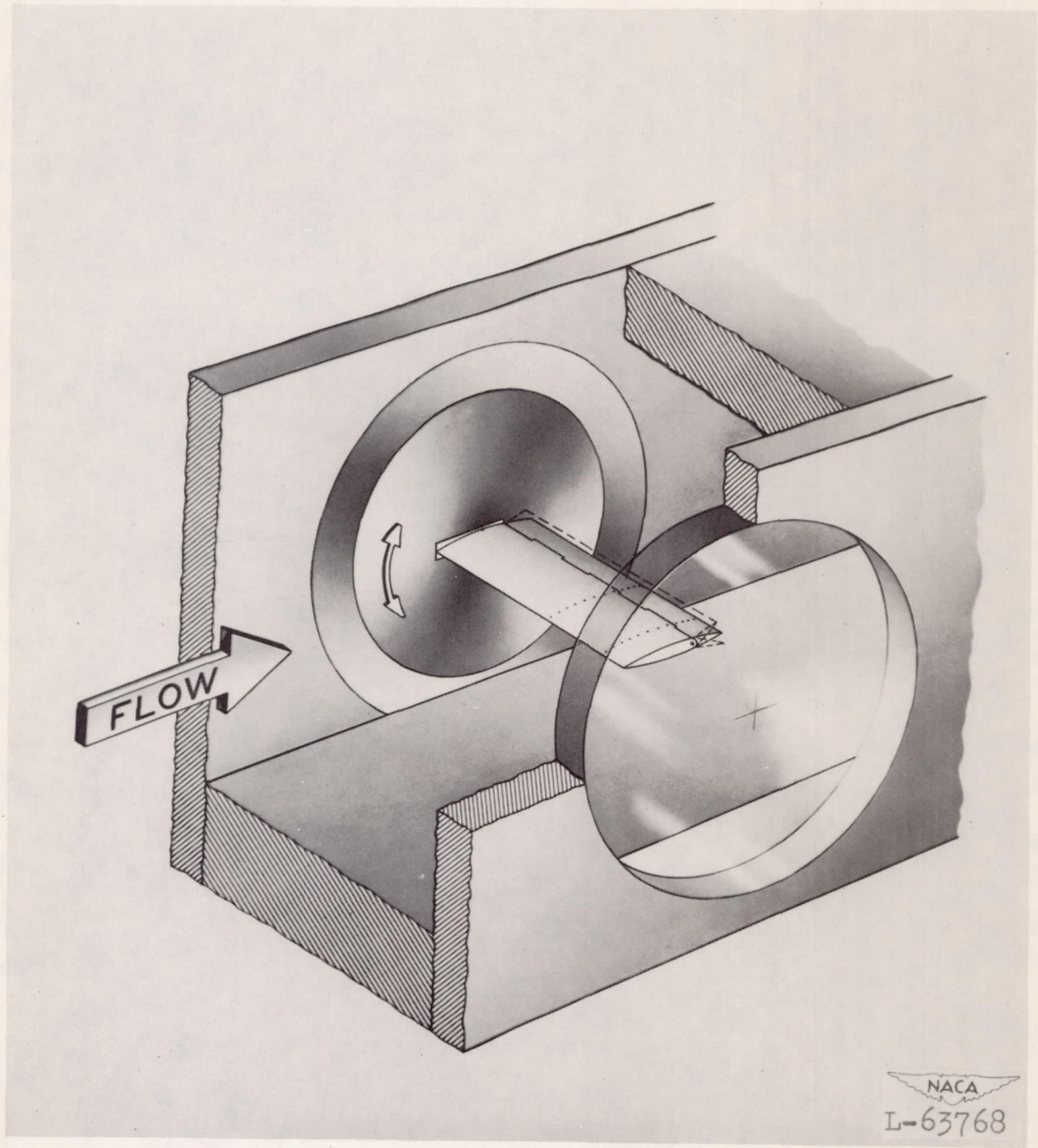

(a) 9-percent-thick wing.

Figure 2.- Illustrations showing general mounting arrangements of 9- and 6-percent-thick models in the tunnel.

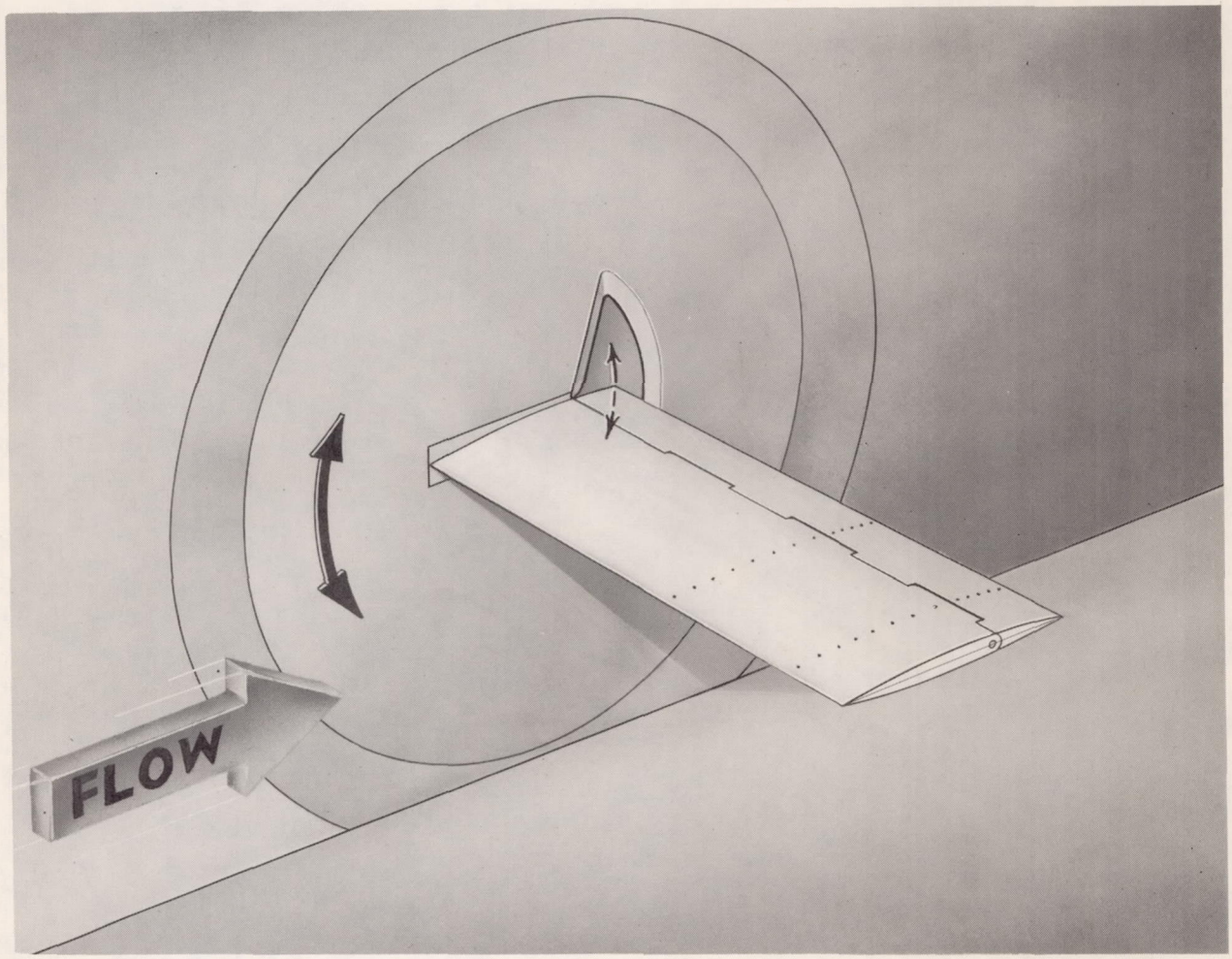

(b) 6-percent-thick wing.

Figure 2.- Concluded.

NACA L-66774.1

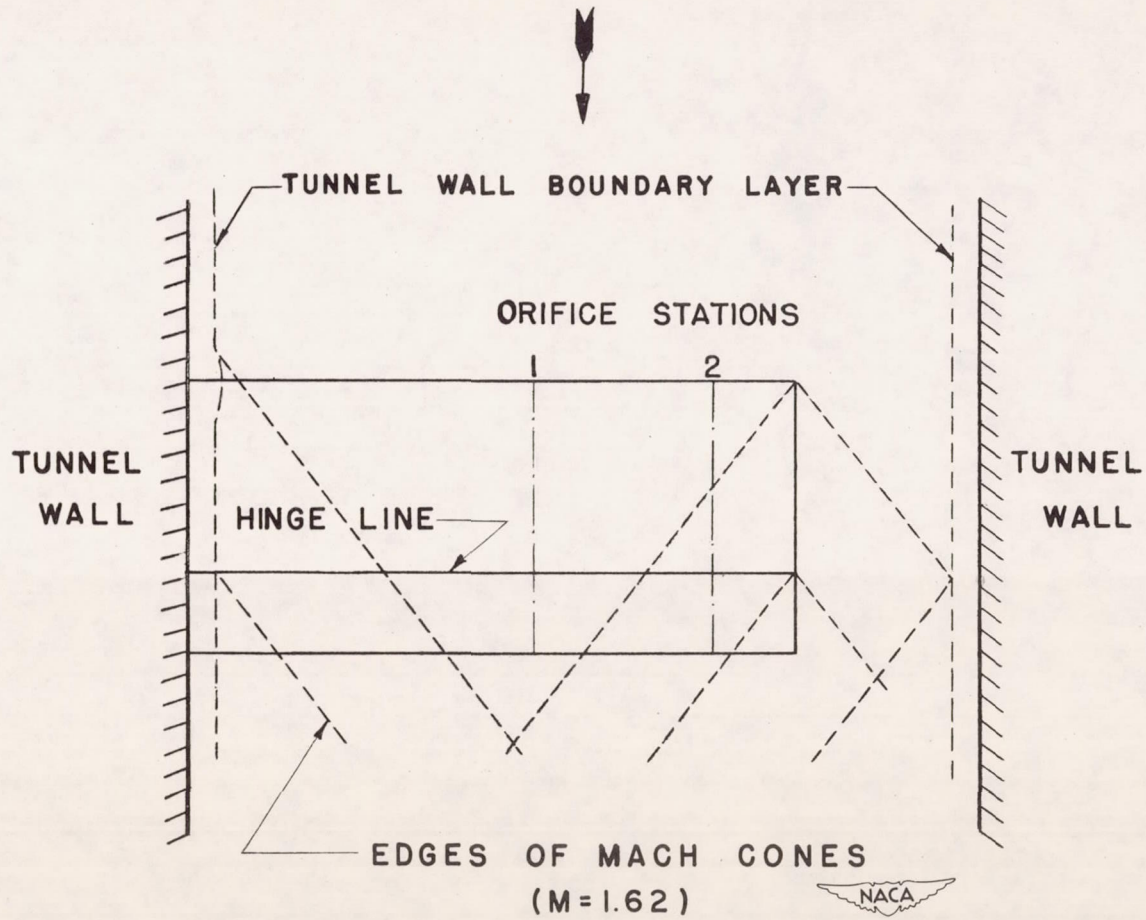

Figure 3.- Pressure-distribution model and its relative location in the wind tunnel.

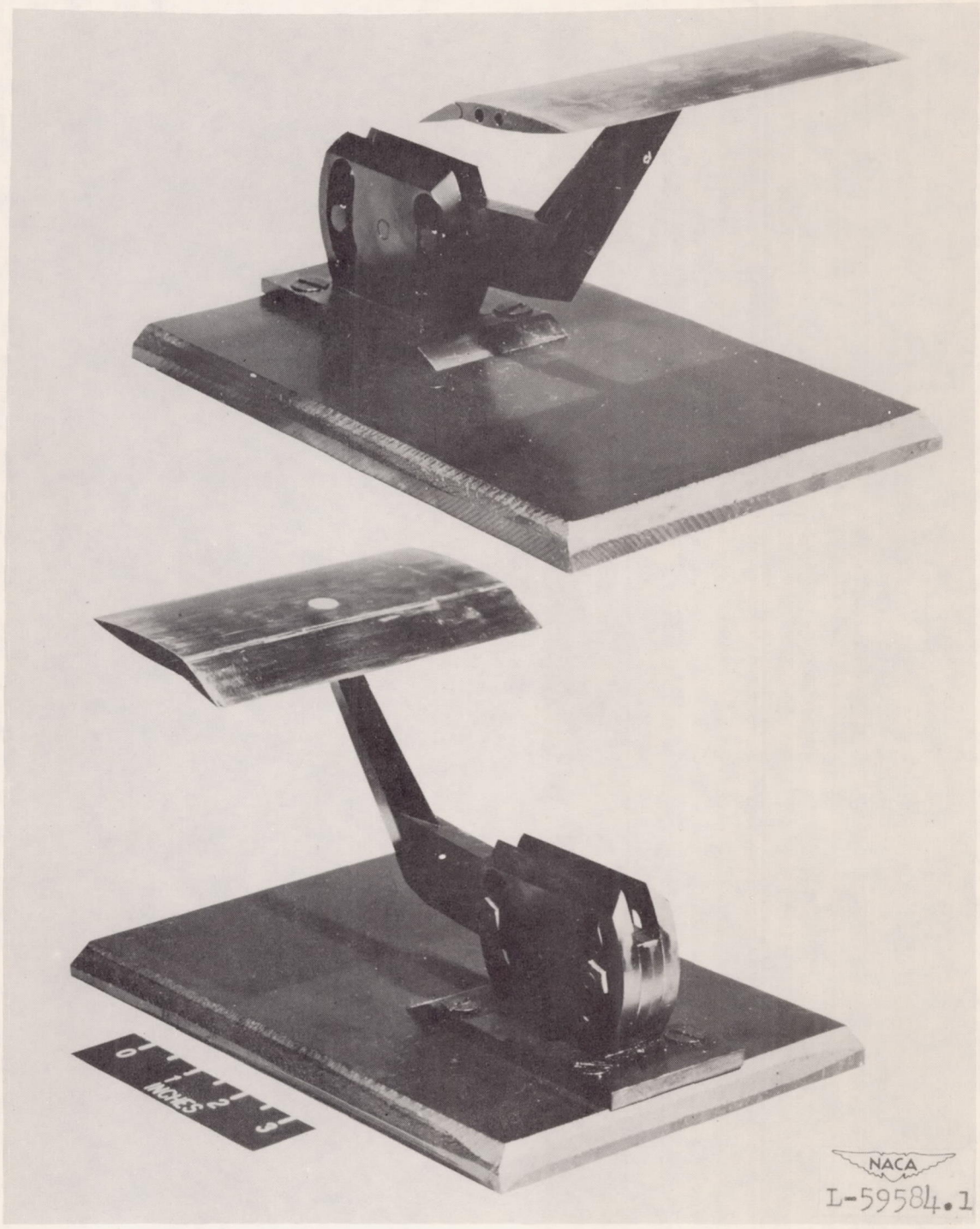

Figure 4.- Front and rear three-quarter views of 9-percent-thick symmetrical circular-arc wing used in schlieren observations.

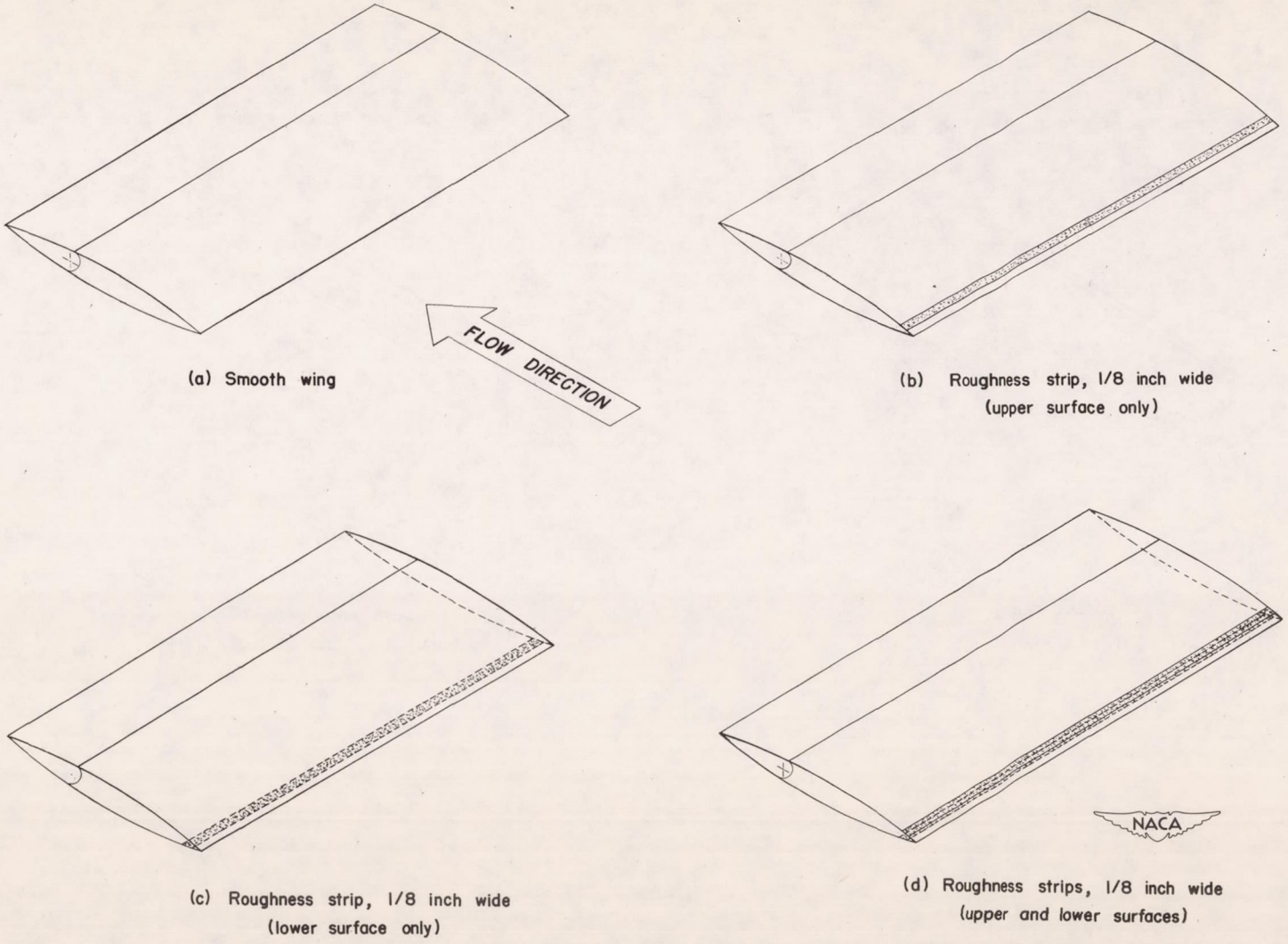

(a) Smooth wing

(b) Roughness strip, 1/8 inch wide (upper surface only)

(c) Roughness strip, 1/8 inch wide (lower surface only)

(d) Roughness strips, 1/8 inch wide (upper and lower surfaces)

Figure 5.- Locations and extent of wing-surface roughness used in transition studies.

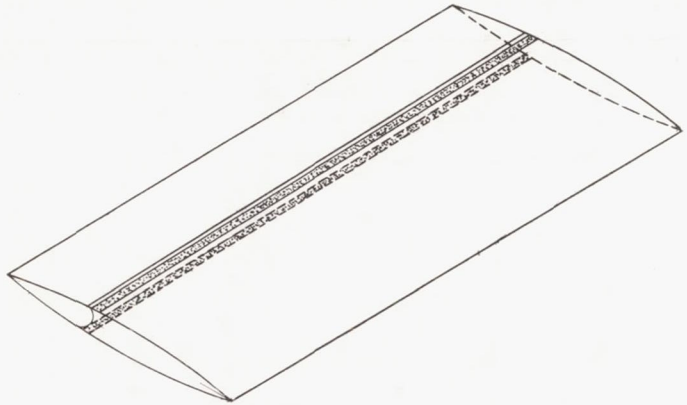

(e) Roughness strips, 1/8 inch wide
(upper and lower surfaces)

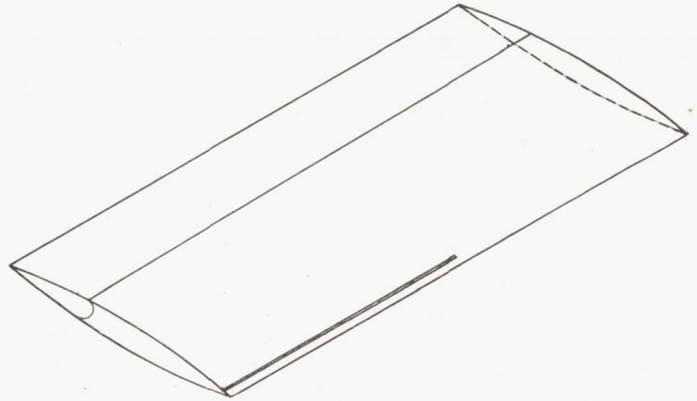

(f) Smooth strip of dope, 1/32 inch wide
(upper surface only)

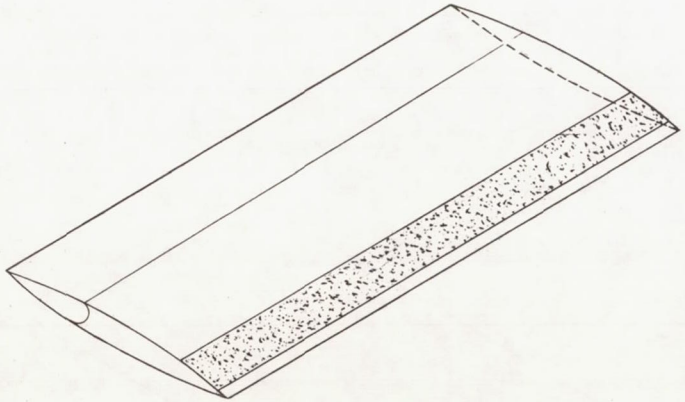

(g) Roughness strip, 3/4 inch wide
(upper surface only)

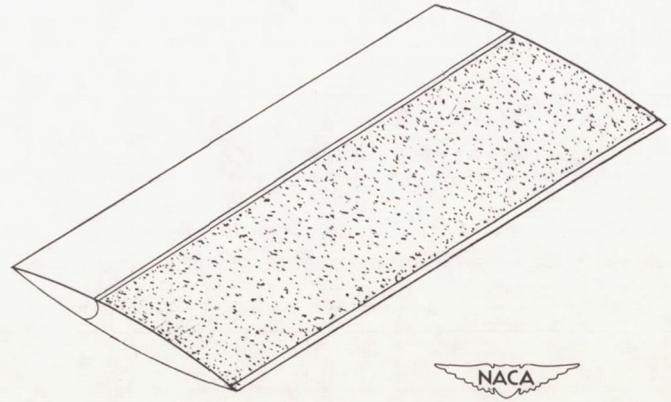

(h) Roughness strip, 2 inches wide
(upper surface only)

Figure 5.- Concluded.

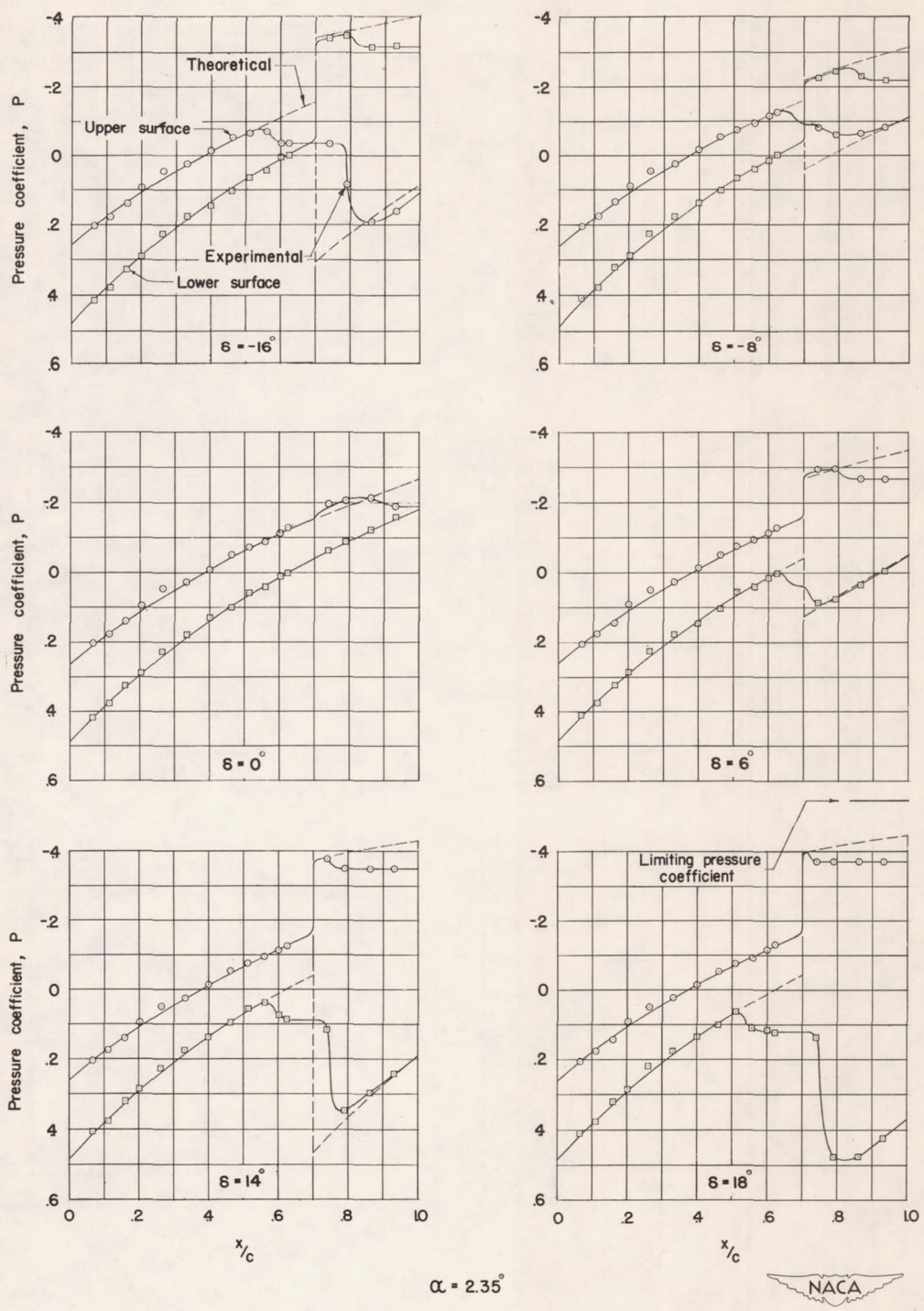

(a) M = 1.62.

Figure 6.- Effect of Mach number on pressure distribution over 9-percent-thick symmetrical circular-arc wing. Station 1.

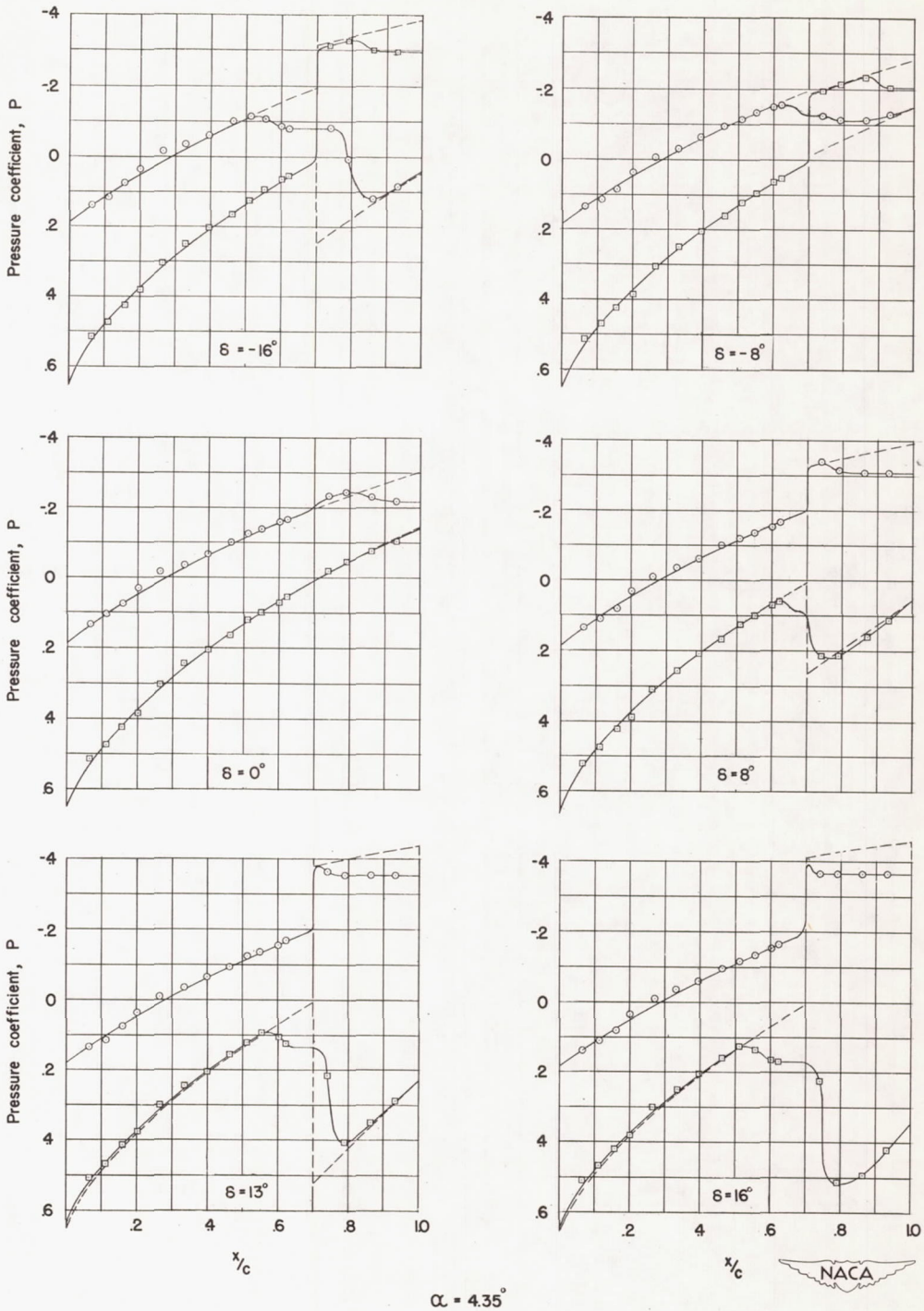

(a) Concluded.

Figure 6.- Continued.

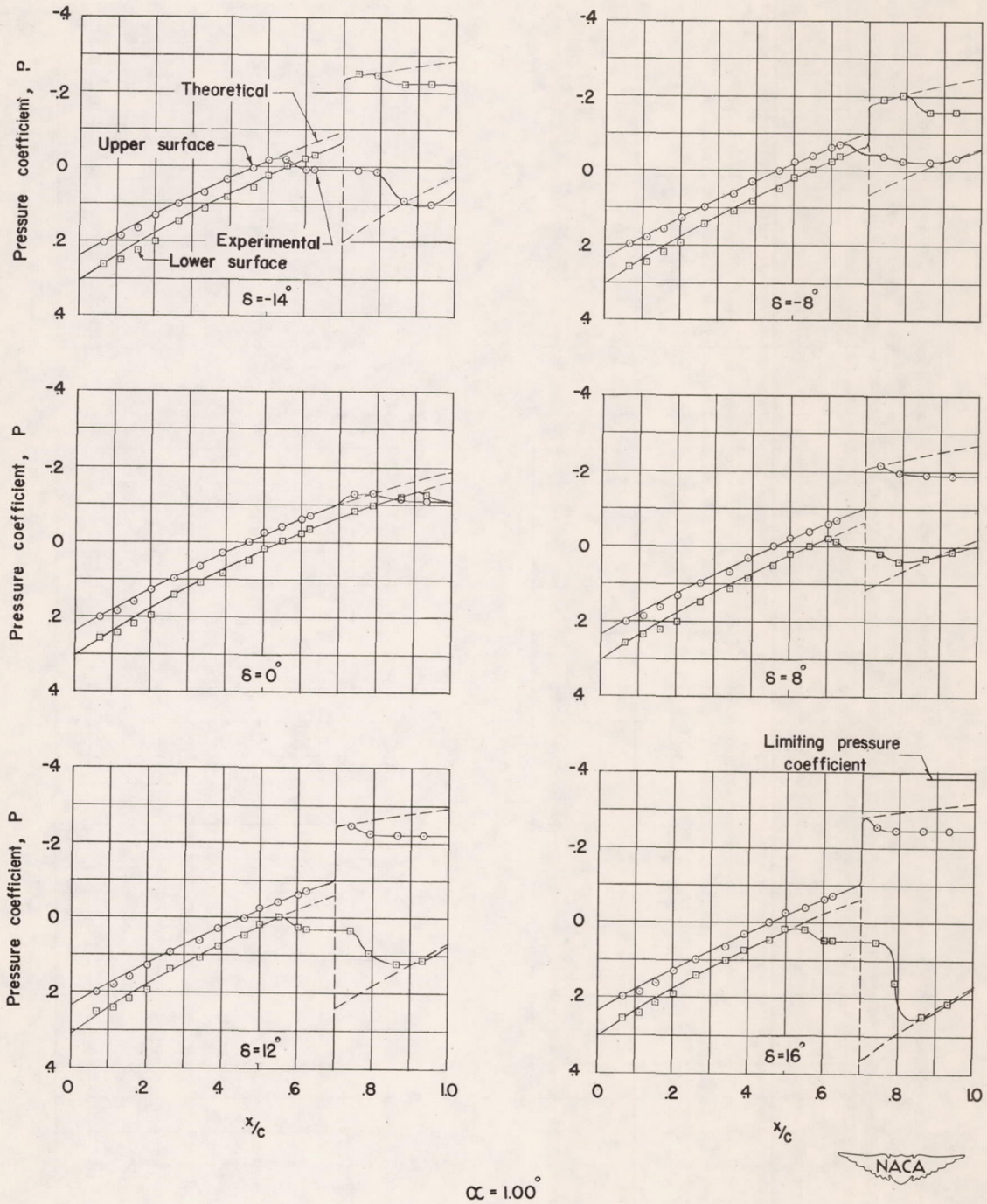

(b) M = 1.93.

Figure 6.- Continued.

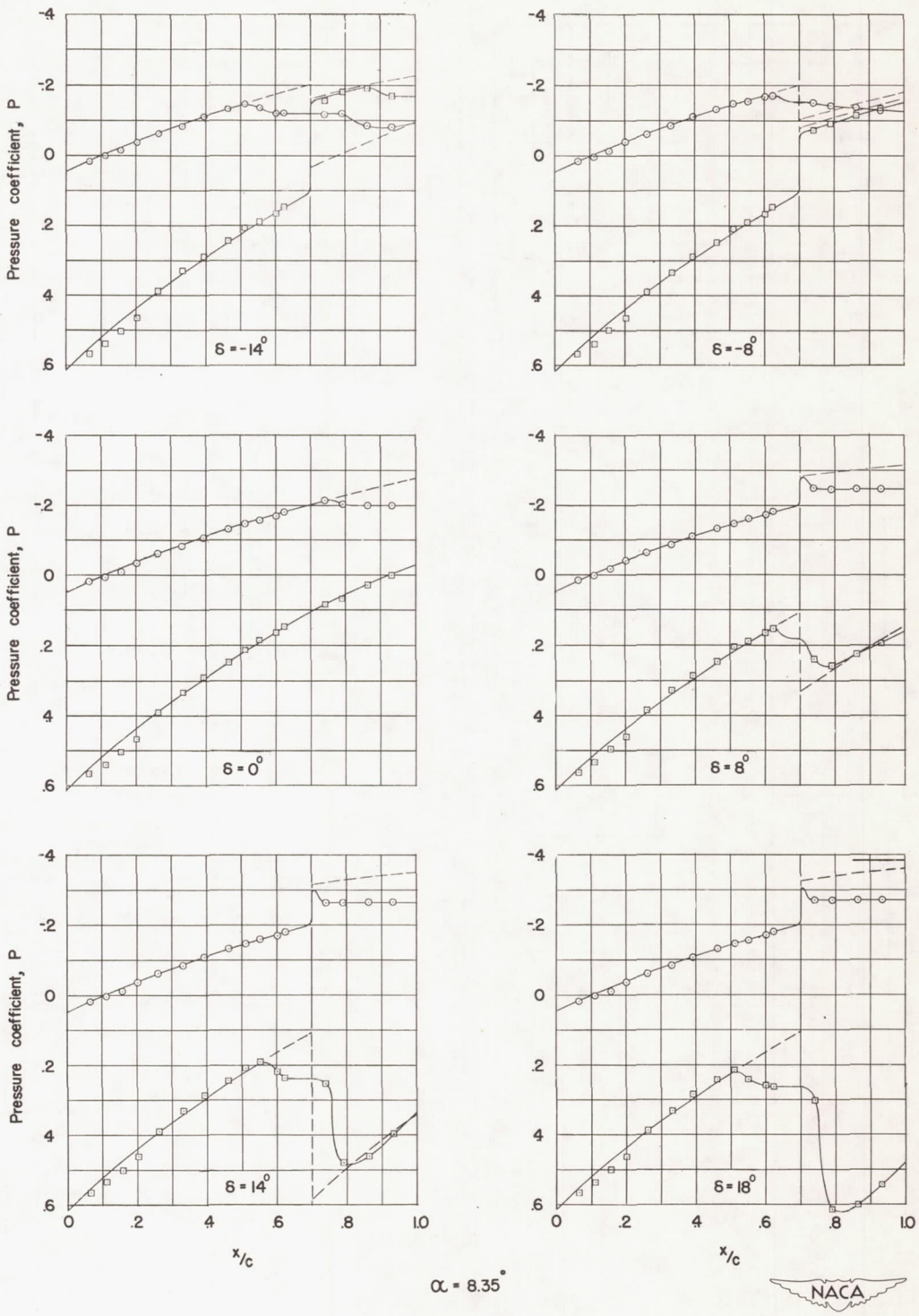

(b) Concluded.

Figure 6.- Continued.

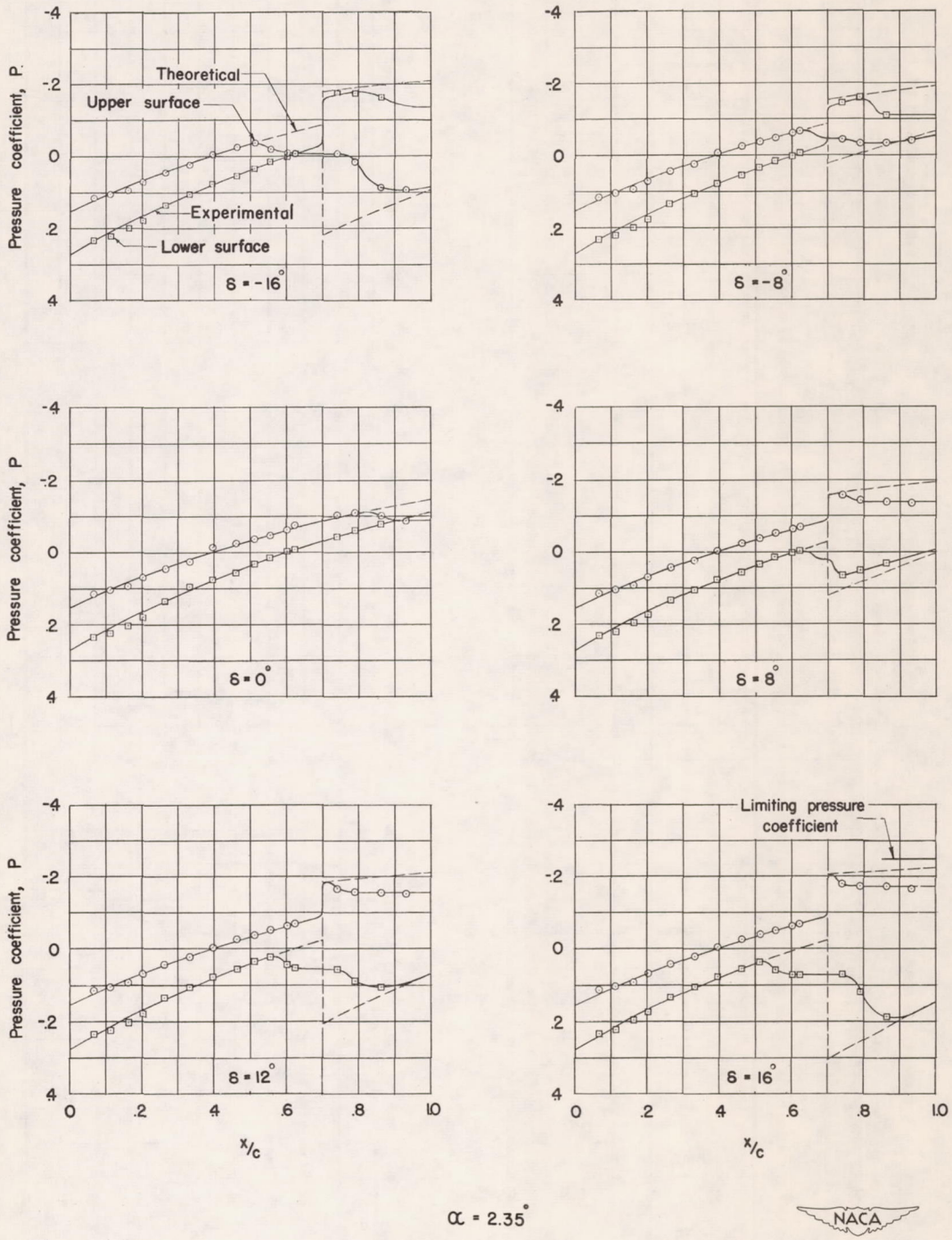

(c) M = 2.40.

Figure 6.- Continued.

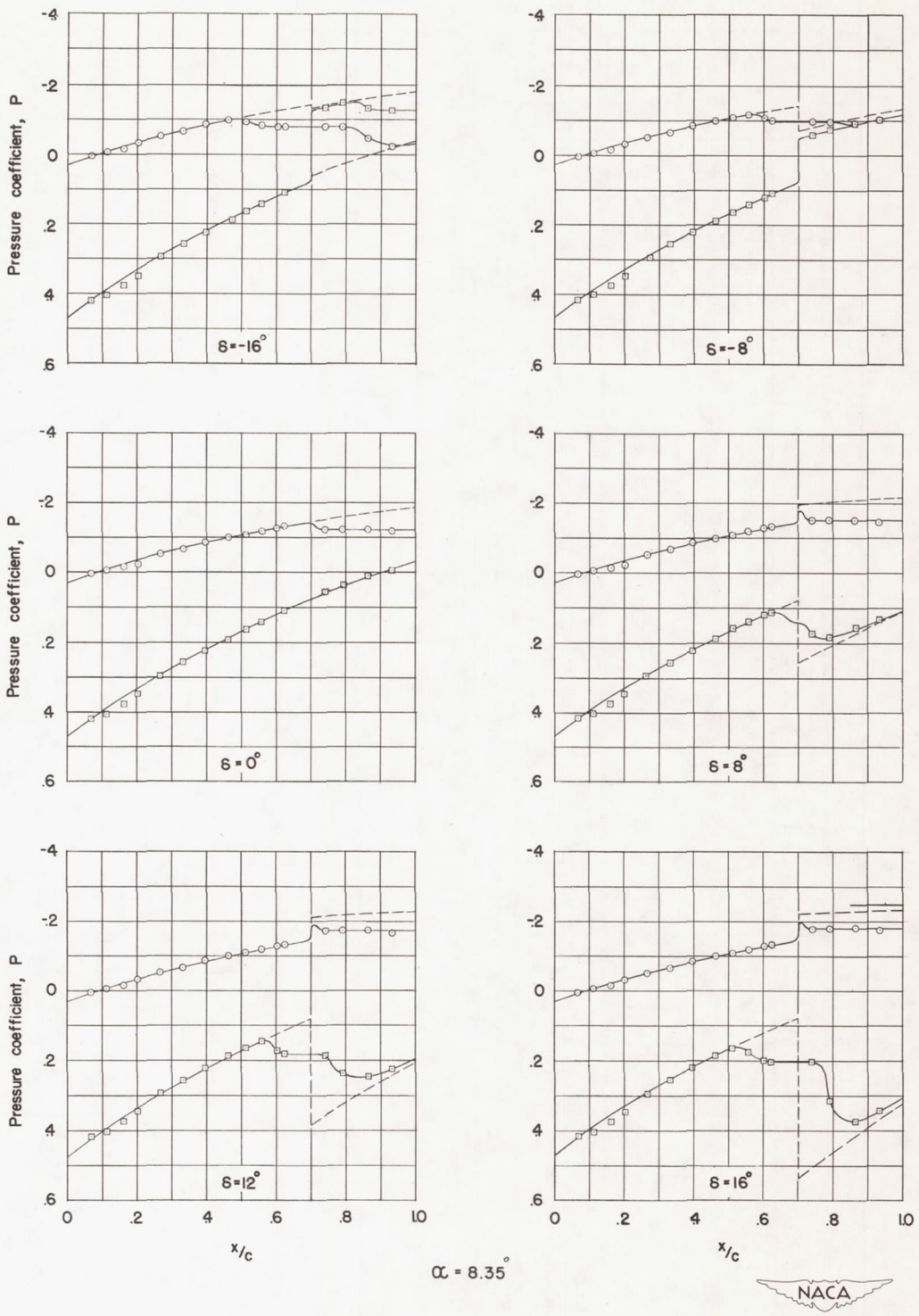

(c) Concluded.

Figure 6.- Concluded.

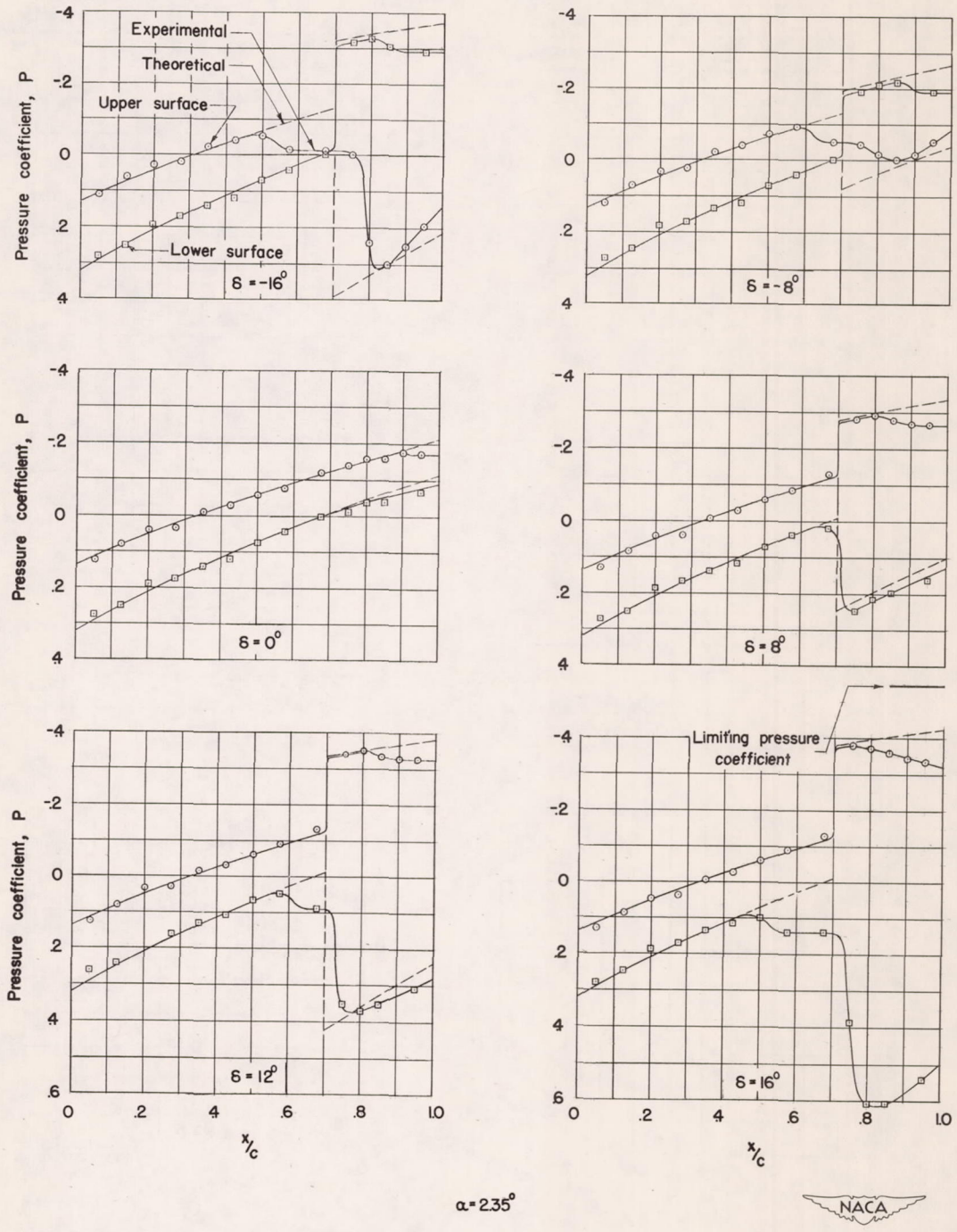

(a) M = 1.62.

Figure 7.- Effect of Mach number on pressure distribution over 6-percent-thick symmetrical circular-arc wing. Station 1.

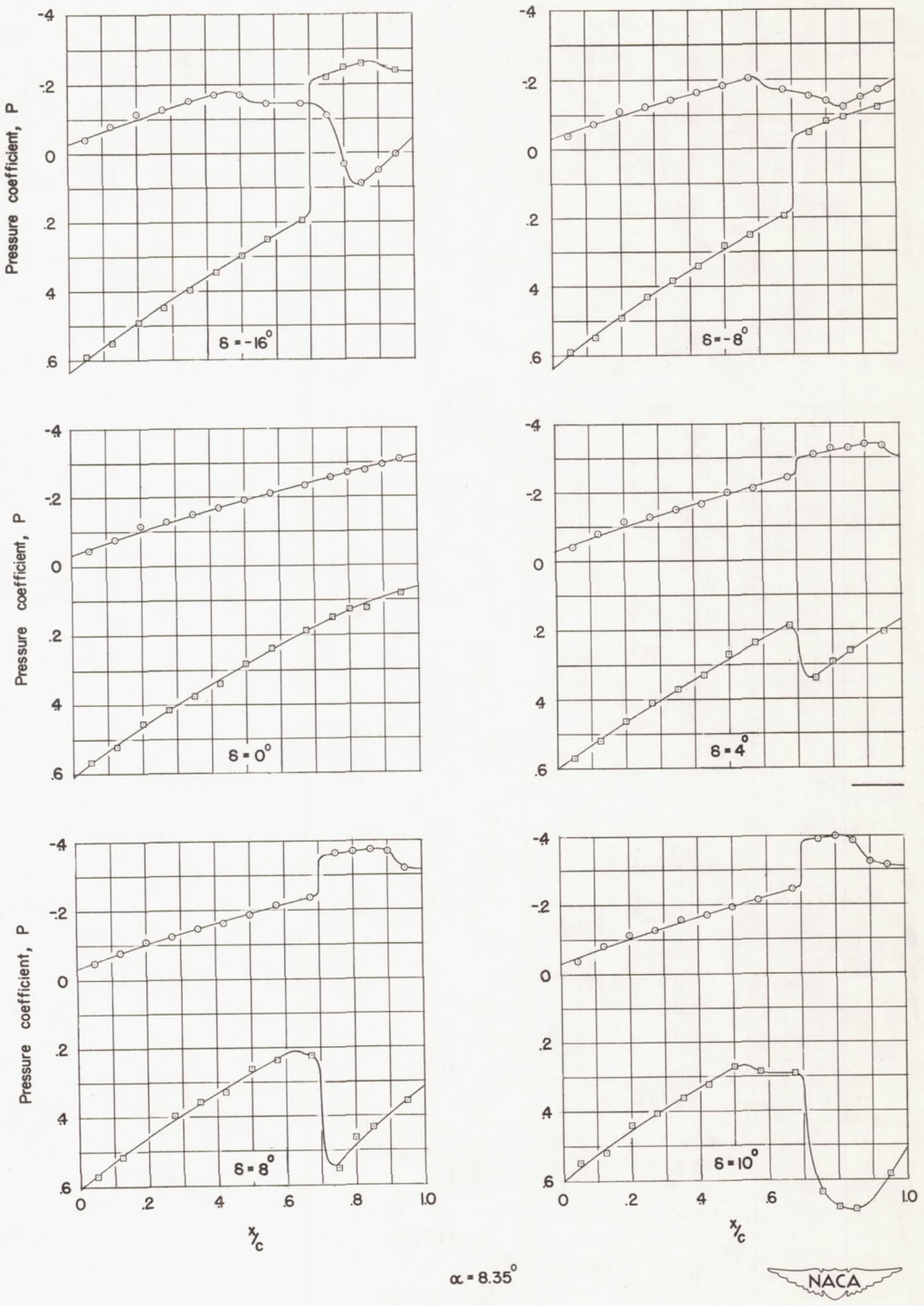

(a) Concluded.

Figure 7.- Continued.

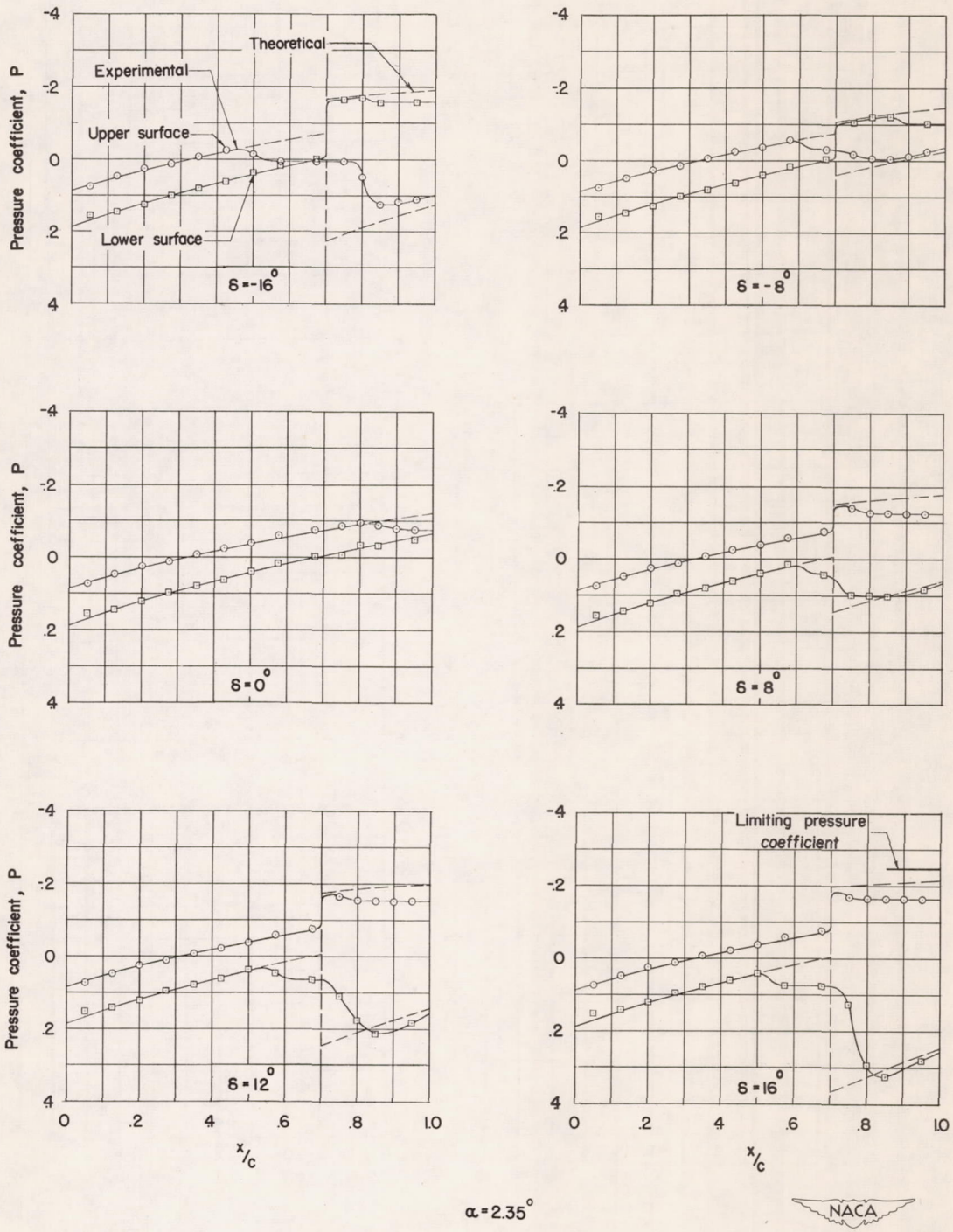

(b) M = 2.40.

Figure 7.- Continued.

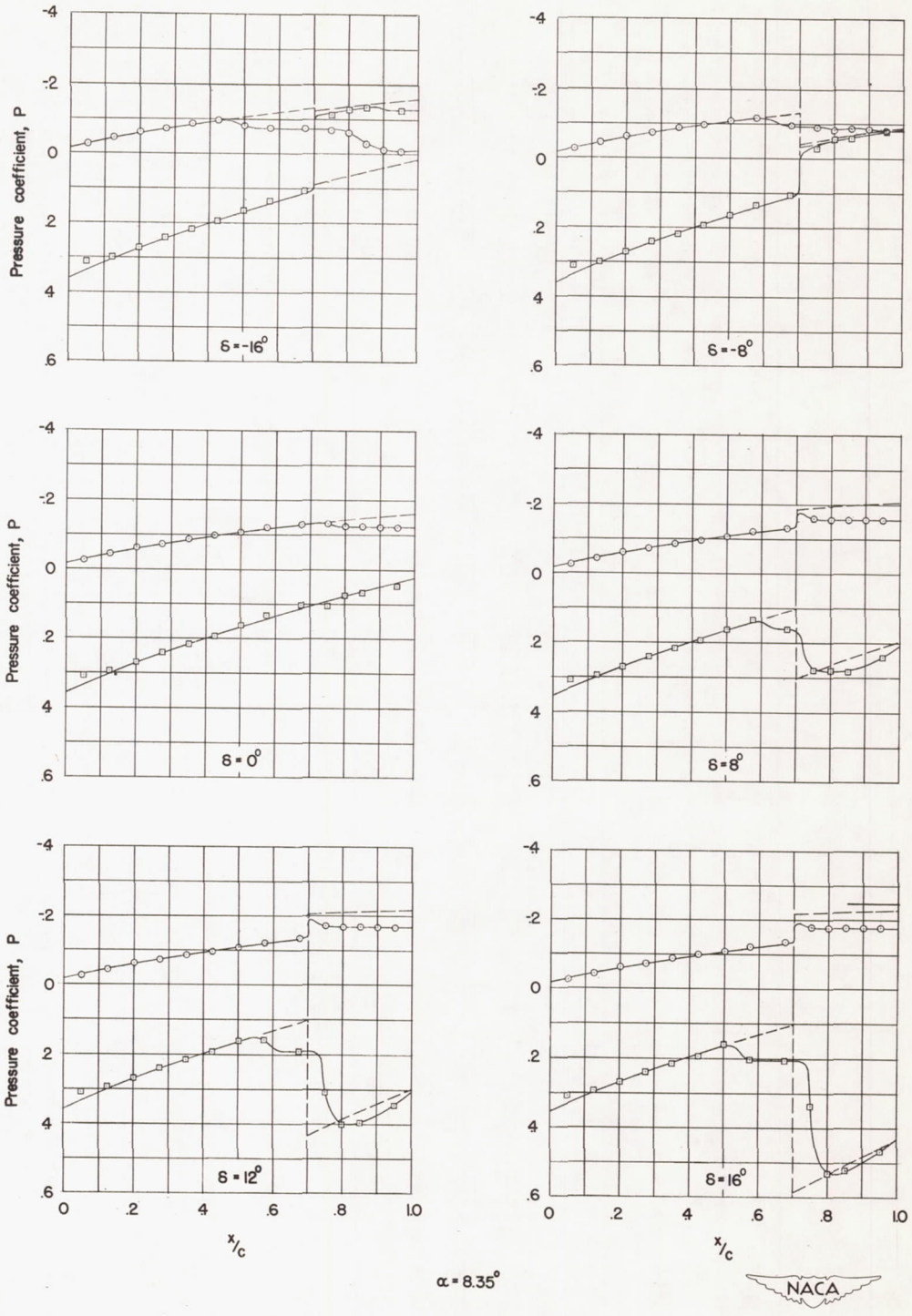

(b) Concluded.

Figure 7.- Concluded.

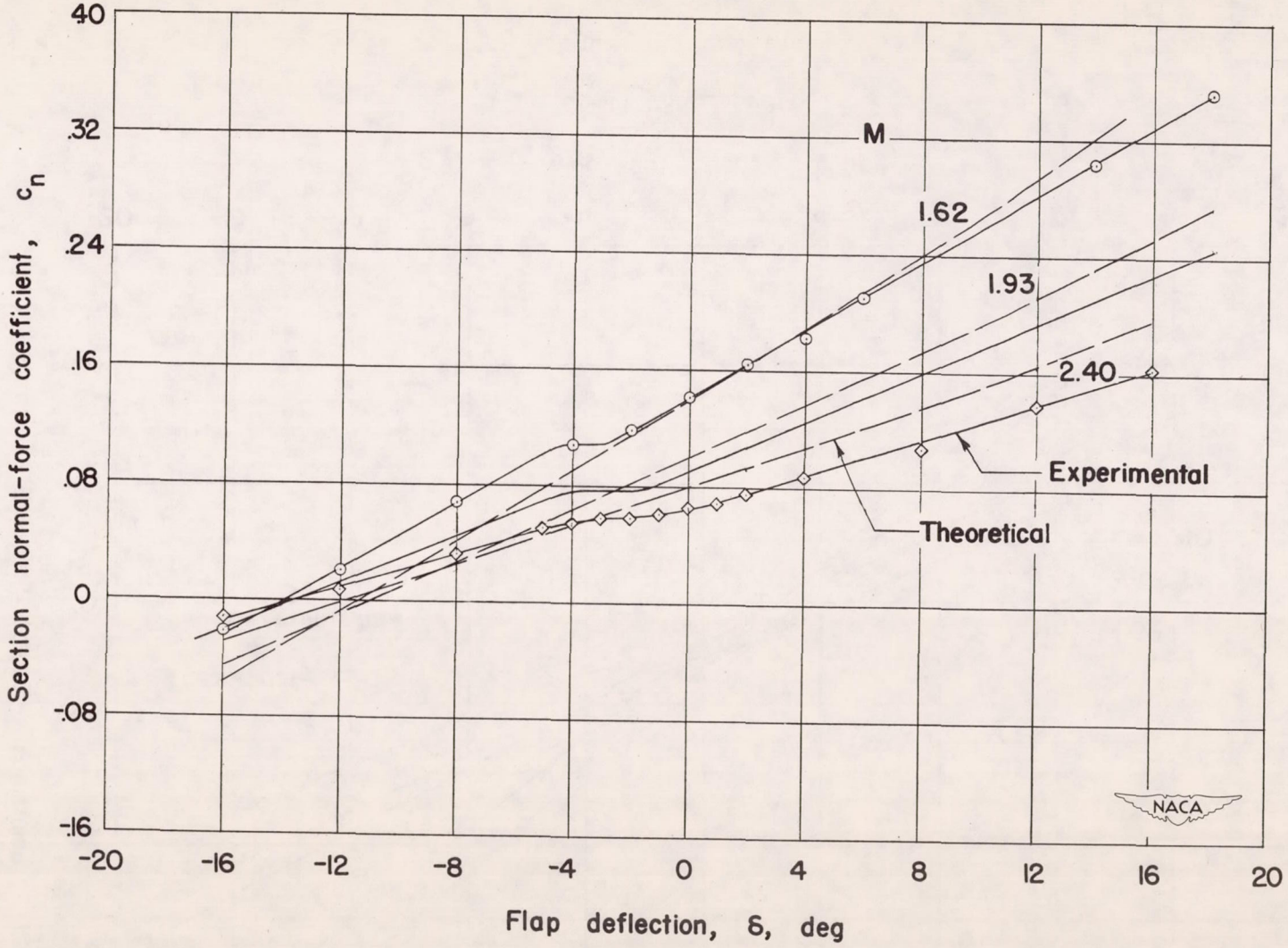

(a) $\alpha = 2.35^{\circ}$.

Figure 8.- Effect of Mach number on the section force and moment characteristics of 9-percent-thick symmetrical circular-arc wing. Station 1.

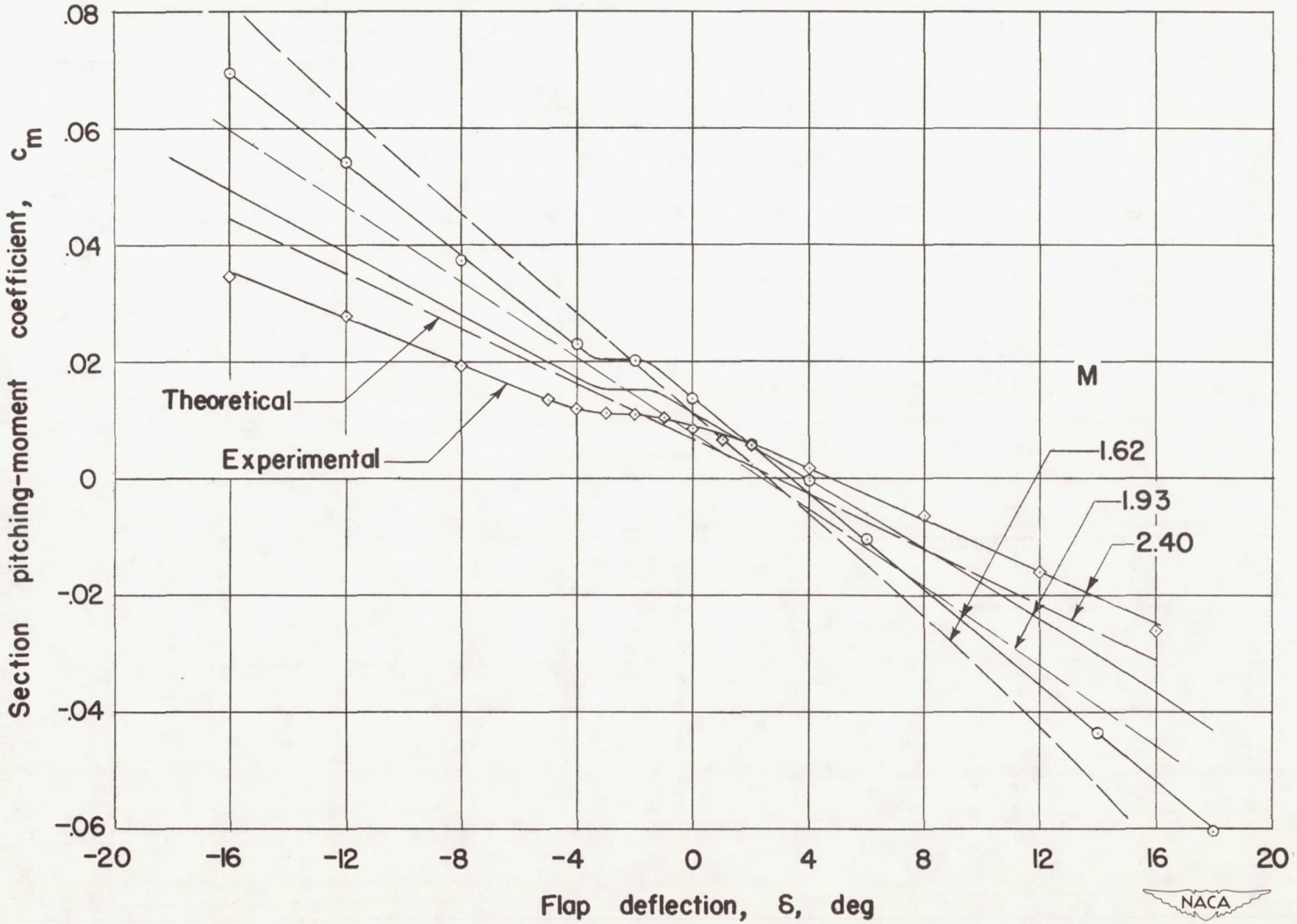

(a) Continued.

Figure 8.- Continued.

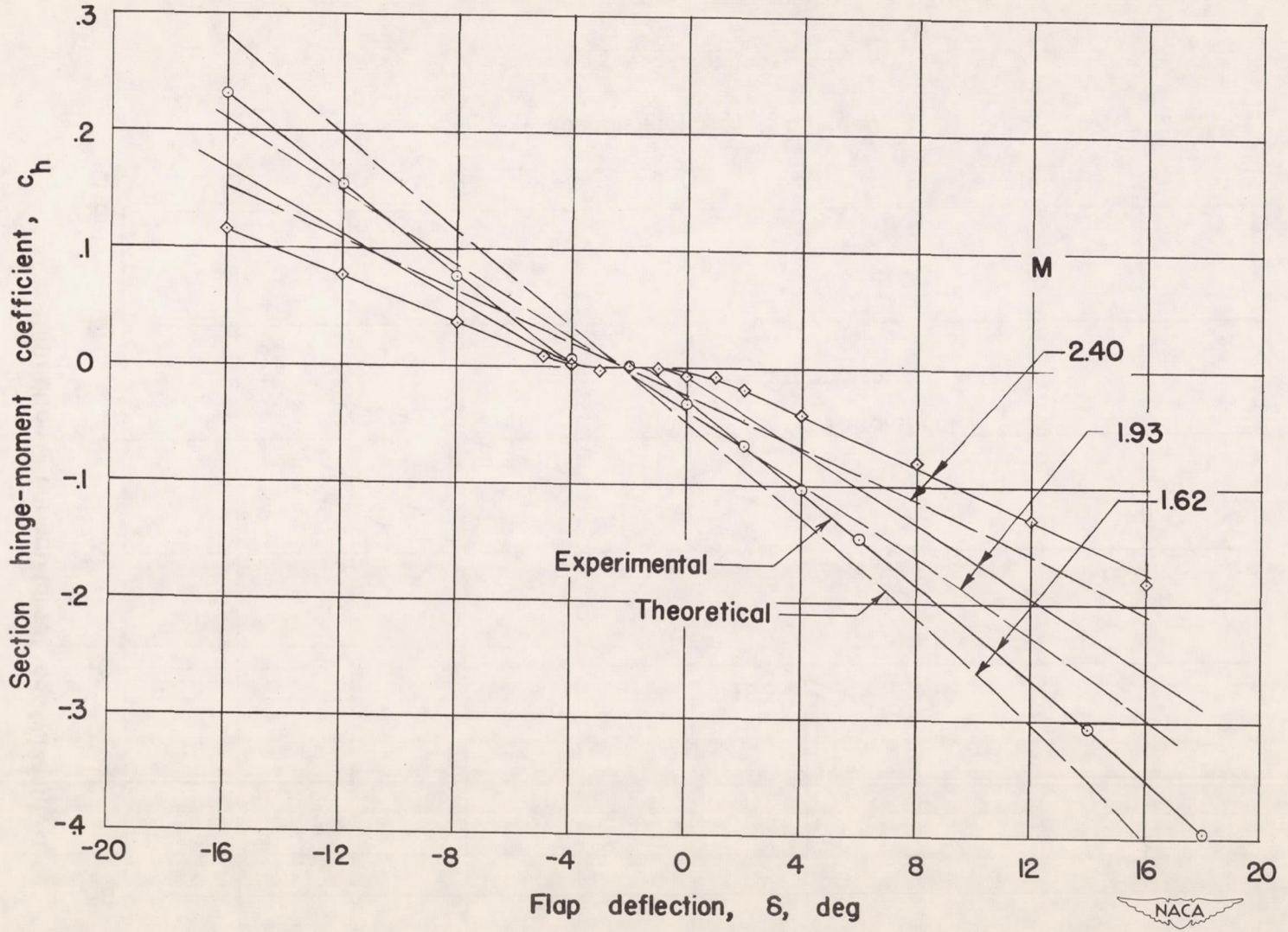

(a) Concluded.

Figure 8.- Continued.

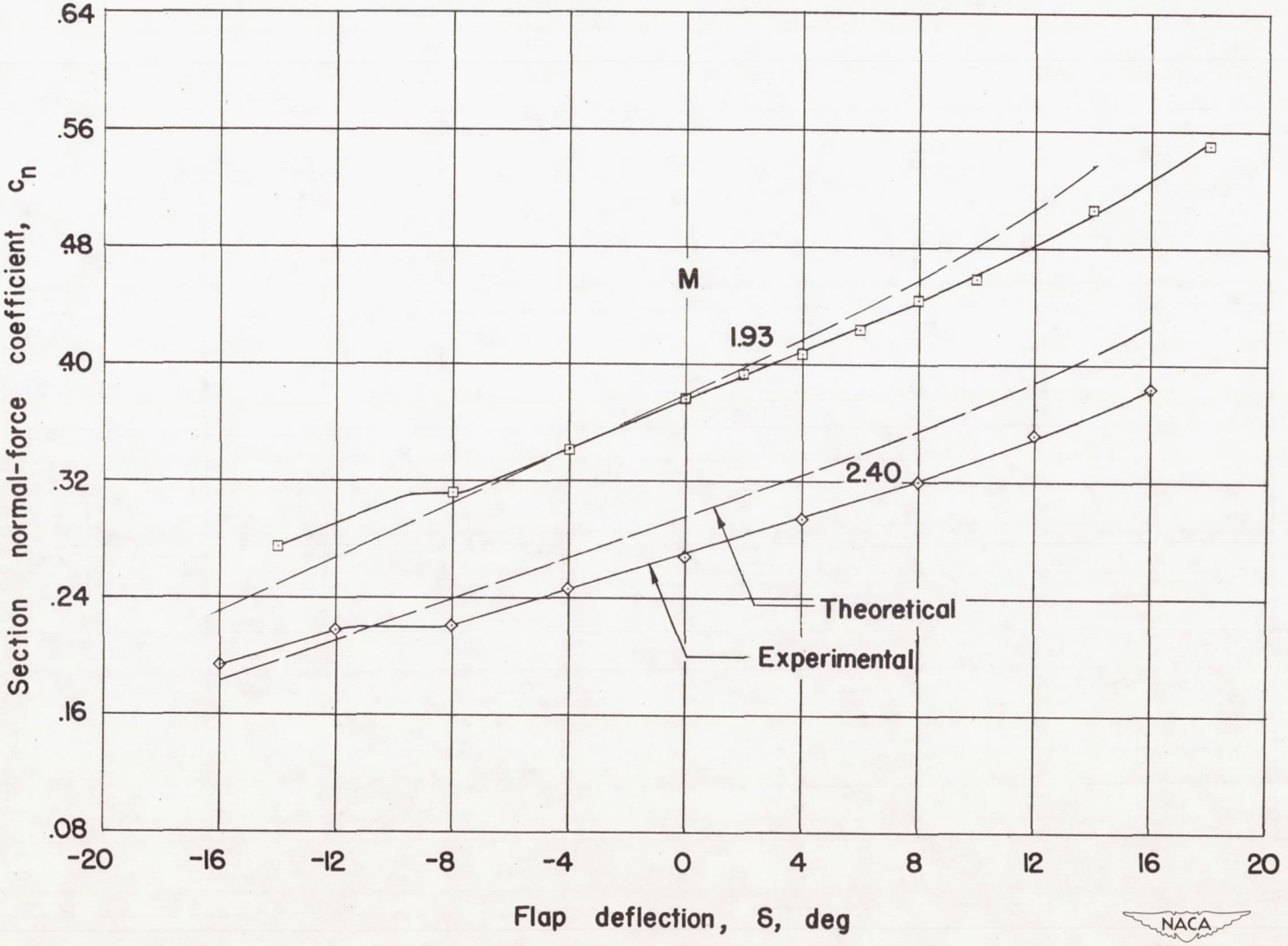

(b) $\alpha = 8.35°$.

Figure 8.- Continued.

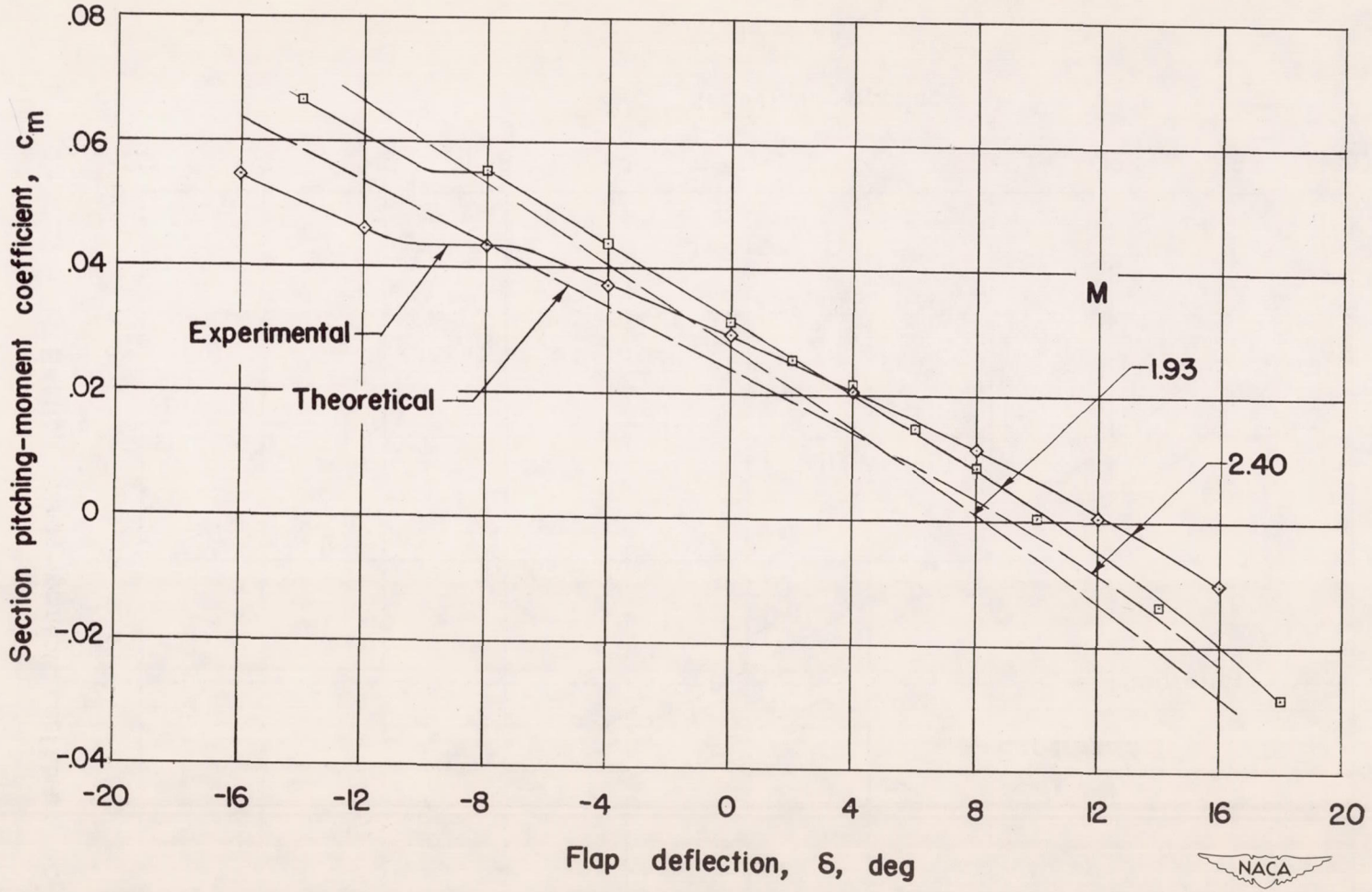

(b) Continued.

Figure 8.- Continued.

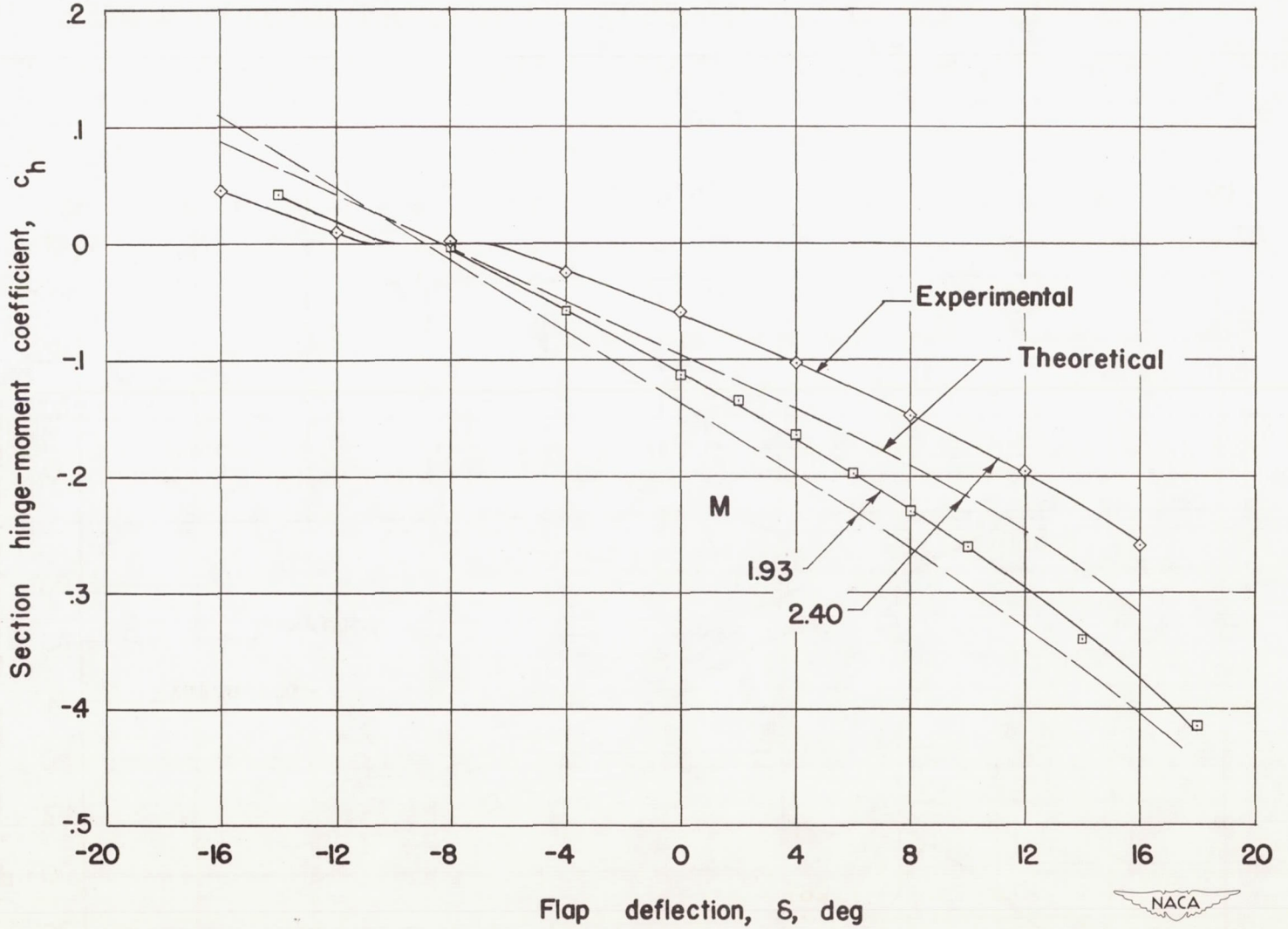

(b) Concluded.

Figure 8.- Concluded.

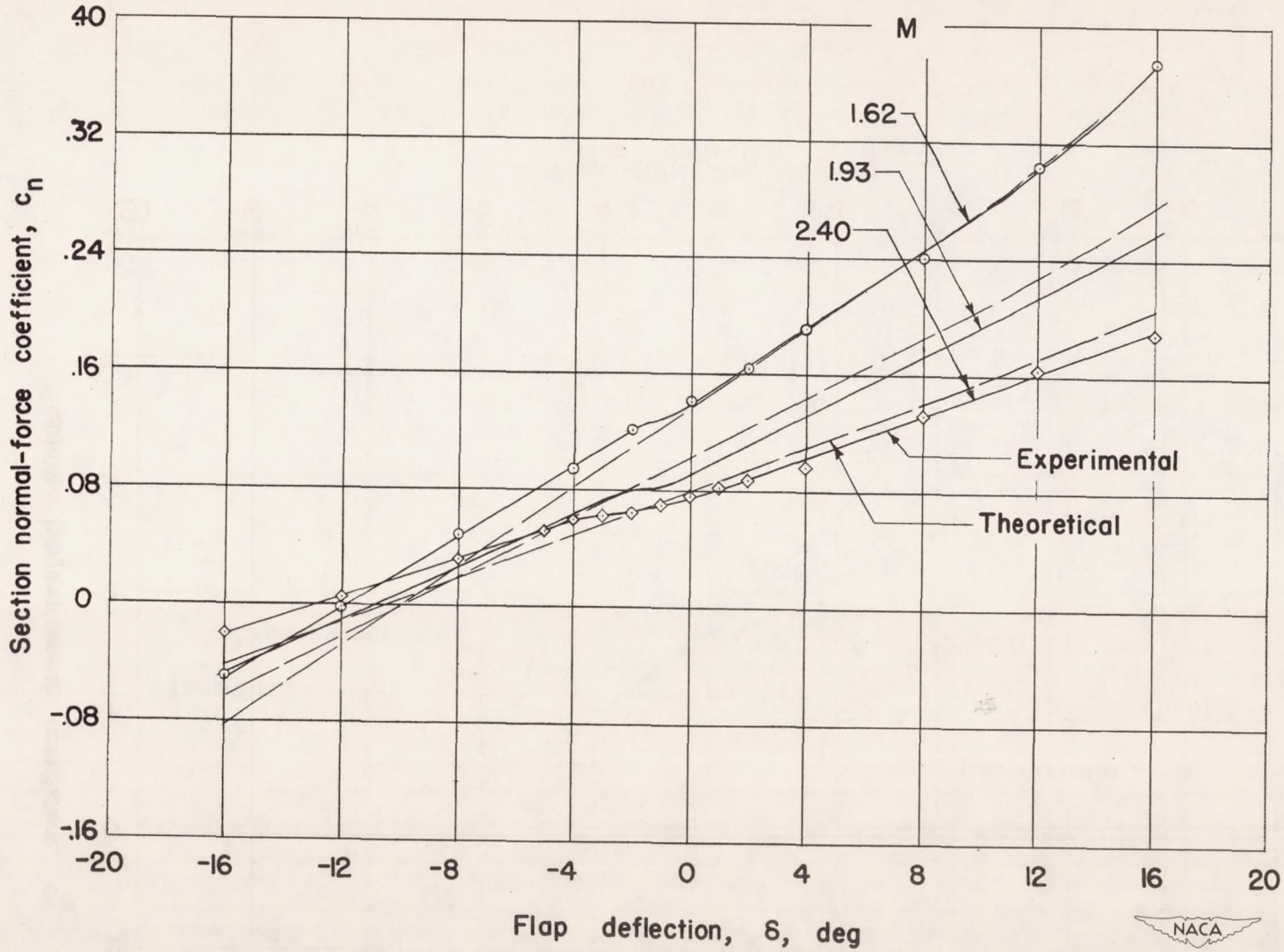

(a) $\alpha = 2.35^\circ$.

Figure 9.- Effect of Mach number on the section force and moment characteristics of 6-percent-thick symmetrical circular-arc wing. Station 1.

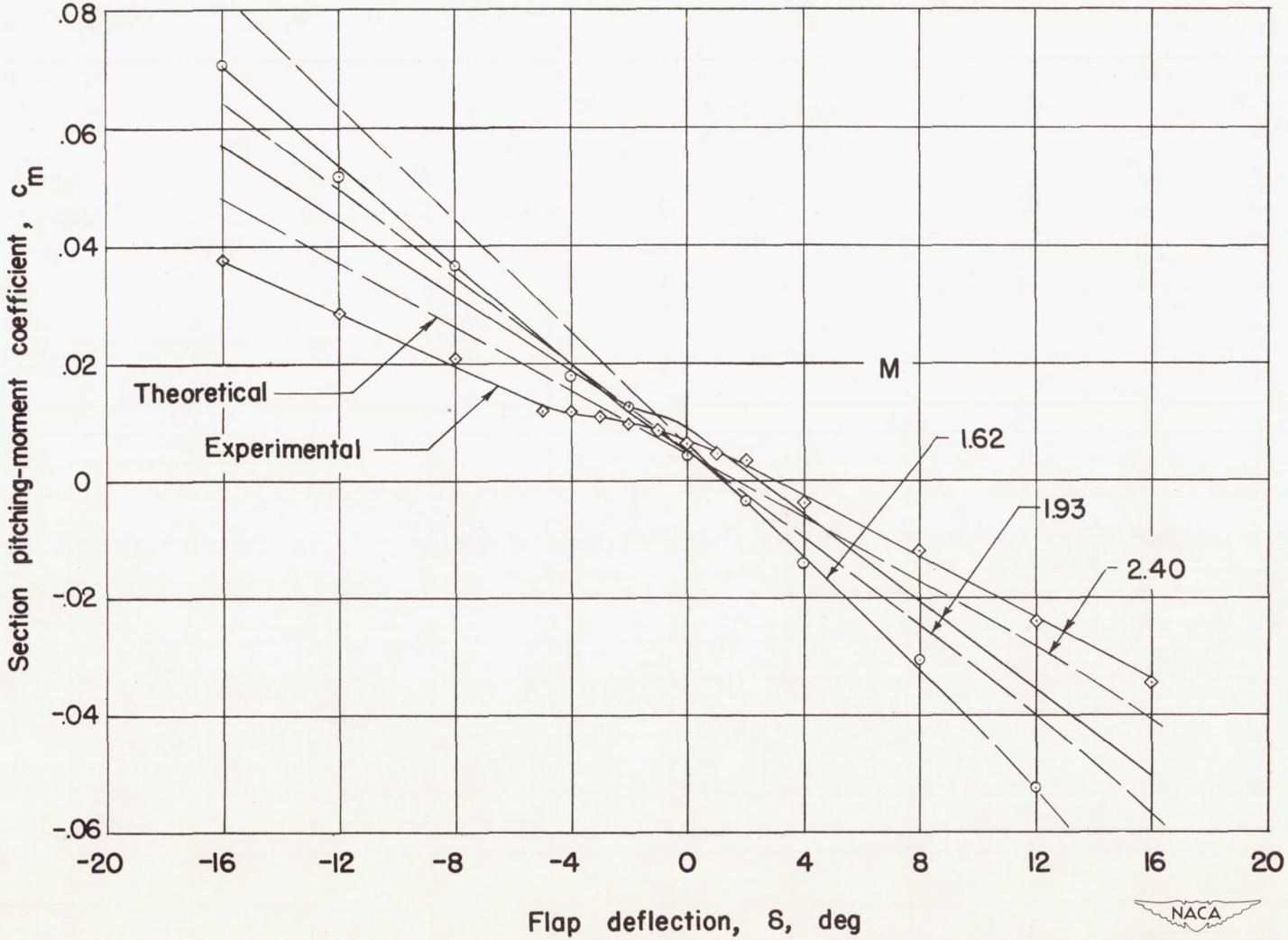

(a) Continued.

Figure 9.- Continued.

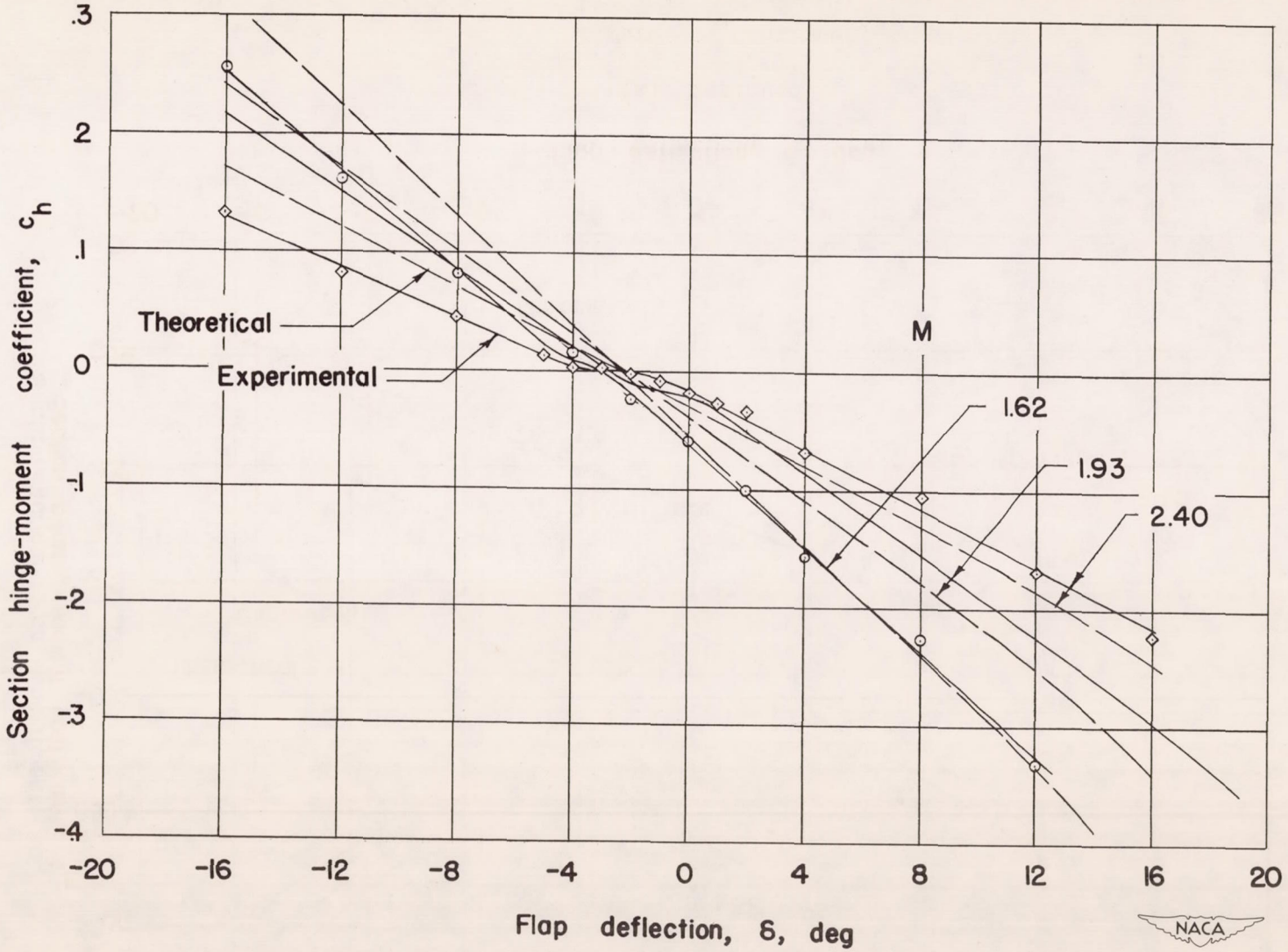

(a) Concluded.

Figure 9.- Continued.

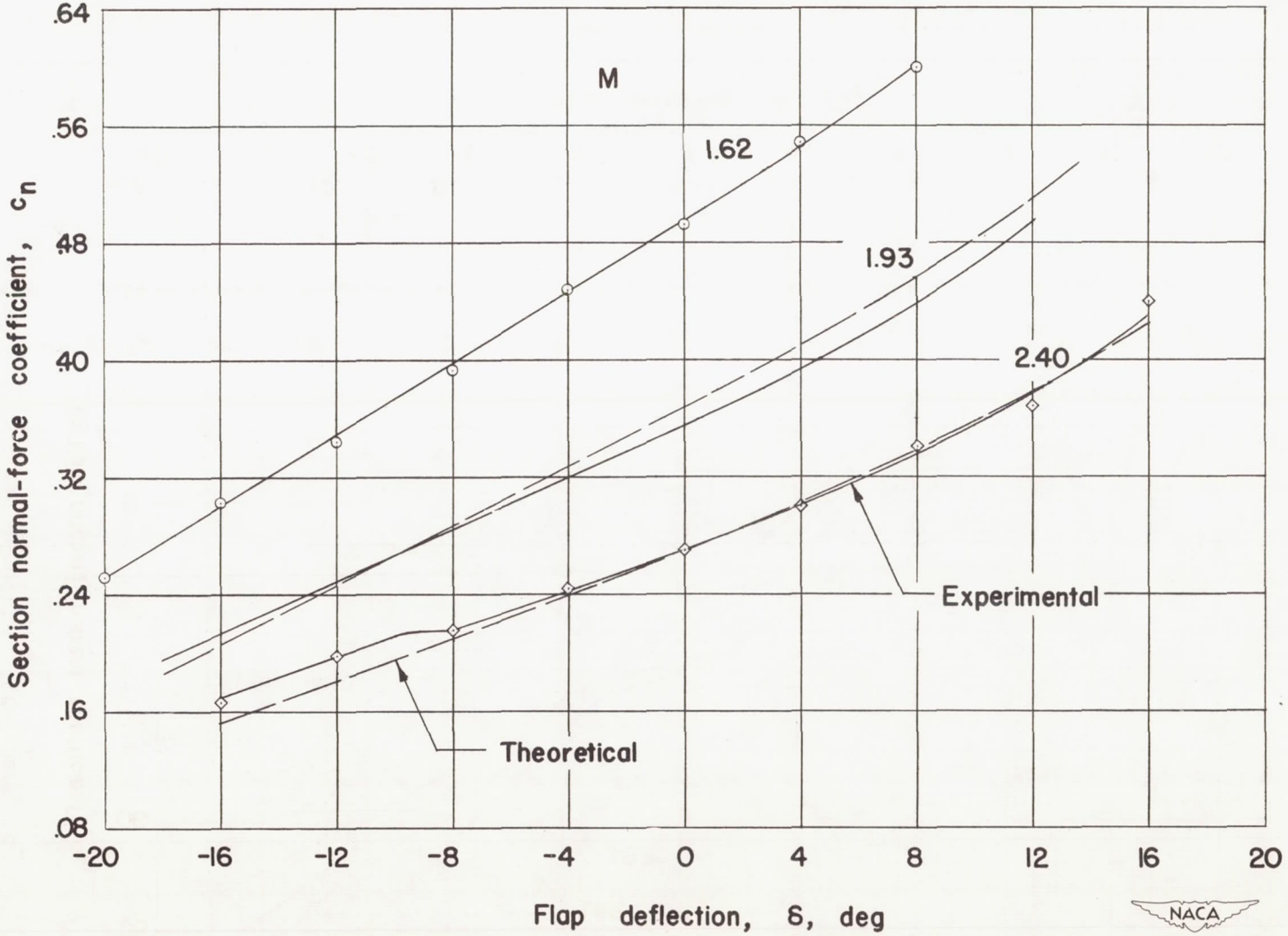

(b) $\alpha = 8.35^\circ$.

Figure 9.- Continued.

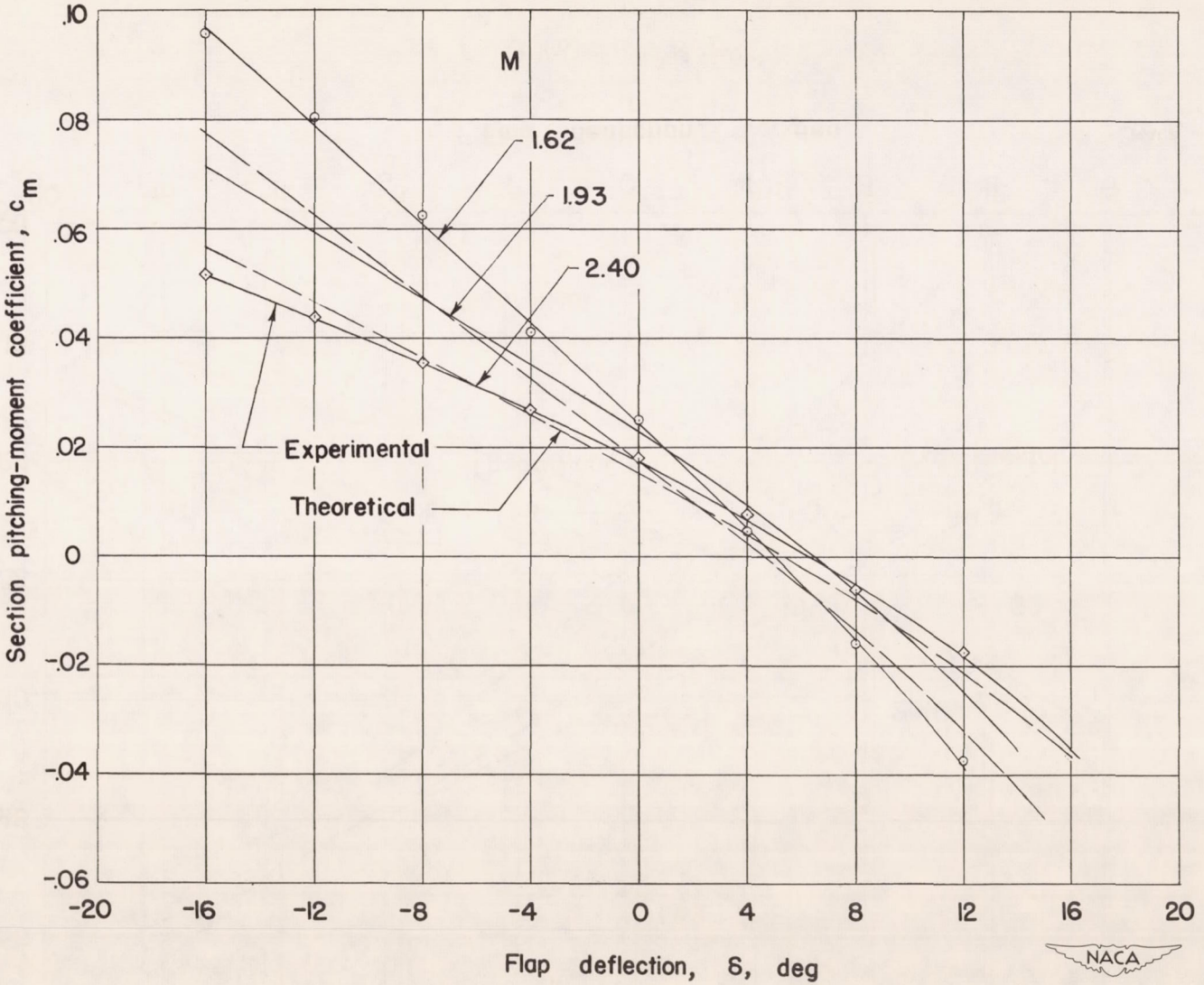

(b) Continued.

Figure 9.- Continued.

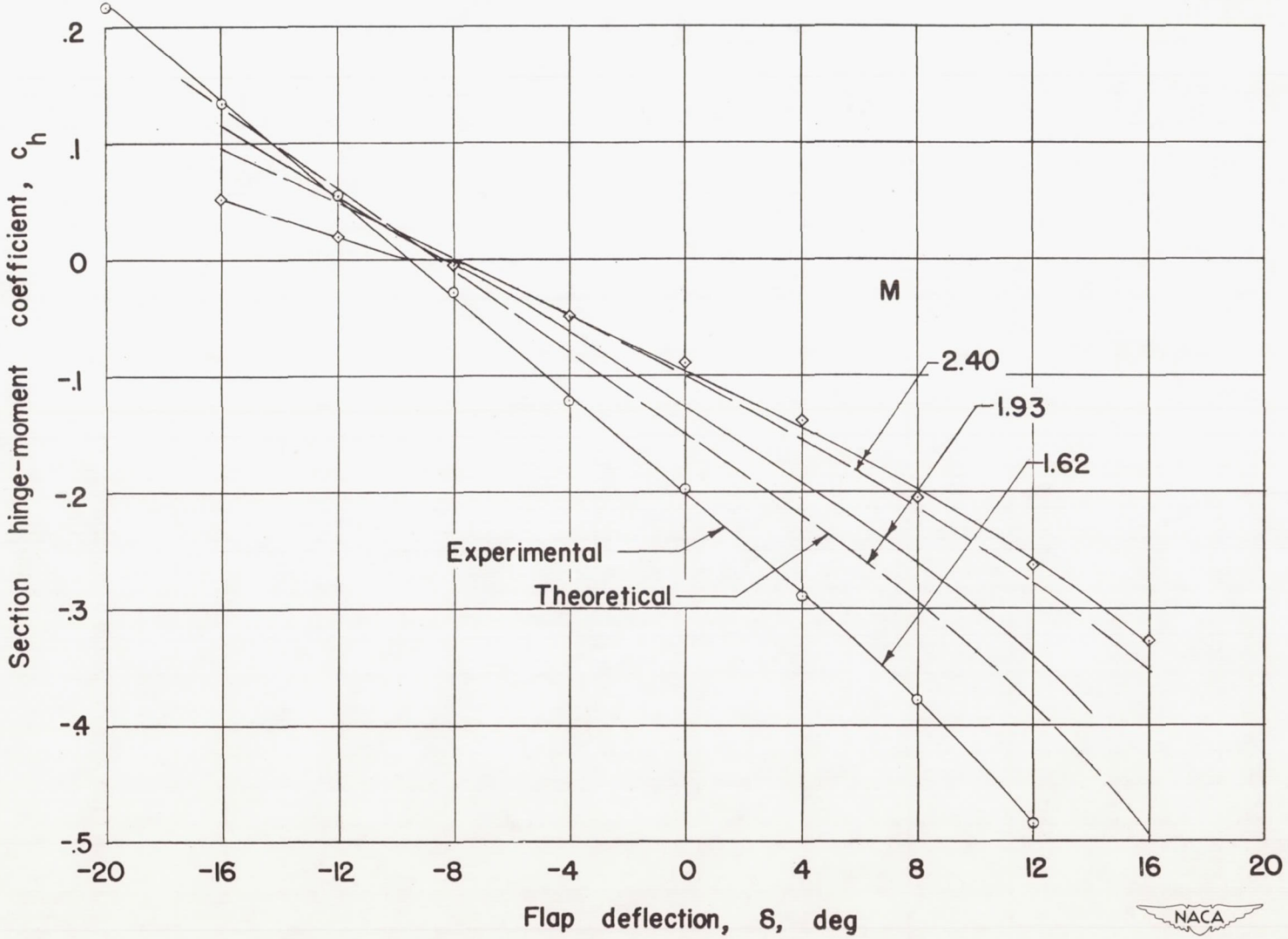

(b) Concluded.

Figure 9.- Concluded.

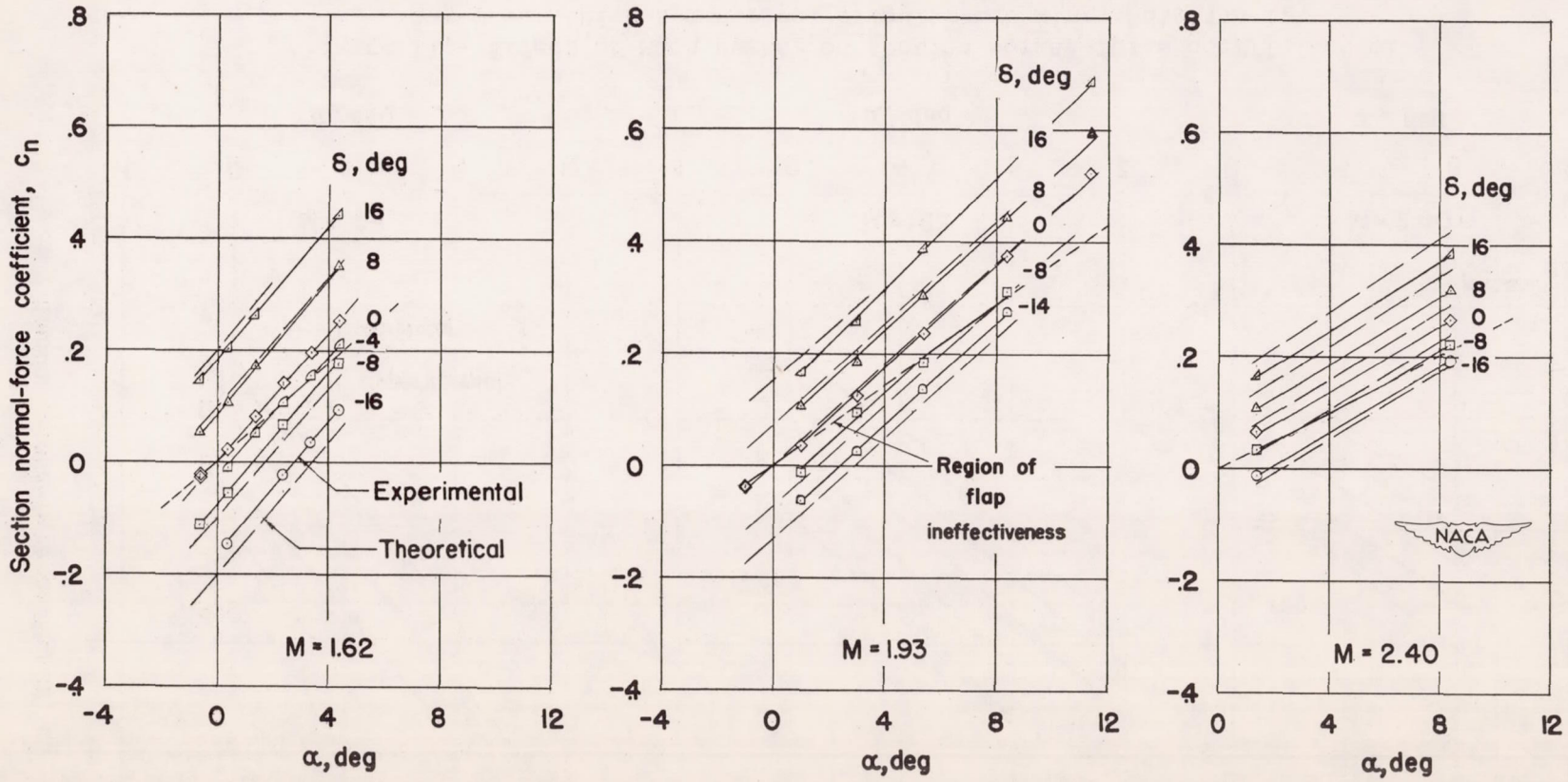

Figure 10.- Effect of Mach number on section normal-force coefficient of 9-percent-thick symmetrical circular-arc wing. Station 1.

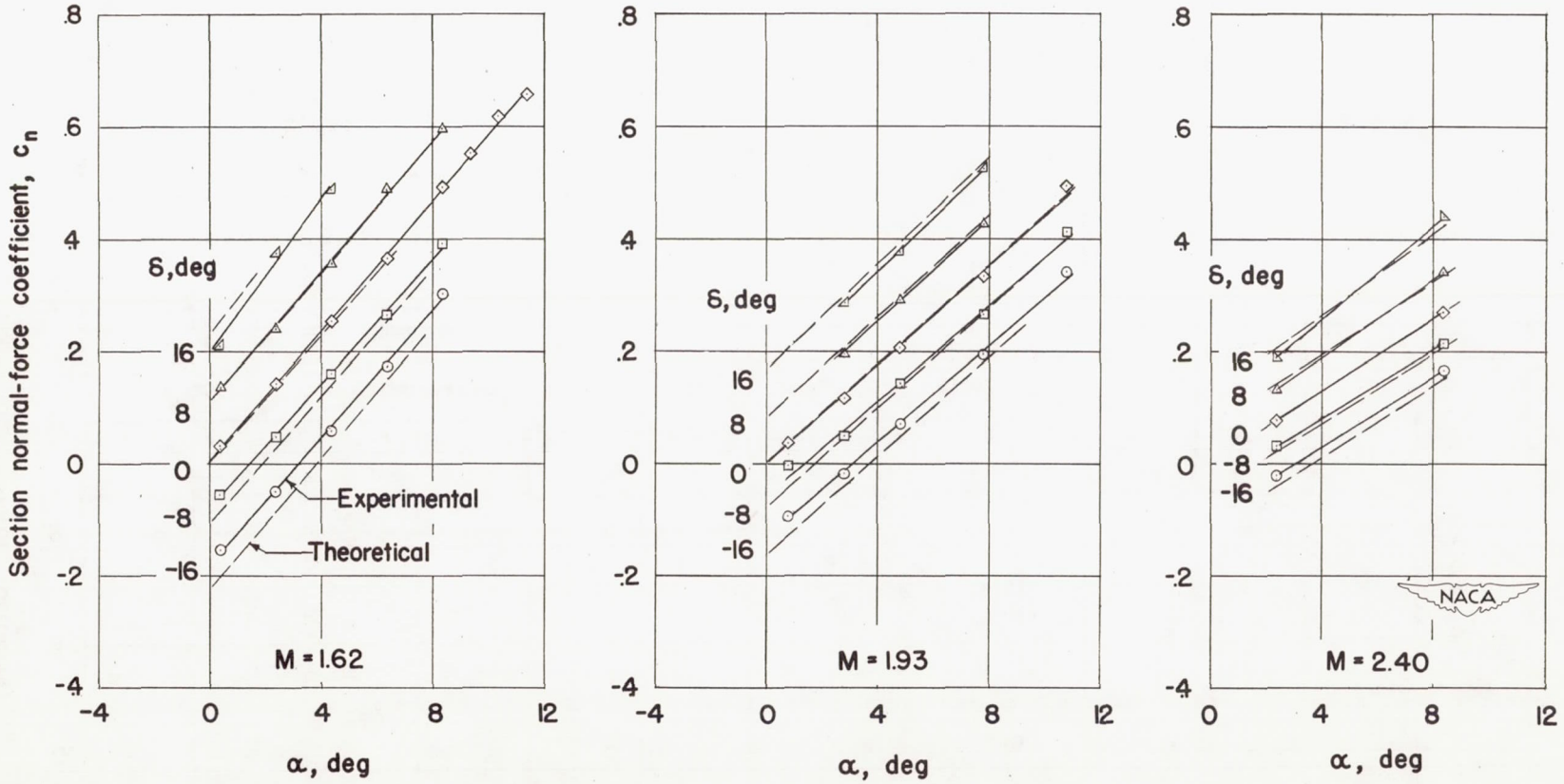

Figure 11.- Effect of Mach number on section normal-force coefficient of 6-percent-thick symmetrical circular-arc wing. Station 1.

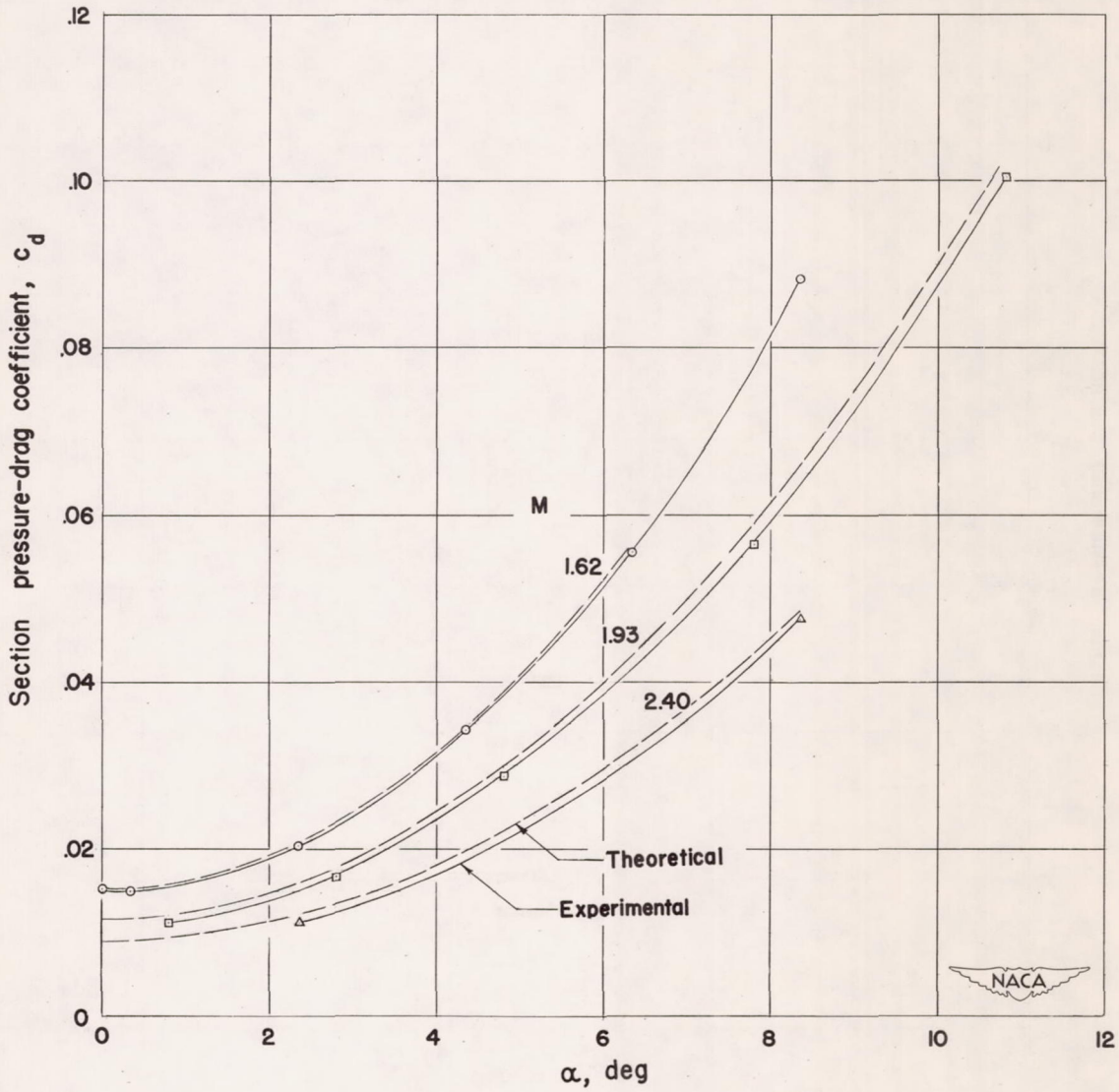

Figure 12.- Effect of Mach number on section pressure-drag coefficient of 6-percent-thick symmetrical circular-arc wing. δ, 0°. Station 1.

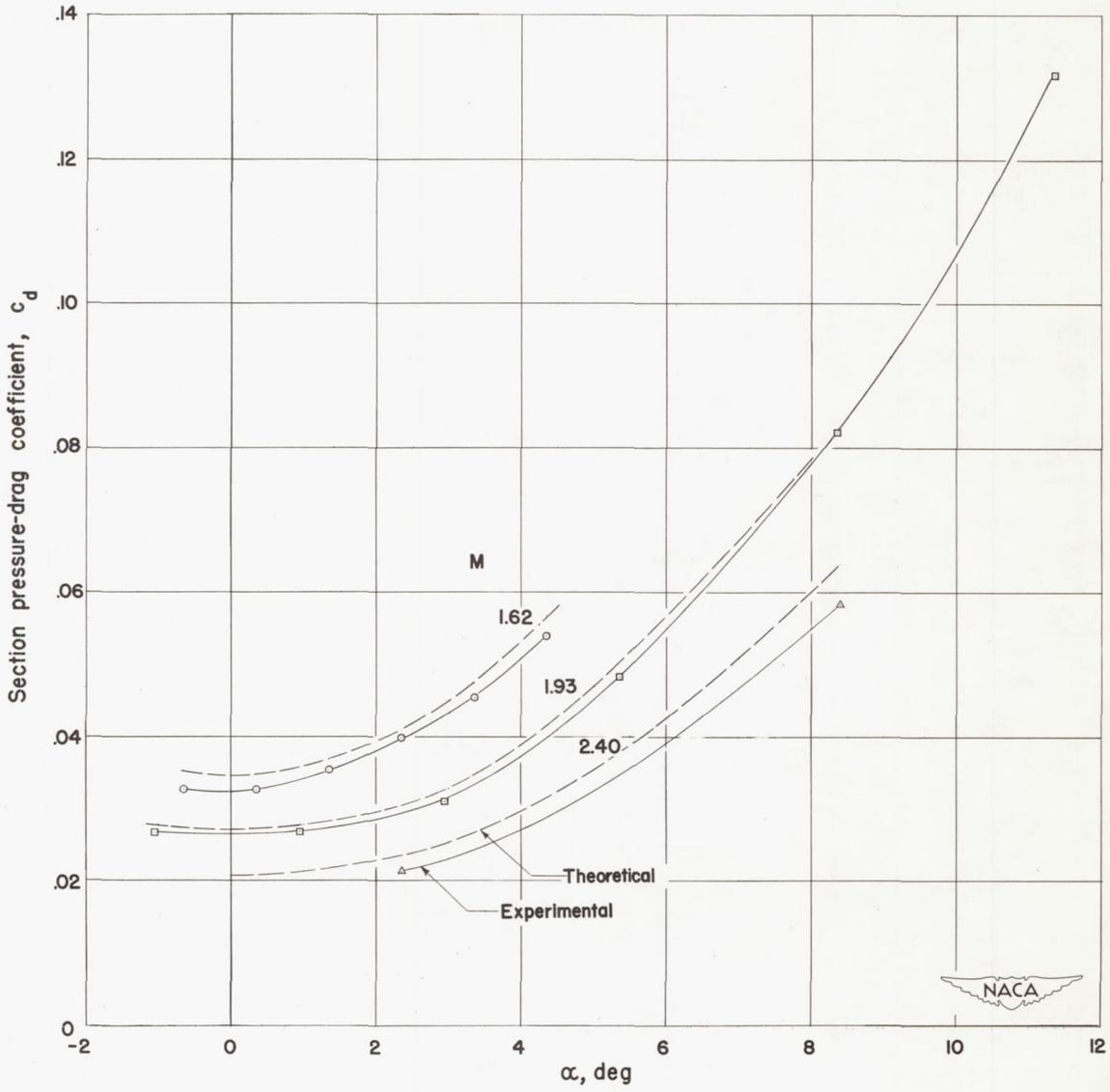

Figure 13.- Effect of Mach number on section pressure-drag coefficient of 9-percent-thick symmetrical circular-arc wing. δ, 0°. Station 1.

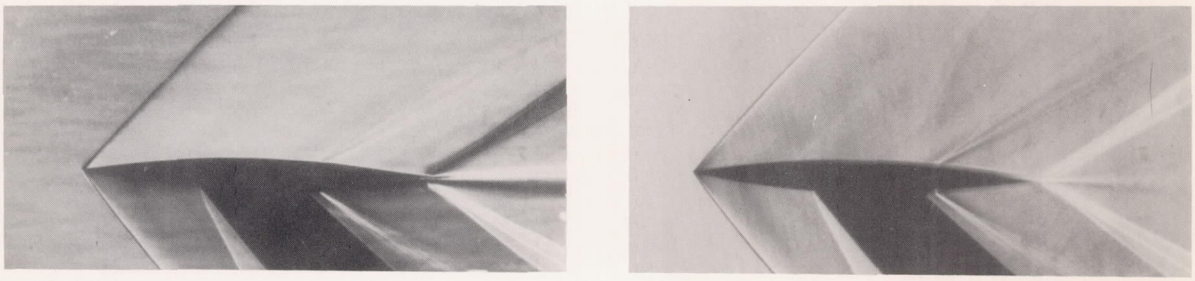

$\alpha = 1.0^{\circ}$, $\delta = 0^{\circ}$.

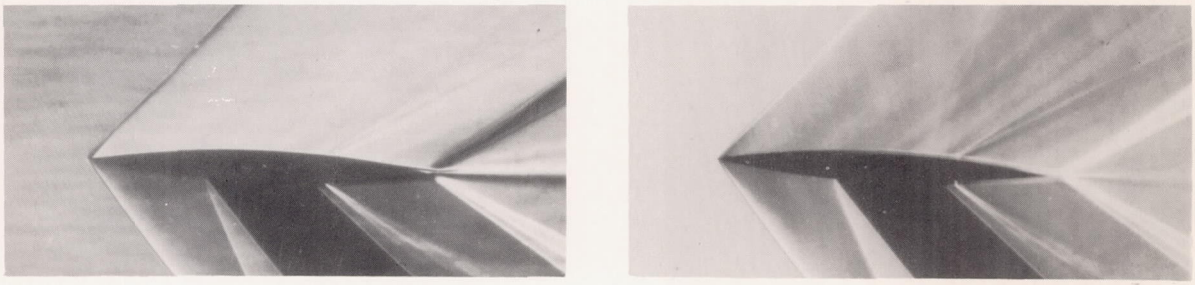

$\alpha = 3.0^{\circ}$, $\delta = 0^{\circ}$.

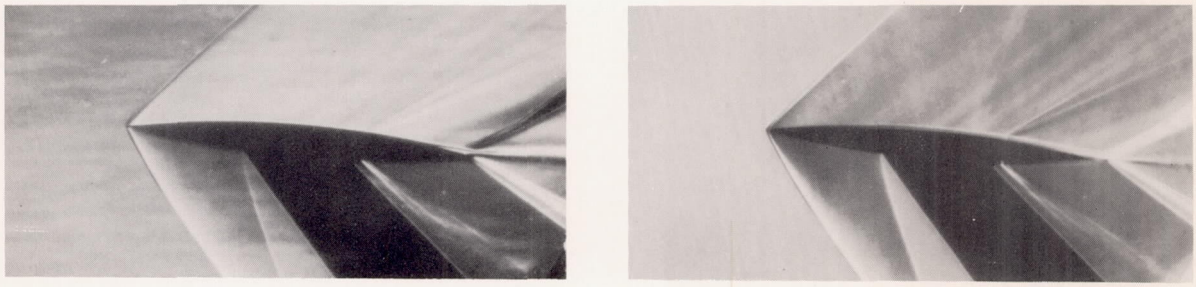

$\alpha = 5.0^{\circ}$, $\delta = 0^{\circ}$.

Horizontal knife edge. Vertical knife edge.

(a) M = 1.62.

(Schlierens)

NACA L-64949

Figure 14.- Schlieren and shadowgraph pictures of flow about 9-percent-thick symmetrical circular-arc wing at $R = 1.07 \times 10^{6}$.

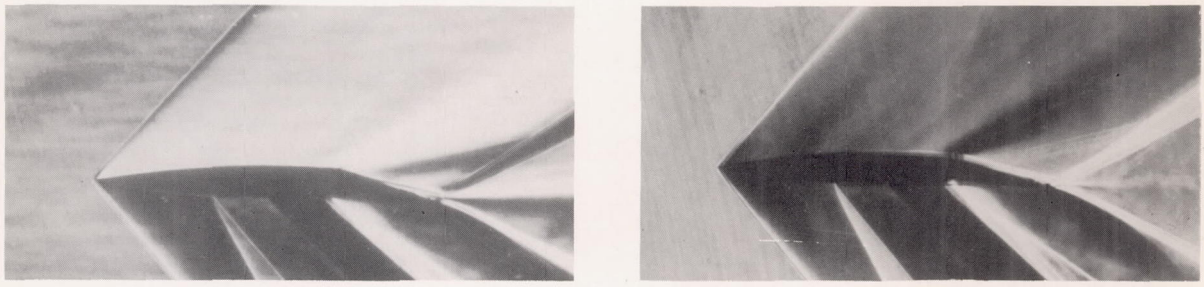

$\alpha = 1.0^{\circ}$, $\delta = 10^{\circ}$.

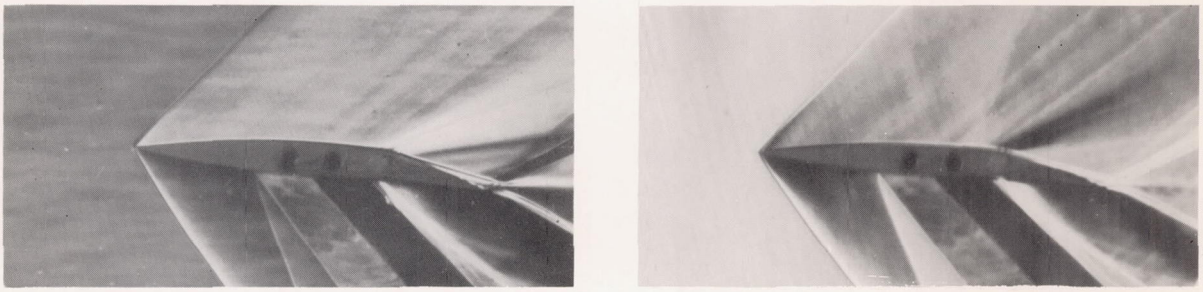

$\alpha = 4.0^{\circ}$, $\delta = 10^{\circ}$.

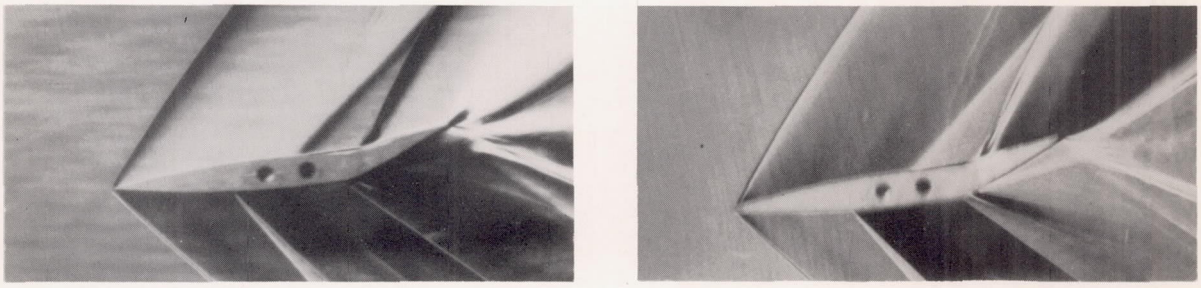

$\alpha = -5.0^{\circ}$, $\delta = -18^{\circ}$.

Horizontal knife edge. Vertical knife edge.

(a) Continued.

Figure 14.- Continued.

NACA L-64950

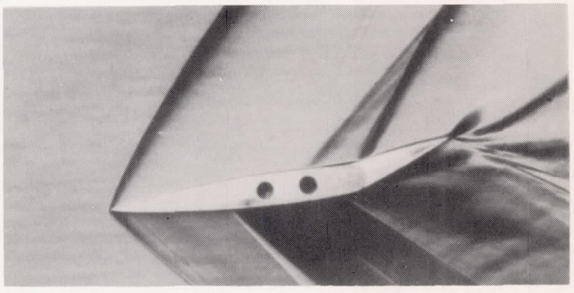

$\alpha = -6.5^{\circ}$, $\delta = -16^{\circ}$.

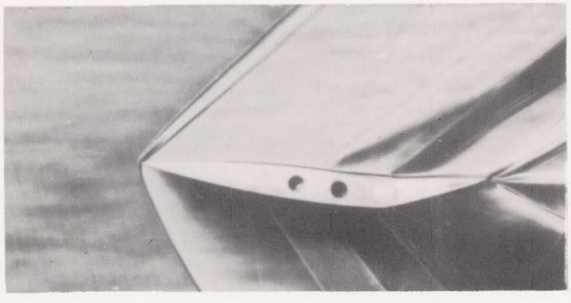

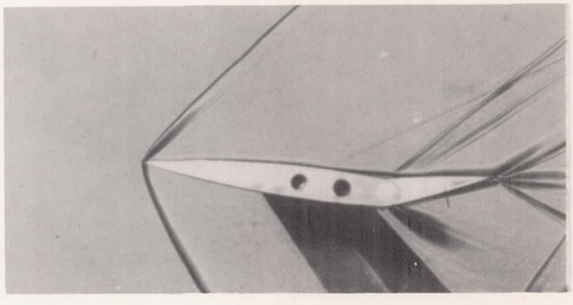

$\alpha = 8.0^{\circ}$, $\delta = -16^{\circ}$.

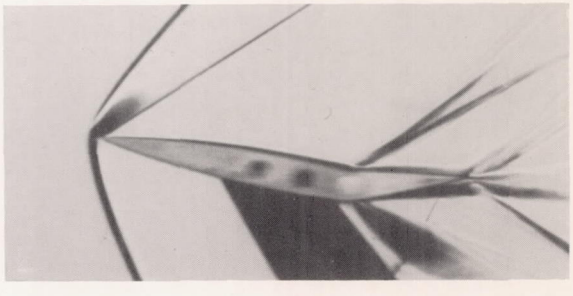

$\alpha = 10.8^{\circ}$, $\delta = -16^{\circ}$.

Horizontal knife edge. Shadowgraph.

(a) Concluded.

Figure 14.- Continued.

NACA L-64951

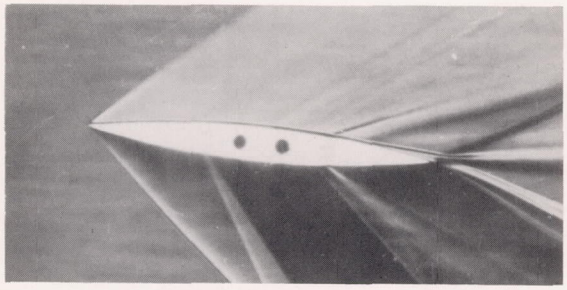
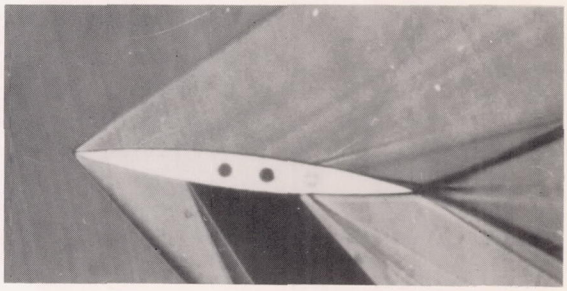

$\alpha = 6^{\circ}$, $\delta = 0^{\circ}$.

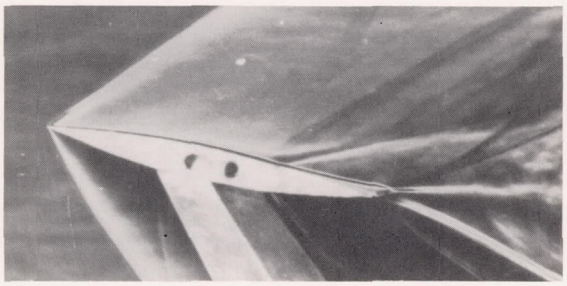
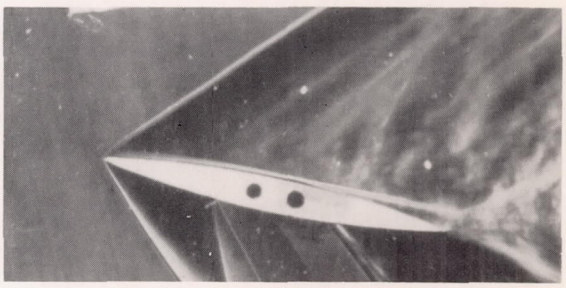

$\alpha = 12^{\circ}$, $\delta = 0^{\circ}$.


$\alpha = -12^{\circ}$, $\delta = 0^{\circ}$.

Horizontal knife edge. Vertical knife edge.

(b) M = 1.93.

(Schlierens)

Figure 14.- Continued.

NACA L-64952

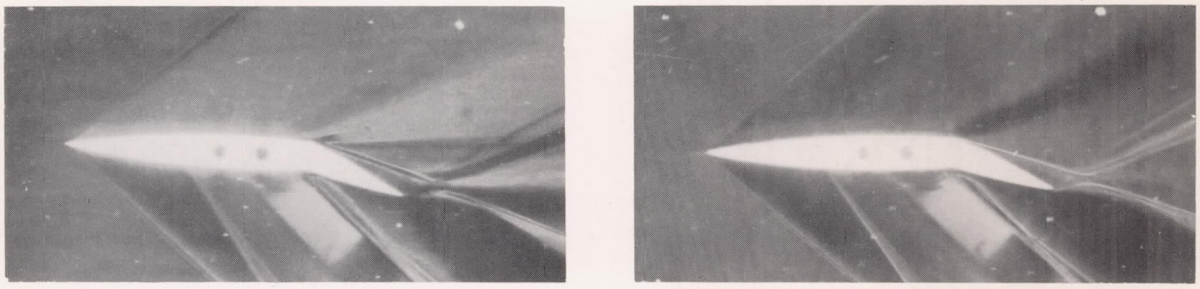

$\alpha = 2^{\circ}$, $\delta = 20^{\circ}$.

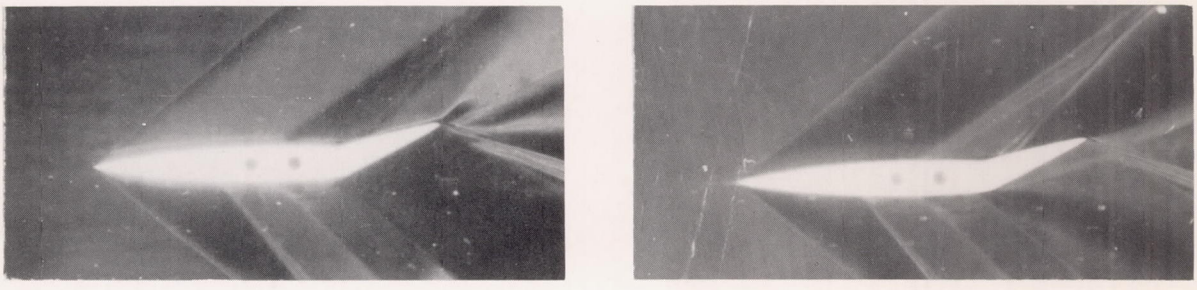

$\alpha = -2^{\circ}$, $\delta = -20^{\circ}$.

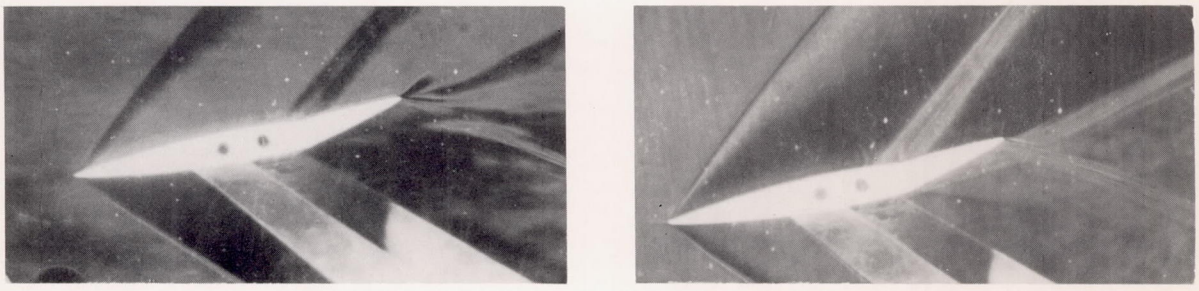

$\alpha = -12^{\circ}$, $\delta = -10^{\circ}$.

Horizontal knife edge. Vertical knife edge.

(b) Concluded.

Figure 14.- Continued.

NACA L- 64953

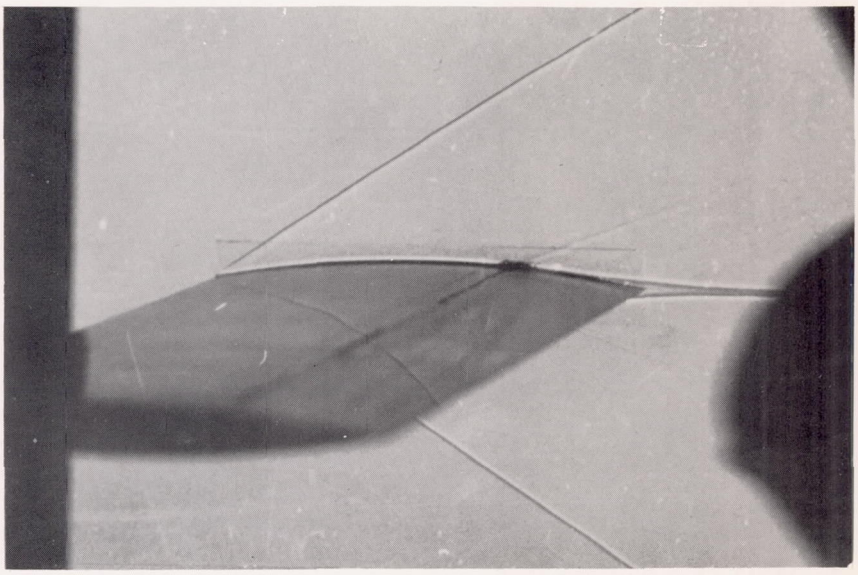

$\alpha = 0^{\circ}$, $\delta = 0^{\circ}$.

(Rear three-quarter view)

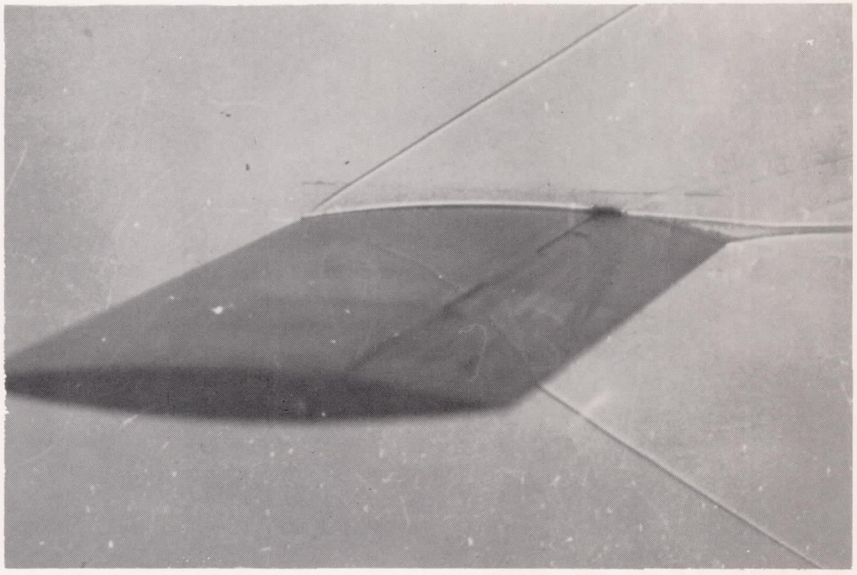

$\alpha = 4^{\circ}$, $\delta = 0^{\circ}$.

(Rear three-quarter view)

(c) M = 2.40.

(Shadowgraphs)

Figure 14.- Continued. NACA L-64954

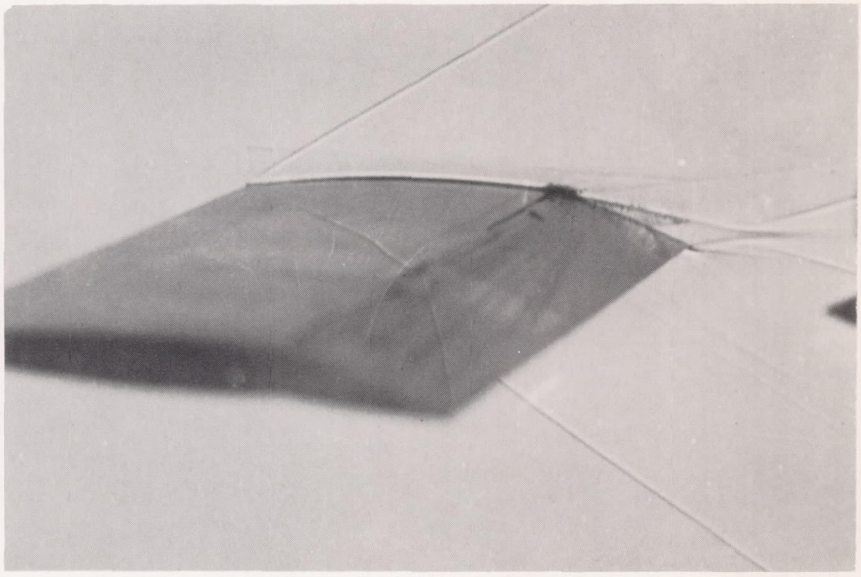

$\alpha = 4^{\circ}$, $\delta = 10^{\circ}$.

(Rear three-quarter view)

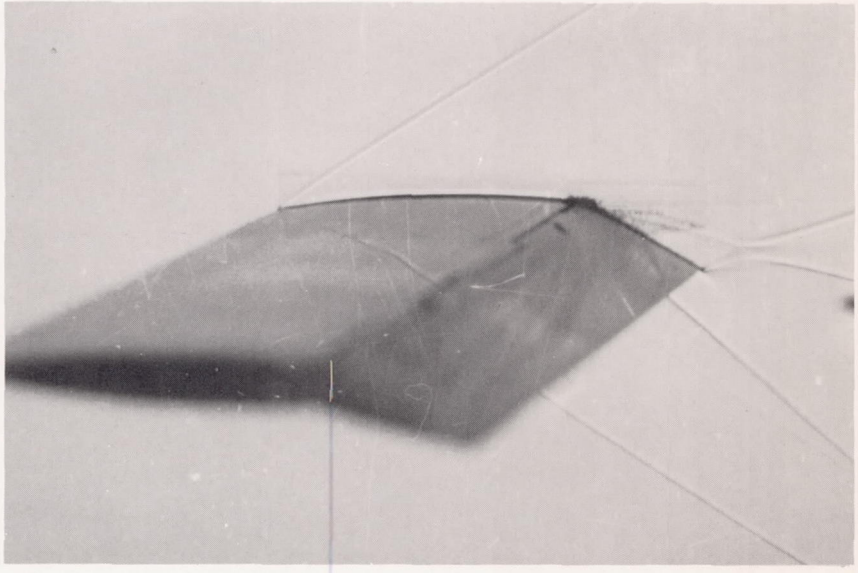

$\alpha = 4^{\circ}$, $\delta = 19^{\circ}$.

(Rear three-quarter view)

(c) Continued.

Figure 14.- Continued.

NACA L-64955

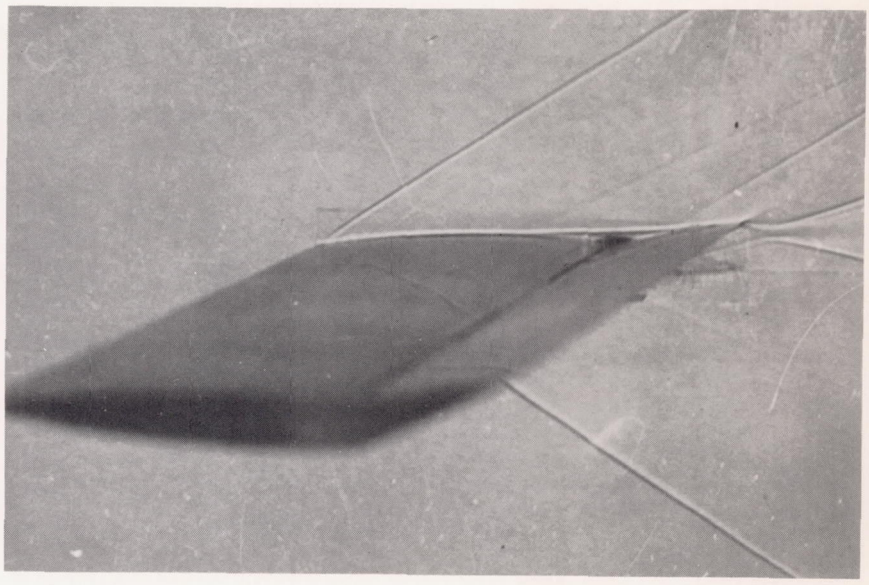

$\alpha = 4^{\circ}$, $\delta = -19^{\circ}$.

(Rear three-quarter view)

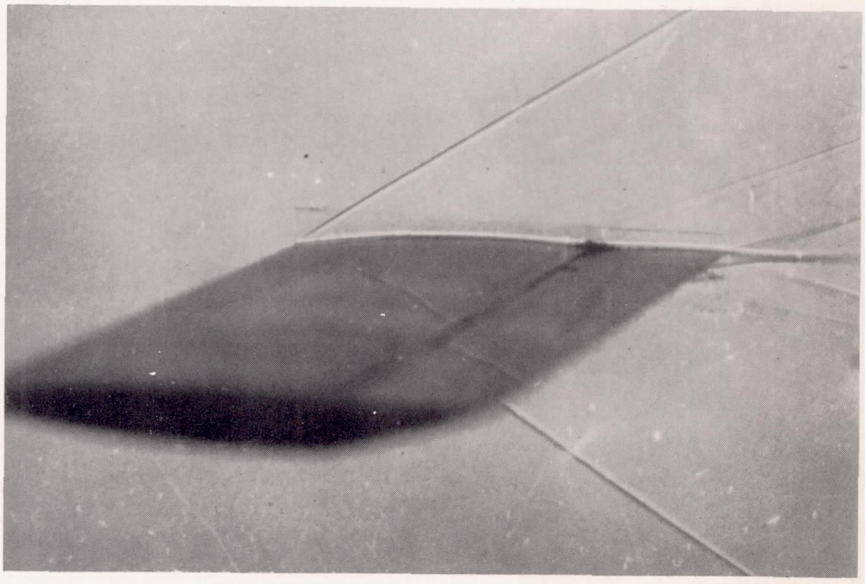

$\alpha = 4^{\circ}$, $\delta = -10^{\circ}$.

(Rear three-quarter view)

(c) Concluded.

Figure 14.- Concluded. NACA L-64956

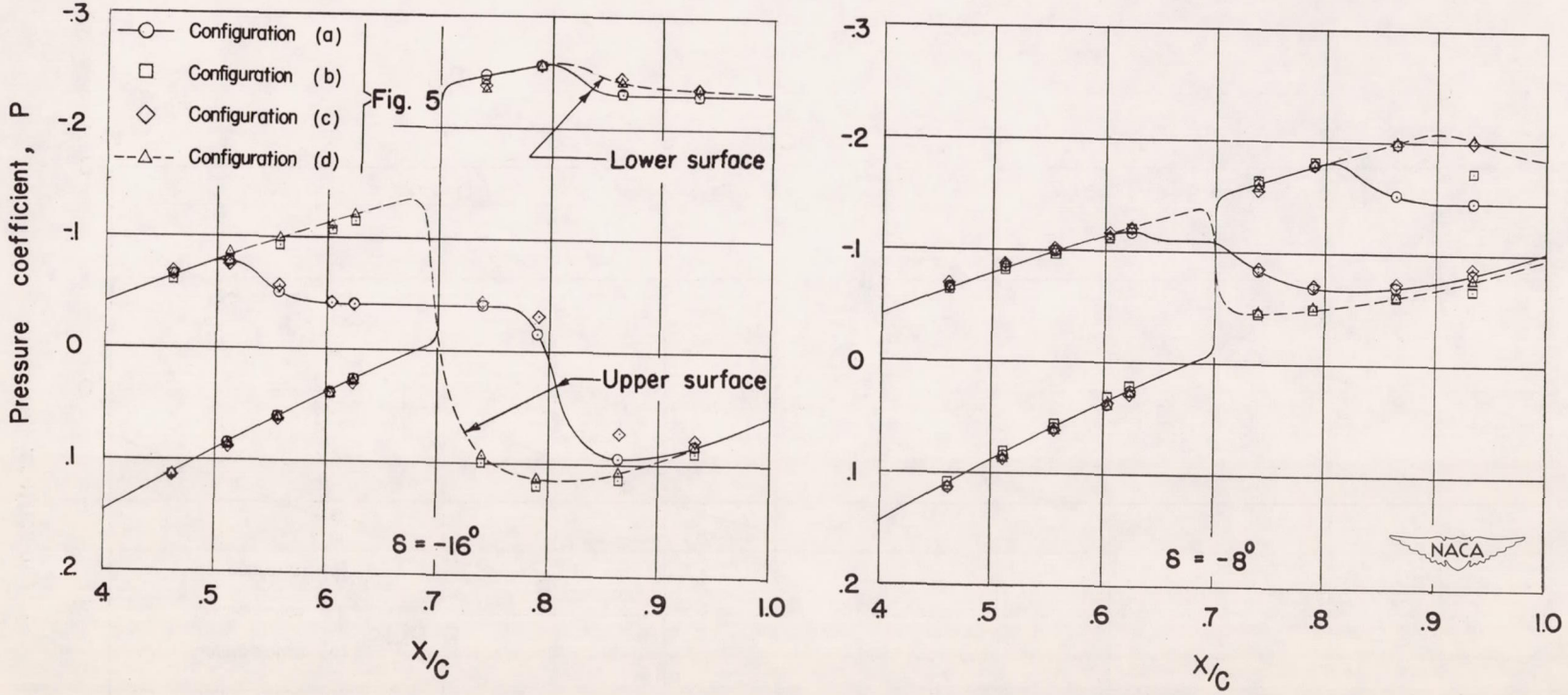

Figure 15.- Effect on pressure distributions of fixing transition near leading edge over 9-percent-thick symmetrical circular-arc wing at M = 1.93. α, 4.00°. Station 1.

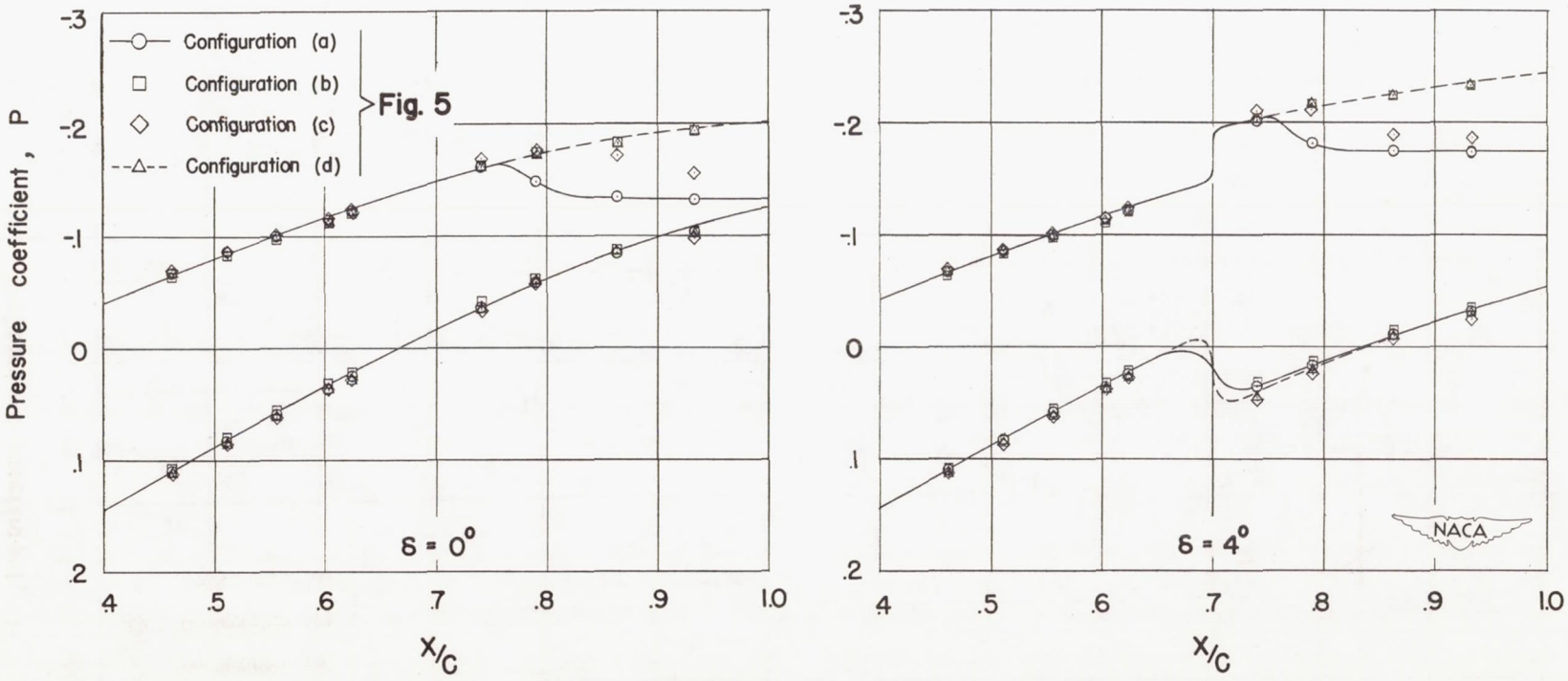

Figure 15.- Continued.

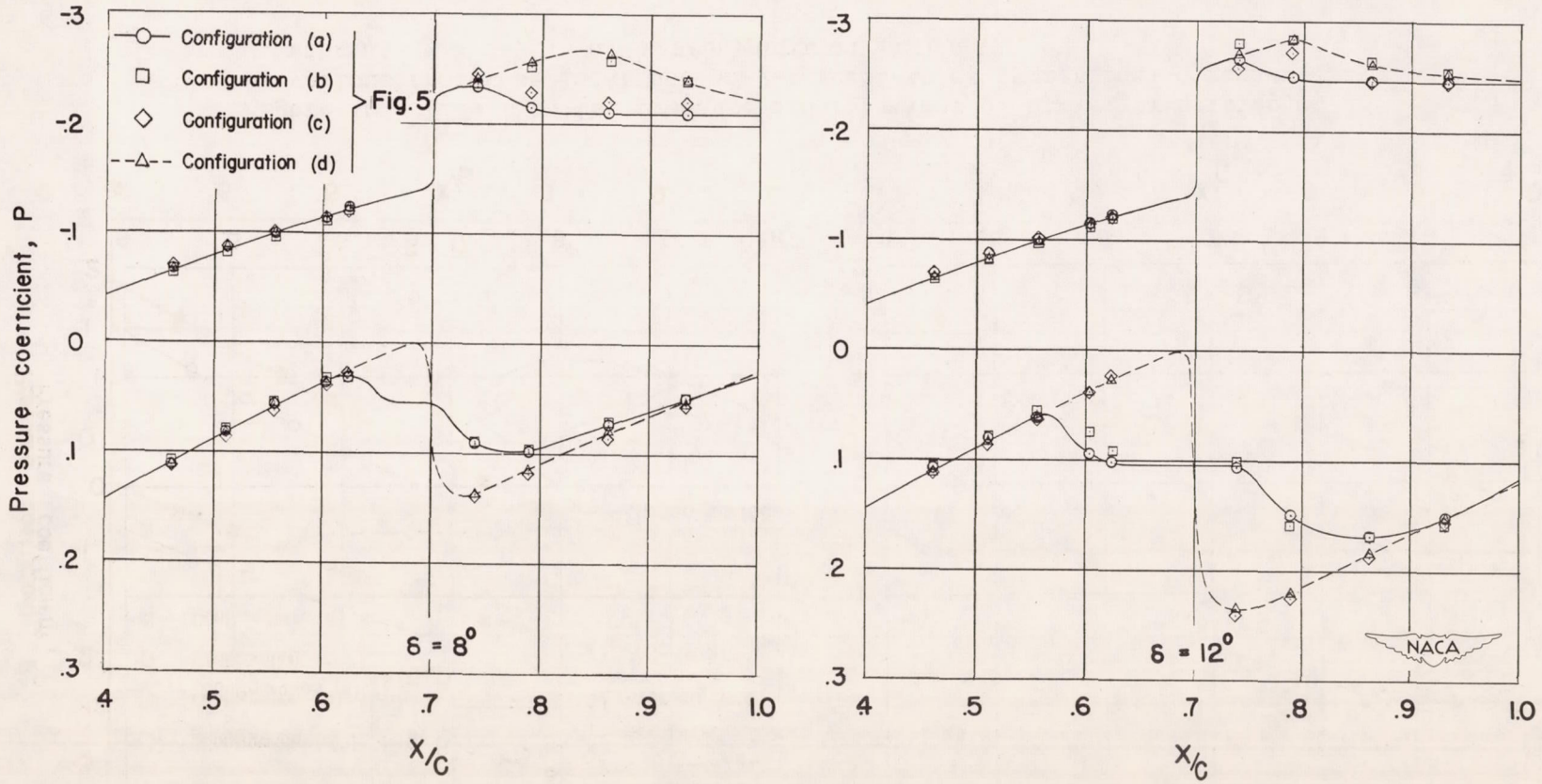

Figure 15.- Concluded.

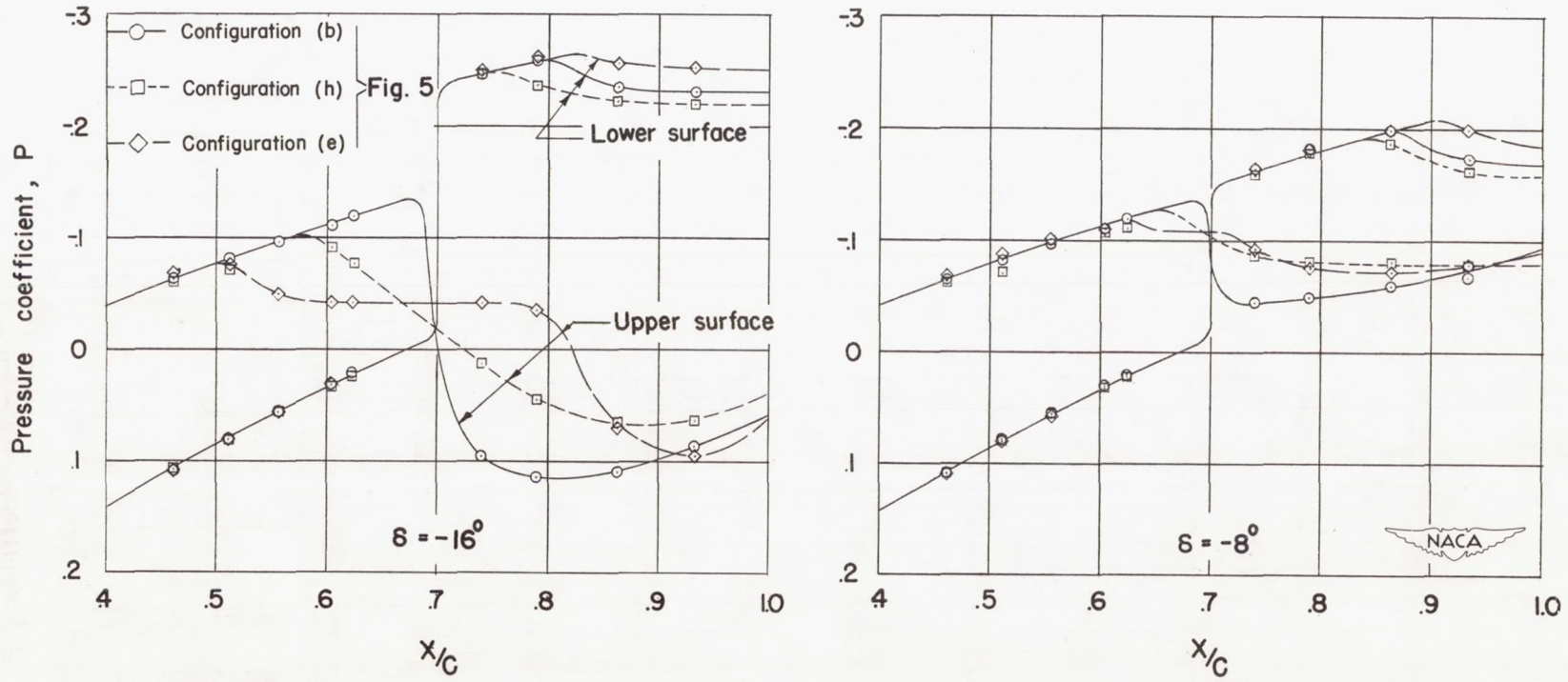

Figure 16.- Effect on the pressure distributions of fixing transition at various chordwise locations on 9-percent-thick symmetrical circular-arc wing at M = 1.93. α, 4.00°. Station 1.

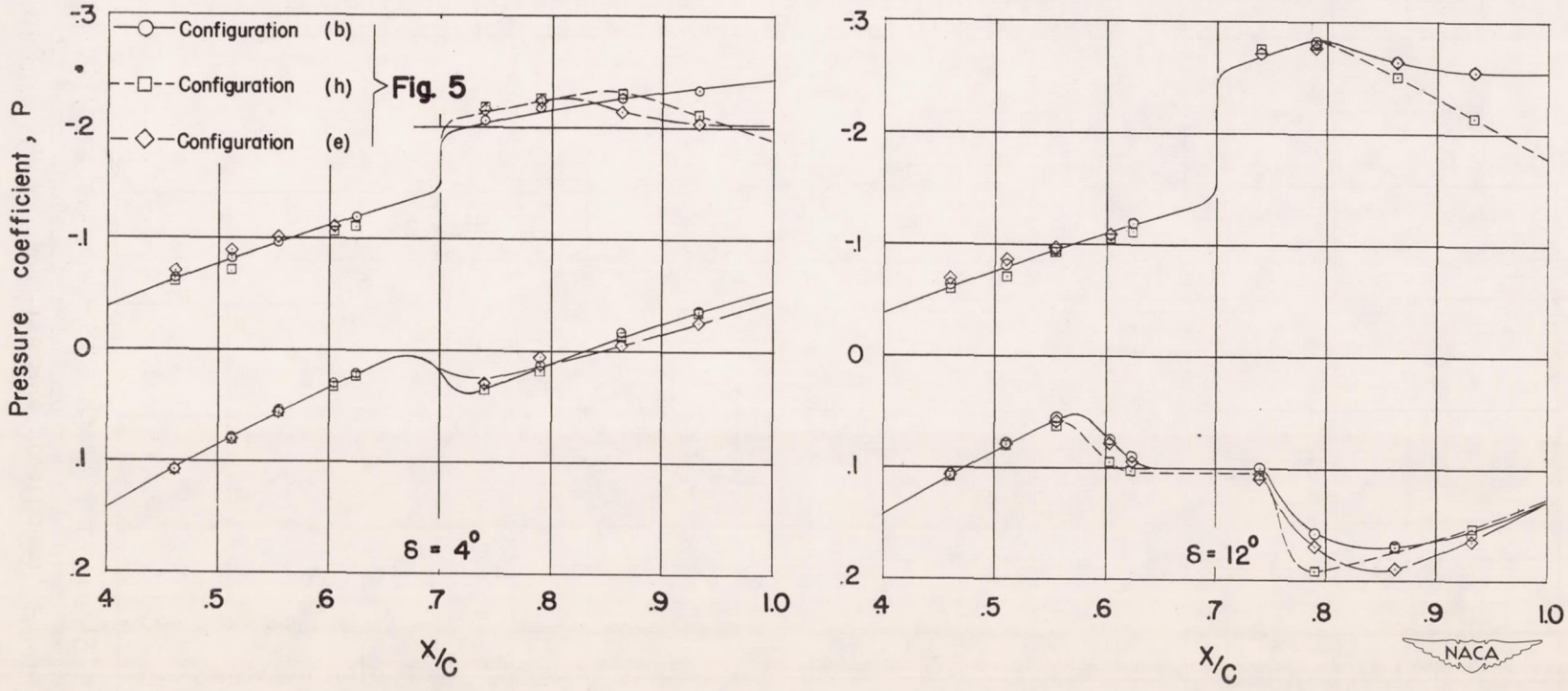

Figure 16.- Concluded.

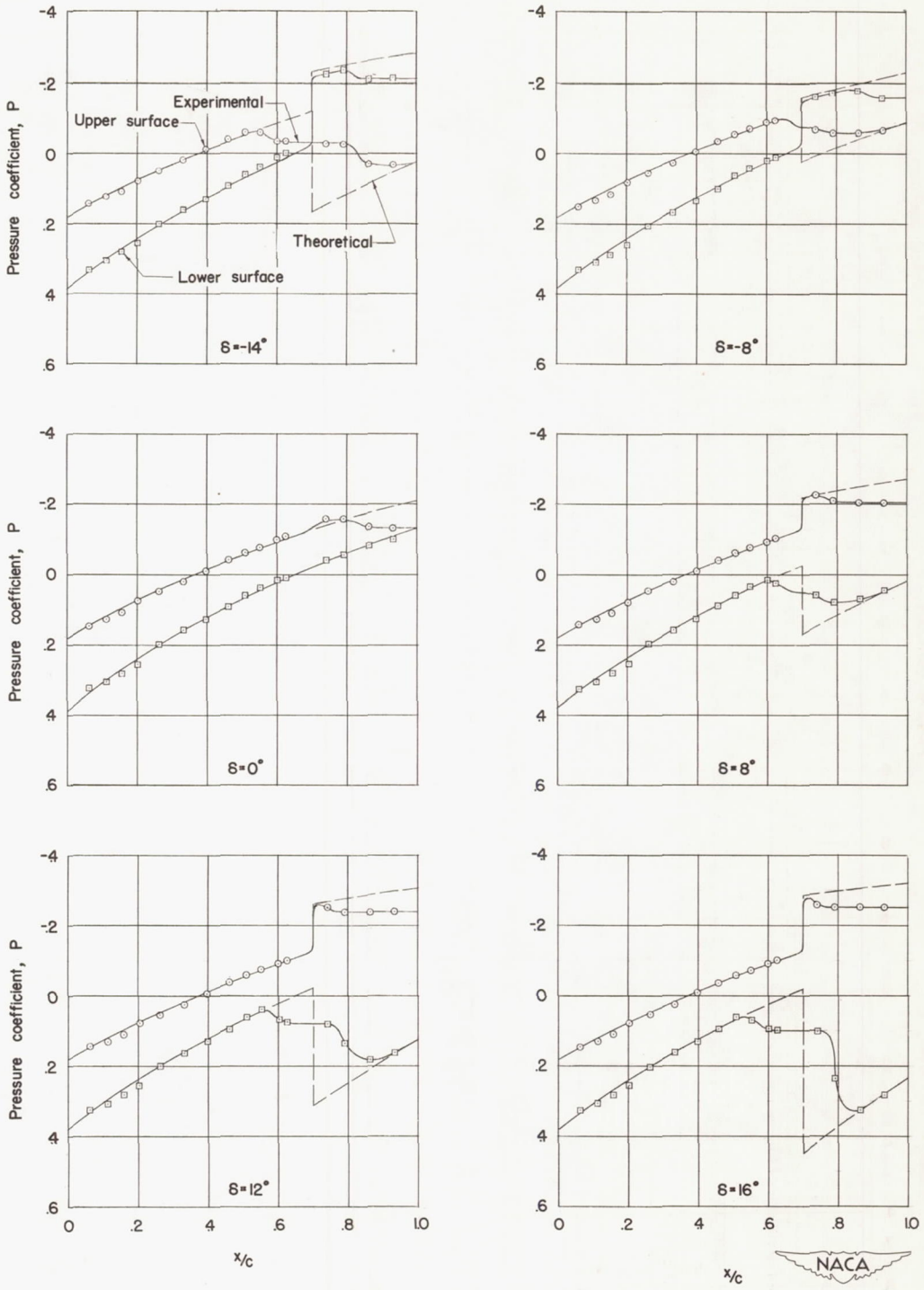

(a) Smooth model, $\alpha = 2.95^{\circ}$.

Figure 17.- Effect of fixing transion on the agreement between the theoretical and experimental pressure distributions over the 9-percent-thick symmetrical circular-arc wing at M = 1.93. Station 1.

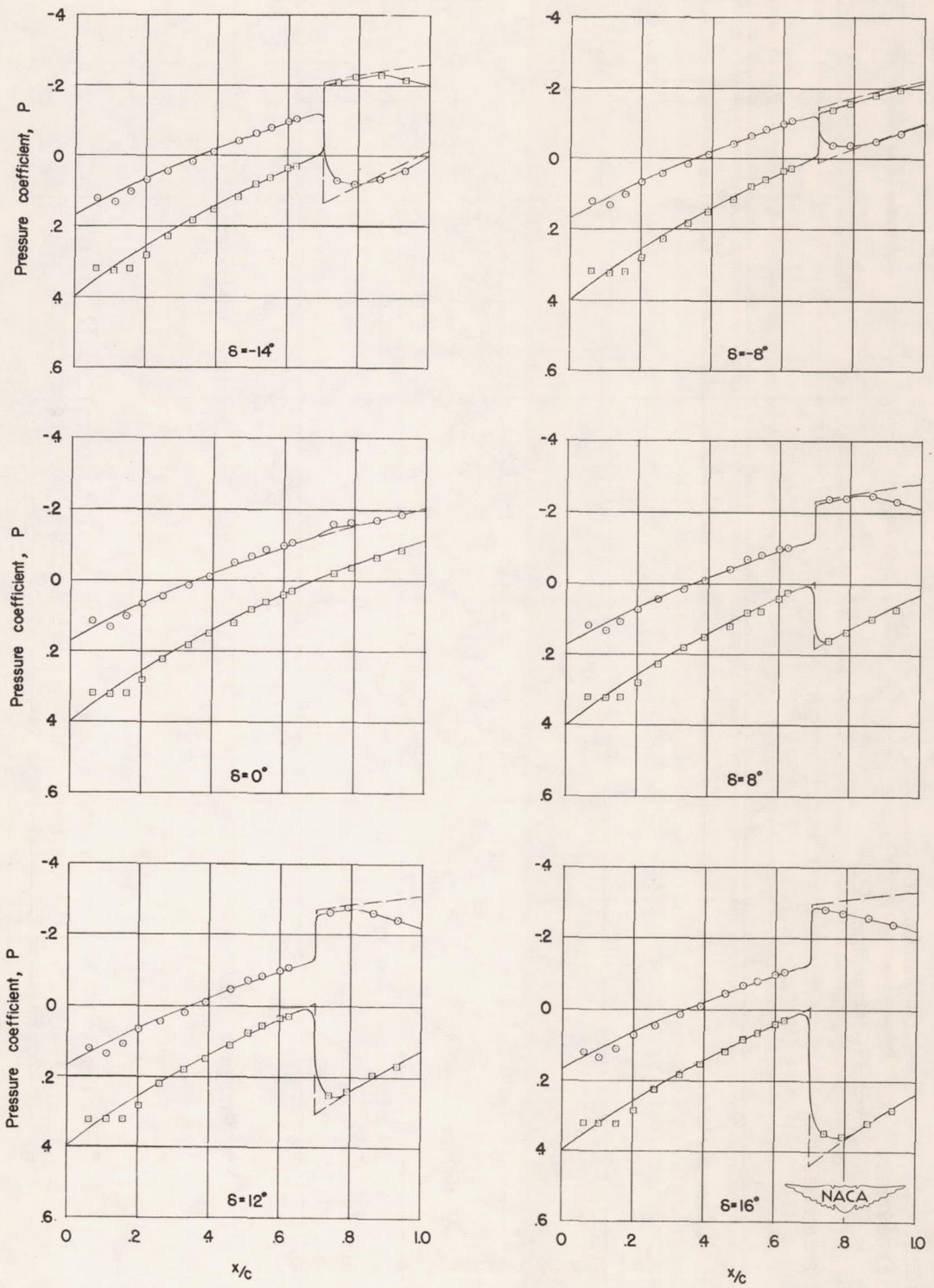

(b) Transition fixed, $\alpha = 3.35^{\circ}$

Figure 17.- Concluded.

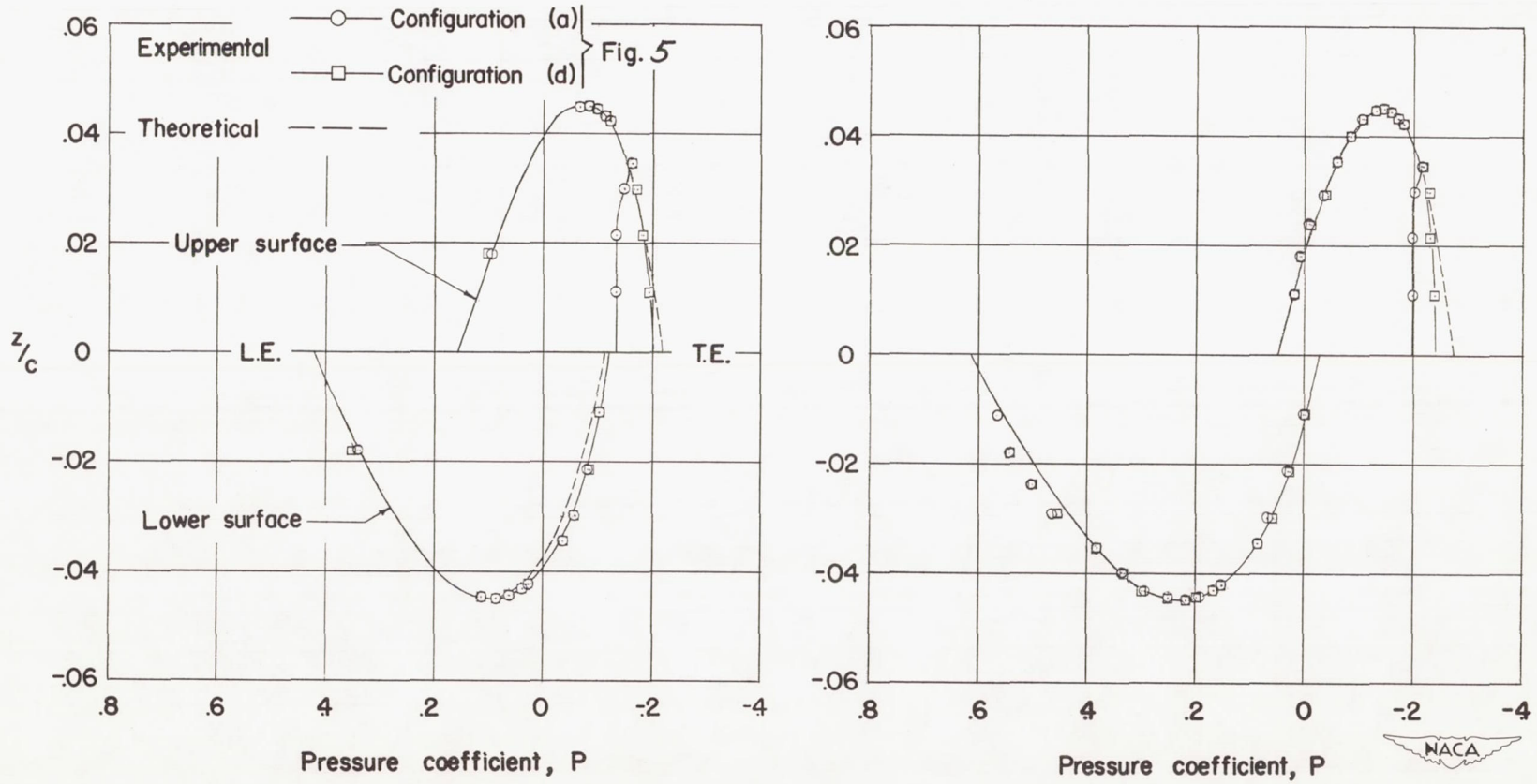

(a) $\alpha = 4.00^{\circ}$.

(b) $\alpha = 8.35^{\circ}$.

Figure 18.- Effect on the pressure distribution (parallel to chord) of fixing transition near leading edge on the 9-percent-thick symmetrical circular-arc wing at M = 1.93. δ, 0°. Station 1.

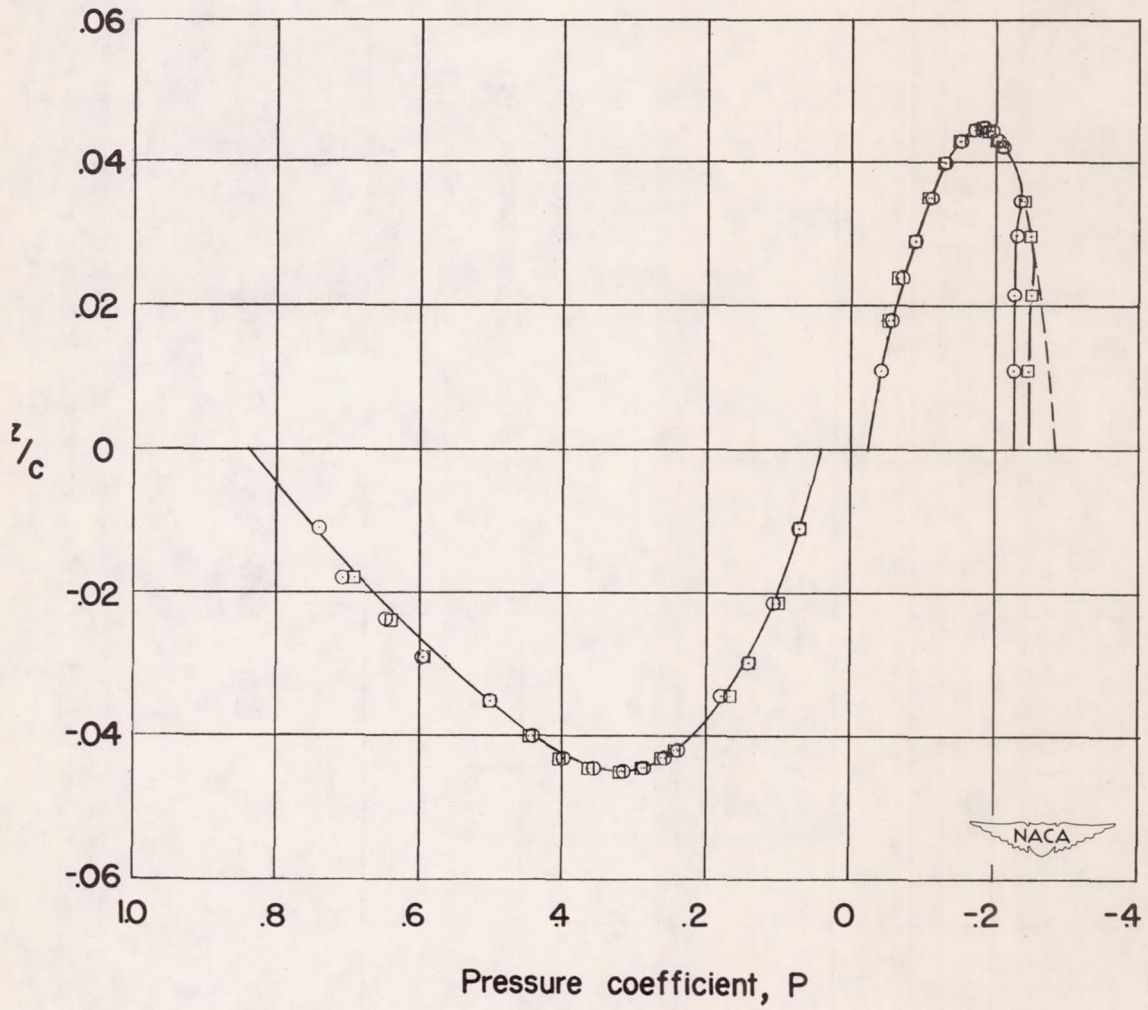

(c) $\alpha = 11.35^{\circ}$.

Figure 18.- Concluded.

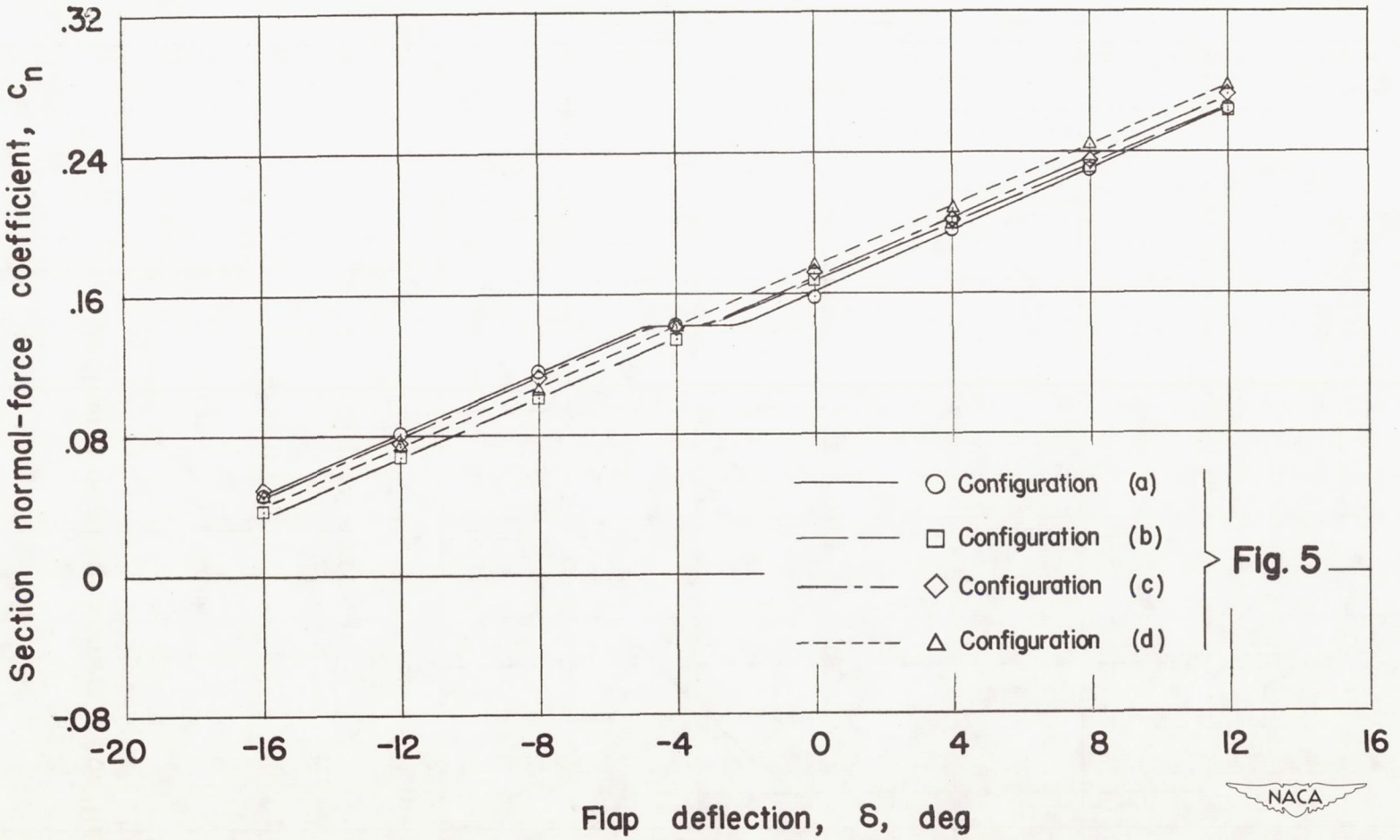

(a) Normal force.

Figure 19.- Effect of fixing transition near leading edge on the section force and moment characteristics of 9-percent-thick symmetrical circular-arc wing at $M = 1.93$. α, 4.00°. Station 1.

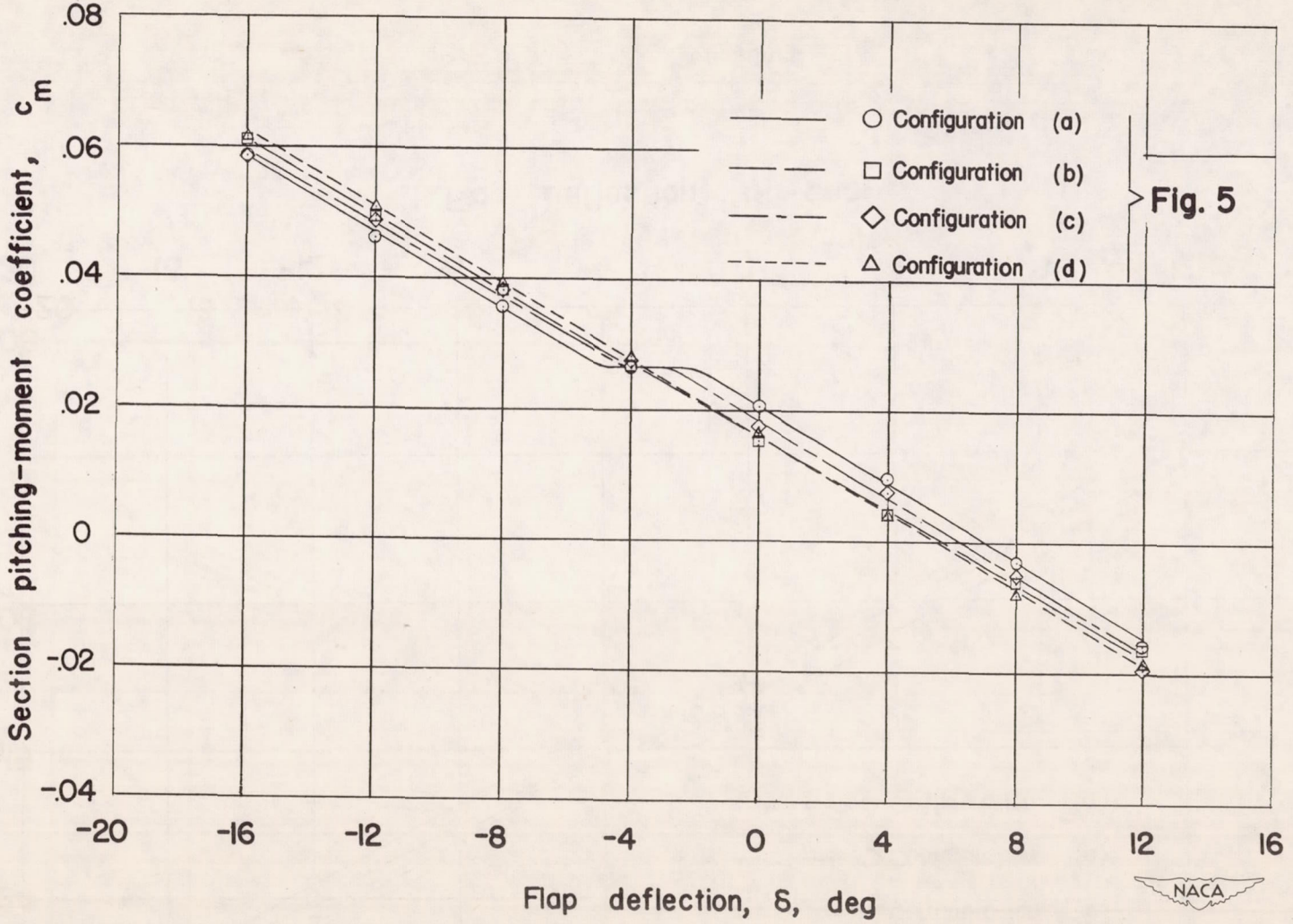

(b) Pitching moment.

Figure 19.- Continued.

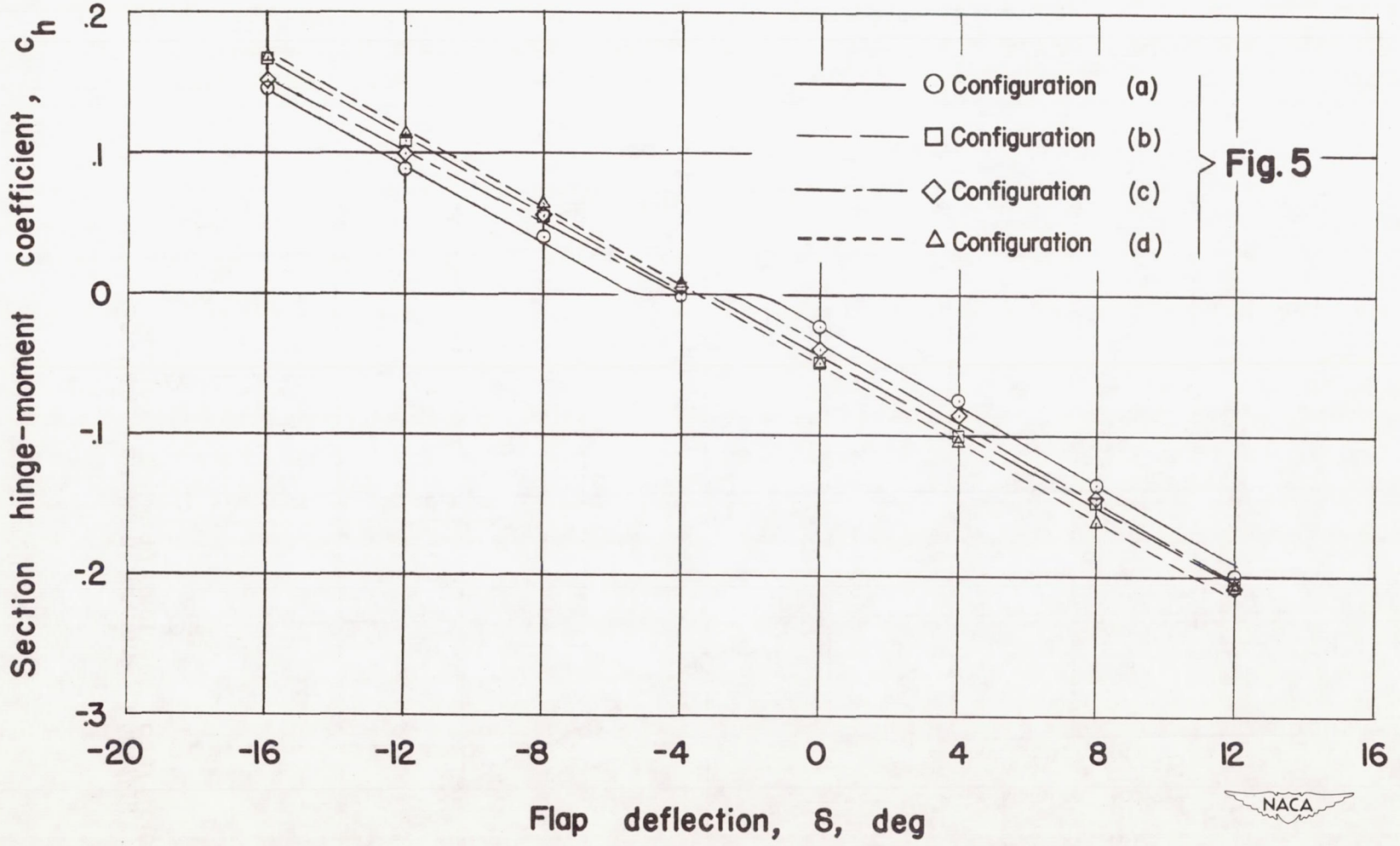

(c) Hinge moment.

Figure 19.- Concluded.

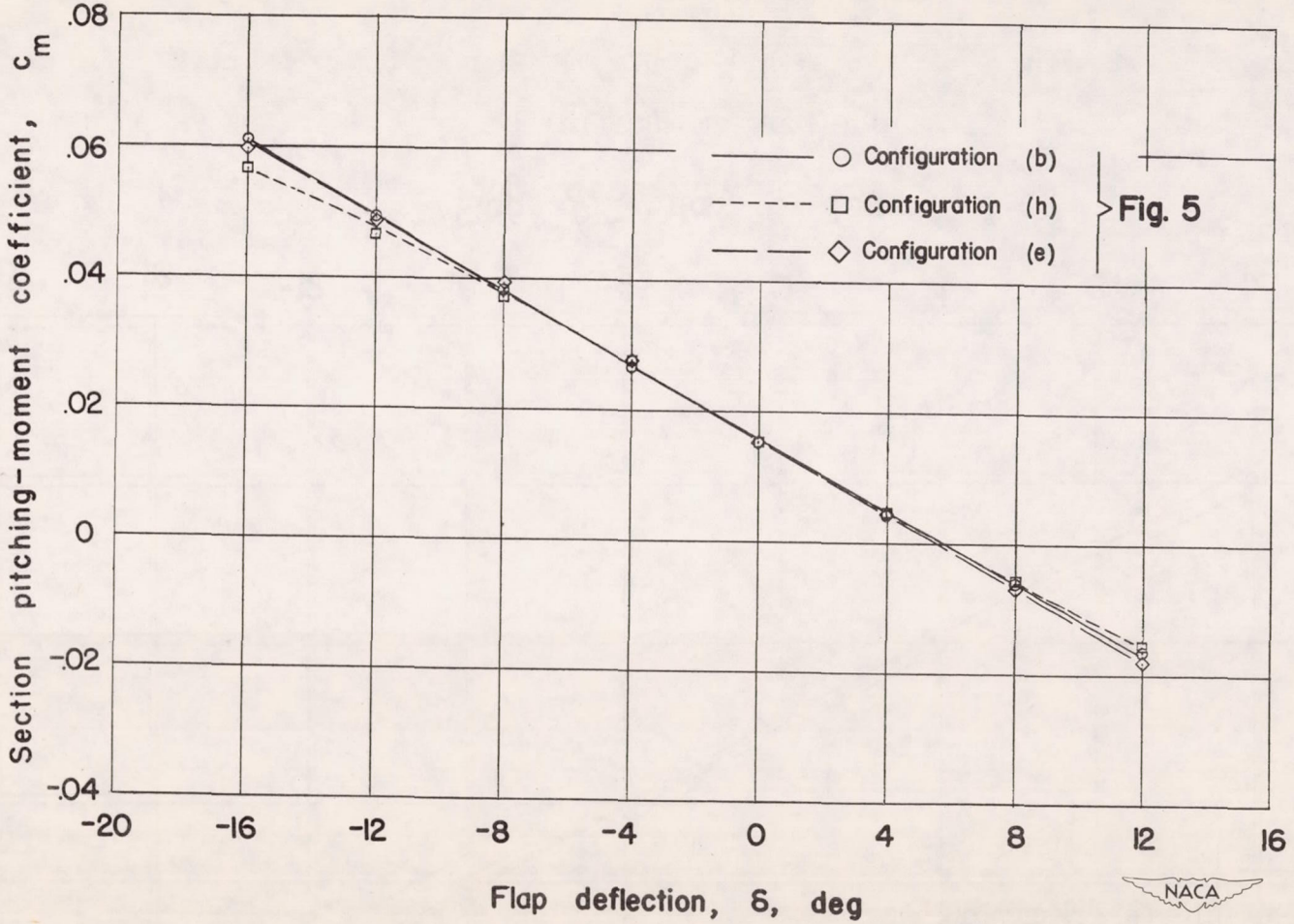

(a) Pitching moment.

Figure 20.- Effect of fixing transition at various chordwise locations on the section moment characteristics of 9-percent-thick symmetrical circular-arc wing at M = 1.93. α, 4.00°. Station 1.

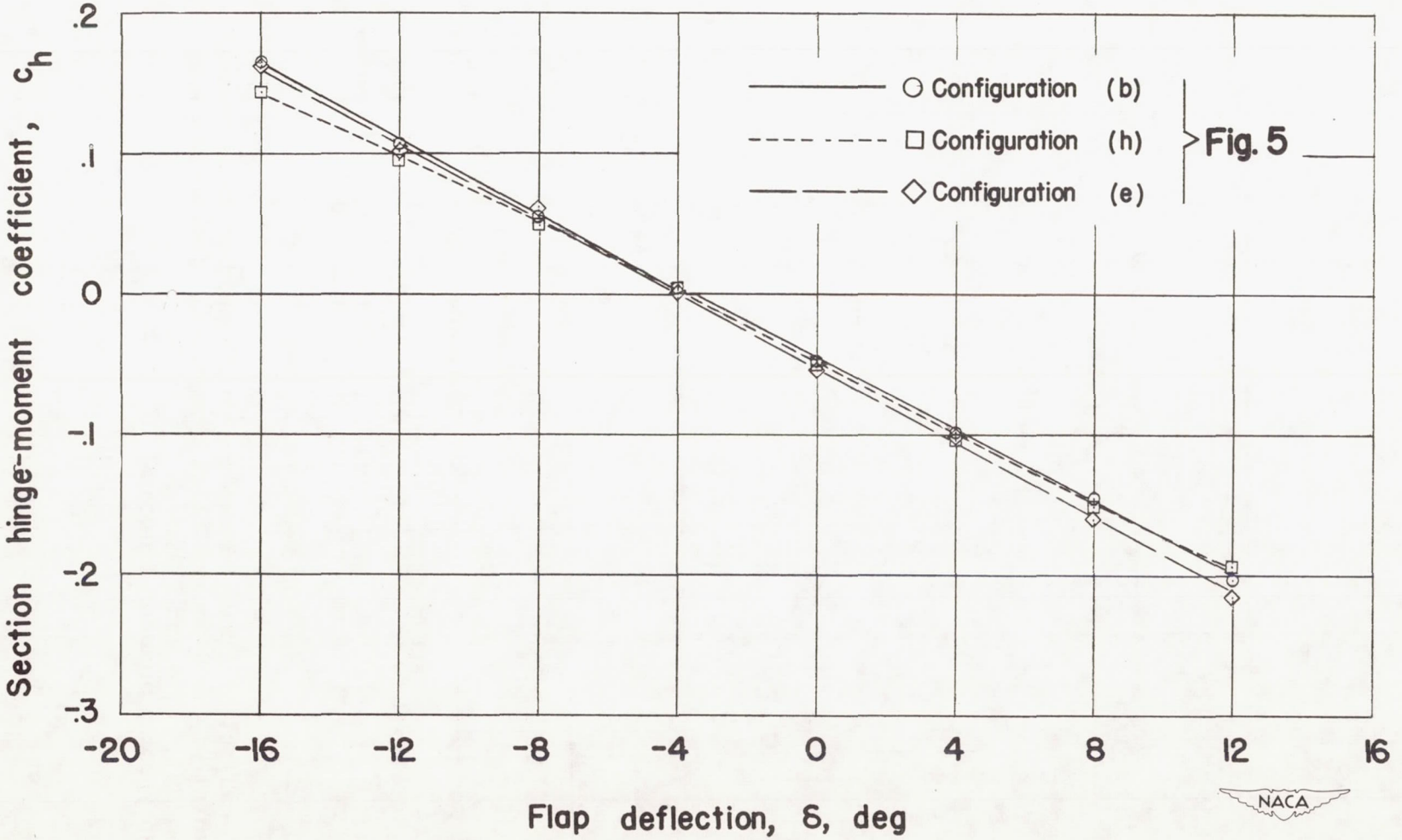

(b) Hinge moment.

Figure 20.- Concluded.

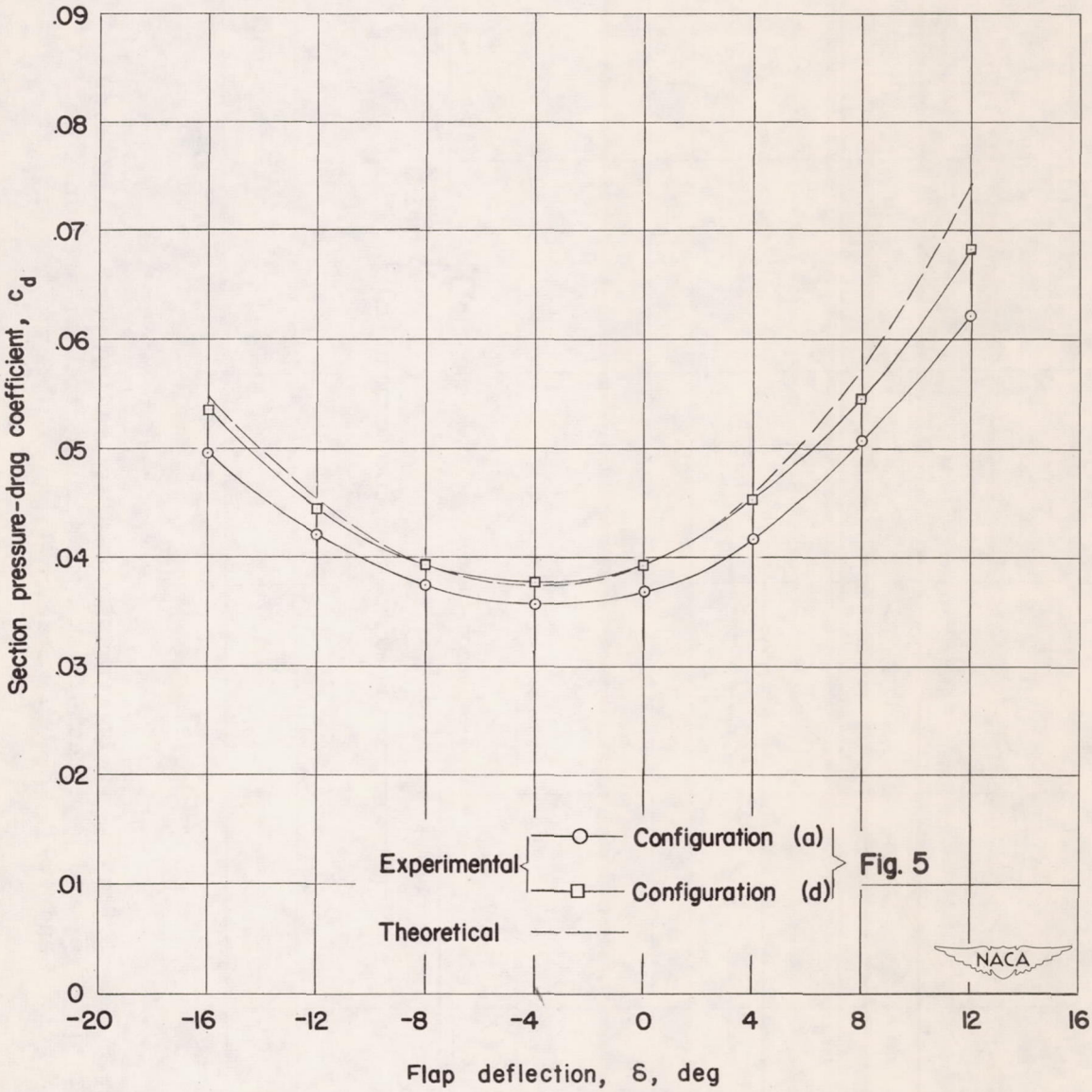

Figure 21.- Effect of fixing transition on the section pressure-drag coefficient of the 9-percent-thick symmetrical circular-arc wing at M = 1.93. α, 4.00°. Station 1.

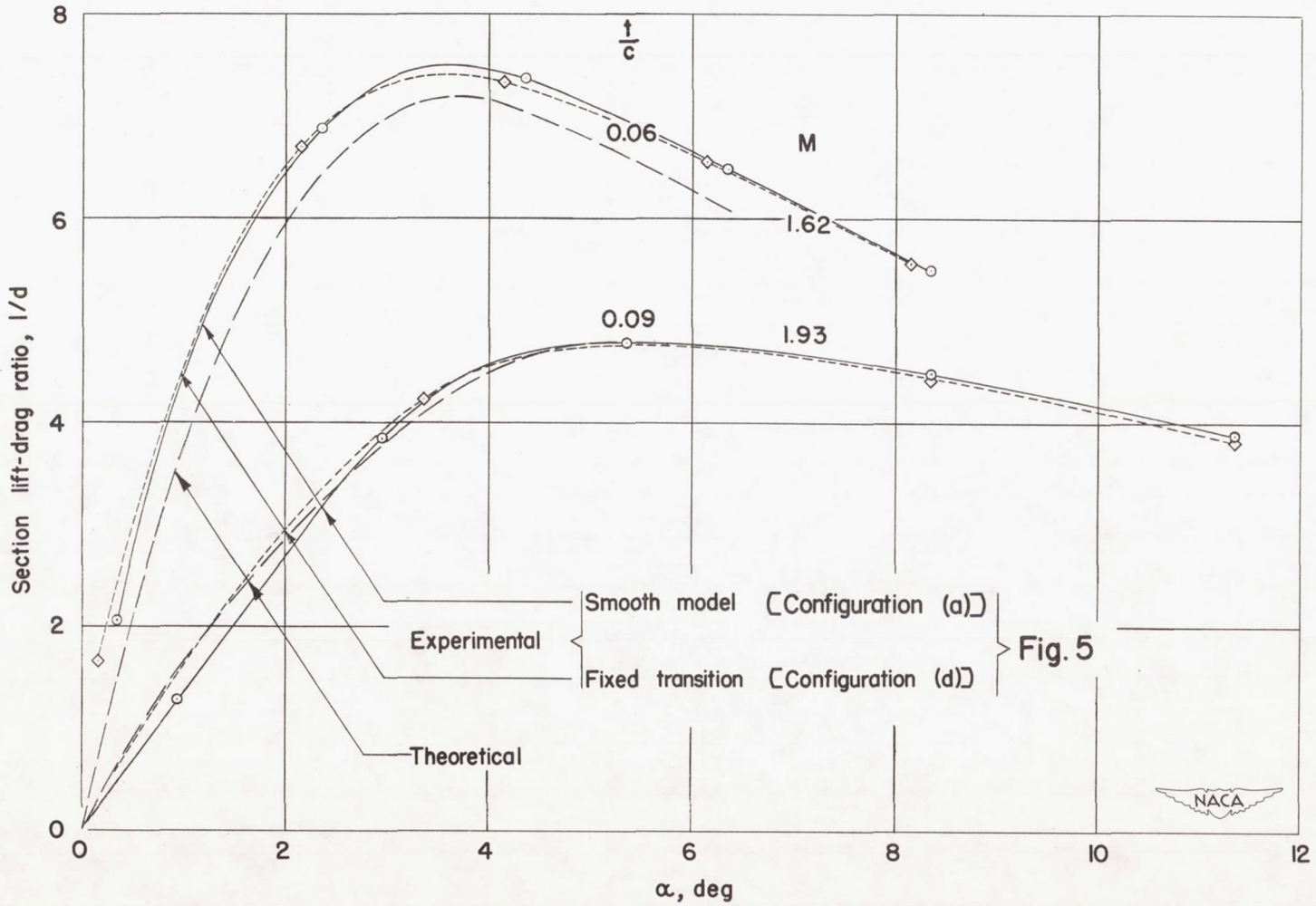

Figure 22.- Effect of fixing transition near leading edge on lift-drag ratio of 6- and 9-percent-thick symmetrical circular-arc wings at M = 1.62 and 1.93. δ, 0°. Station 1.

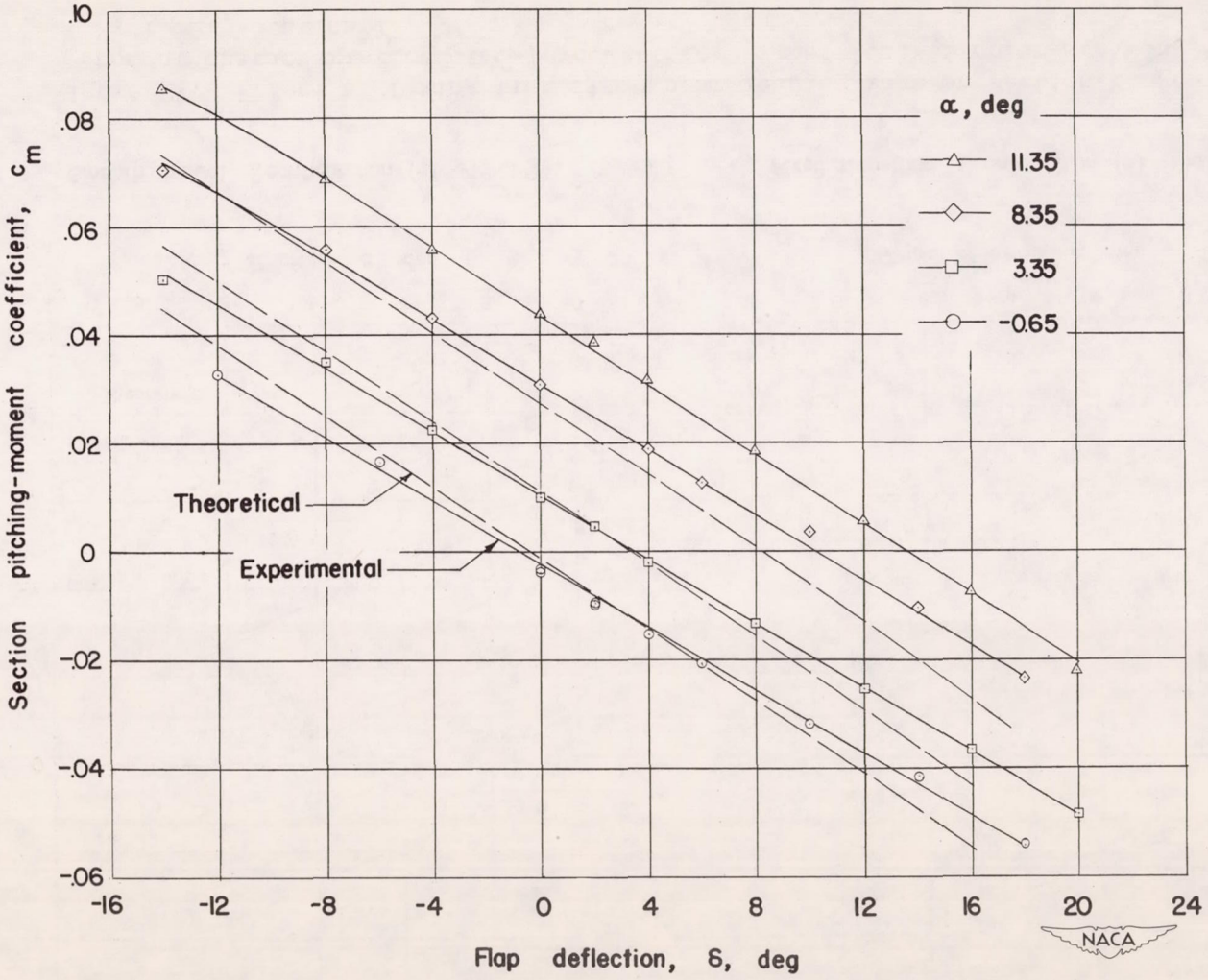

Figure 23.- Section pitching-moment characteristics of 9-percent-thick symmetrical circular-arc wing with fixed transition. Configuration (d), figure 5. M, 1.93. Station 1.

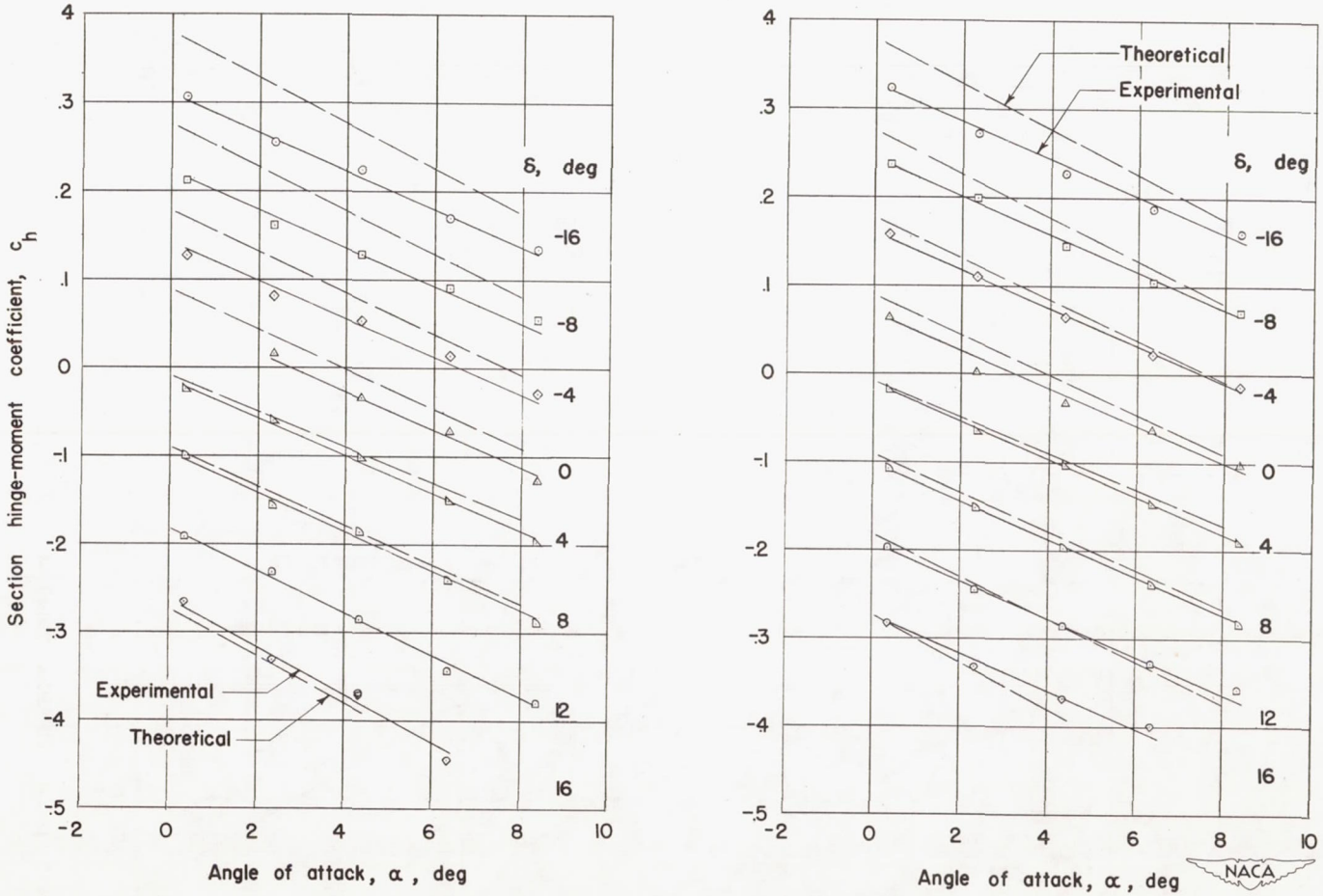

Figure 24.- Effect of fixing transition near leading edge on section hinge-moment characteristics of 6-percent-thick symmetrical circular-arc wing. M, 1.62. Station 1.

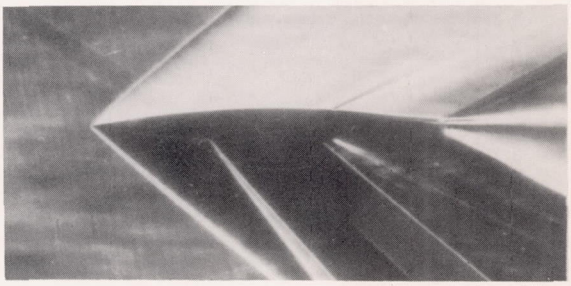

$\alpha = -1^{\circ}$, $\delta = 0^{\circ}$.

Smooth model.

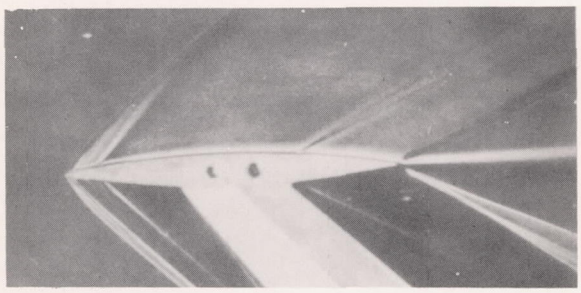

$\alpha = -2^{\circ}$, $\delta = 0^{\circ}$.

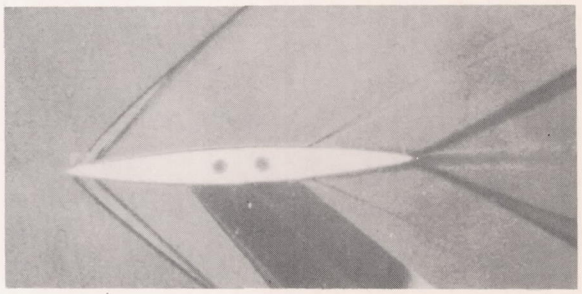

$\alpha = -2^{\circ}$, $\delta = 0^{\circ}$.

Fixed transition.

Horizontal knife edge. Vertical knife edge.

NACA L-64944

Figure 25.- Effect of fixing transition on the flow over a 9-percent-thick symmetrical circular-arc wing at $M = 1.93$ and $R = 1.07 \times 10^6$.

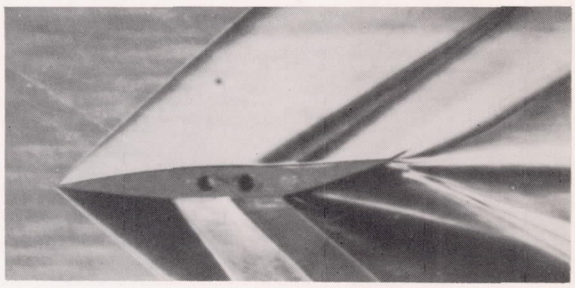

$\alpha = 2^{\circ}$, $\delta = 10^{\circ}$.

Smooth model.

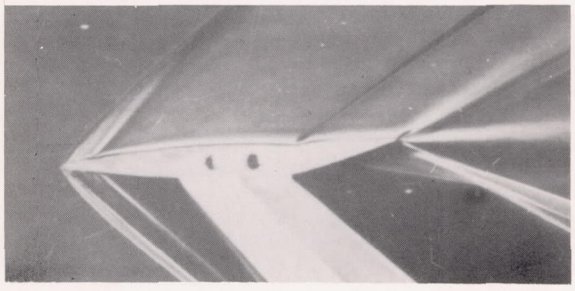

$\alpha = 2^{\circ}$, $\delta = 10^{\circ}$.

Horizontal knife edge.

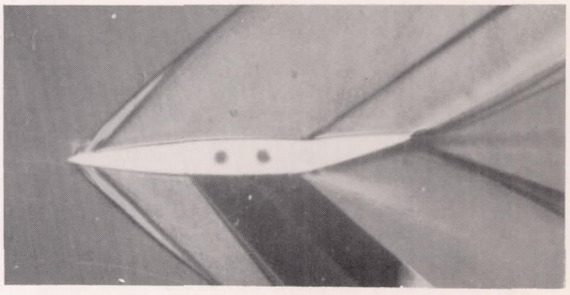

$\alpha = 2^{\circ}$, $\delta = 10^{\circ}$.

Vertical knife edge.

Fixed transition.

Figure 25.- Continued.

NACA L-64945

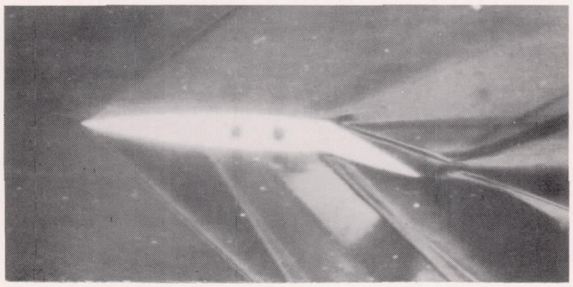

$\alpha = 2^{\circ}$, $\delta = 20^{\circ}$.

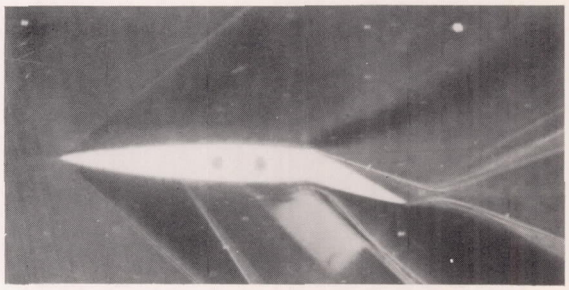

$\alpha = 2^{\circ}$, $\delta = 20^{\circ}$.

Smooth model.

$\alpha = 2^{\circ}$, $\delta = 20^{\circ}$.

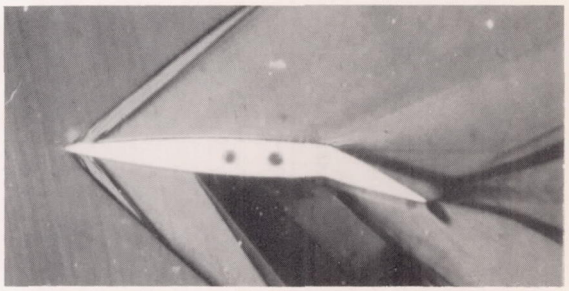

$\alpha = 2^{\circ}$, $\delta = 20^{\circ}$.

Fixed transition.

Horizontal knife edge. Vertical knife edge.

Figure 25.- Continued. L-64946

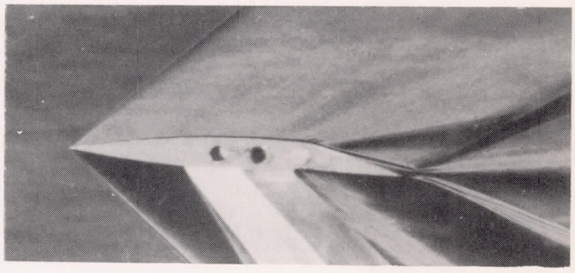

$\alpha = -2^{\circ}$, $\delta = -10^{\circ}$.

Smooth model.

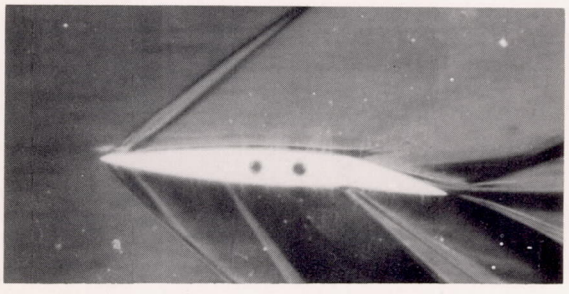

$\alpha = -2^{\circ}$, $\delta = -10^{\circ}$.

Horizontal knife edge.

$\alpha = -2^{\circ}$, $\delta = -10^{\circ}$.

Vertical knife edge.

Fixed transition.

Figure 25.- Continued.

NACA L-64947

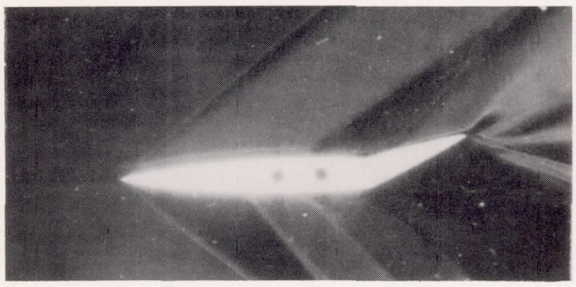

$\alpha = -2^{\circ}$, $\delta = -20^{\circ}$.

$\alpha = -2^{\circ}$, $\delta = -20^{\circ}$.

Smooth model.

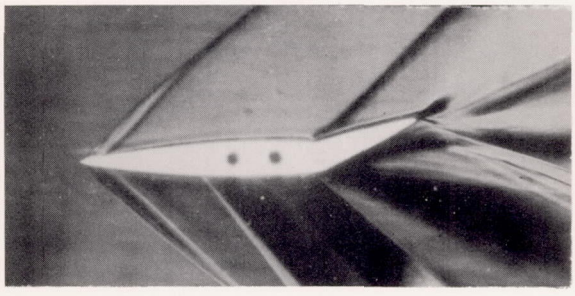

$\alpha = -2^{\circ}$, $\delta = -20^{\circ}$.

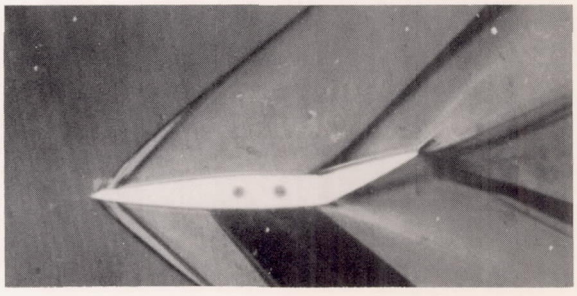

$\alpha = -2^{\circ}$, $\delta = -20^{\circ}$.

Fixed transition.

Horizontal knife edge. Vertical knife edge.

Figure 25.- Concluded.

NACA L-64948

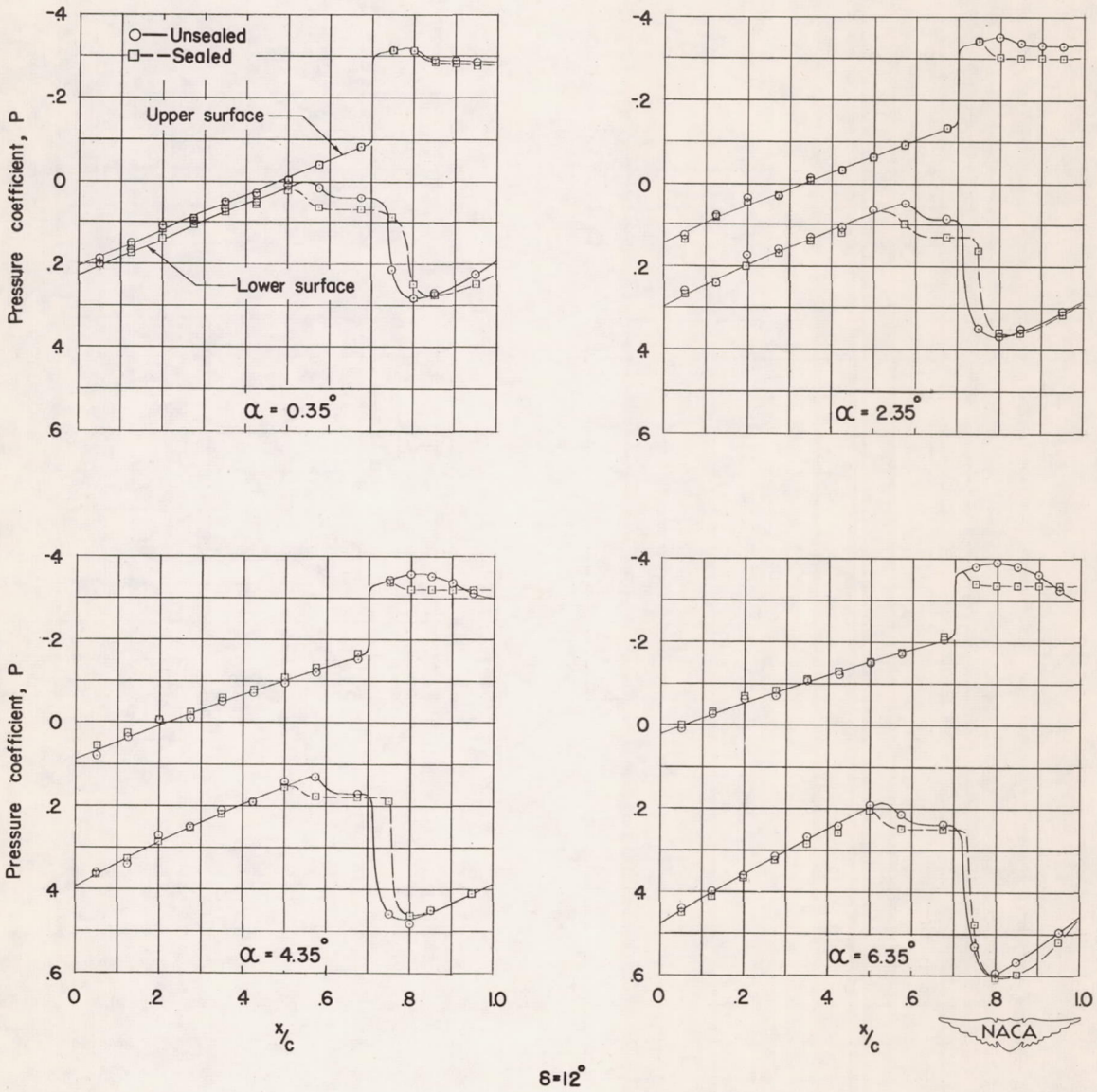

Figure 26.- Effect of sealing hinge gap on experimental pressure distribution over 6-percent-thick symmetrical circular-arc wing. M, 1.62. Station 1.

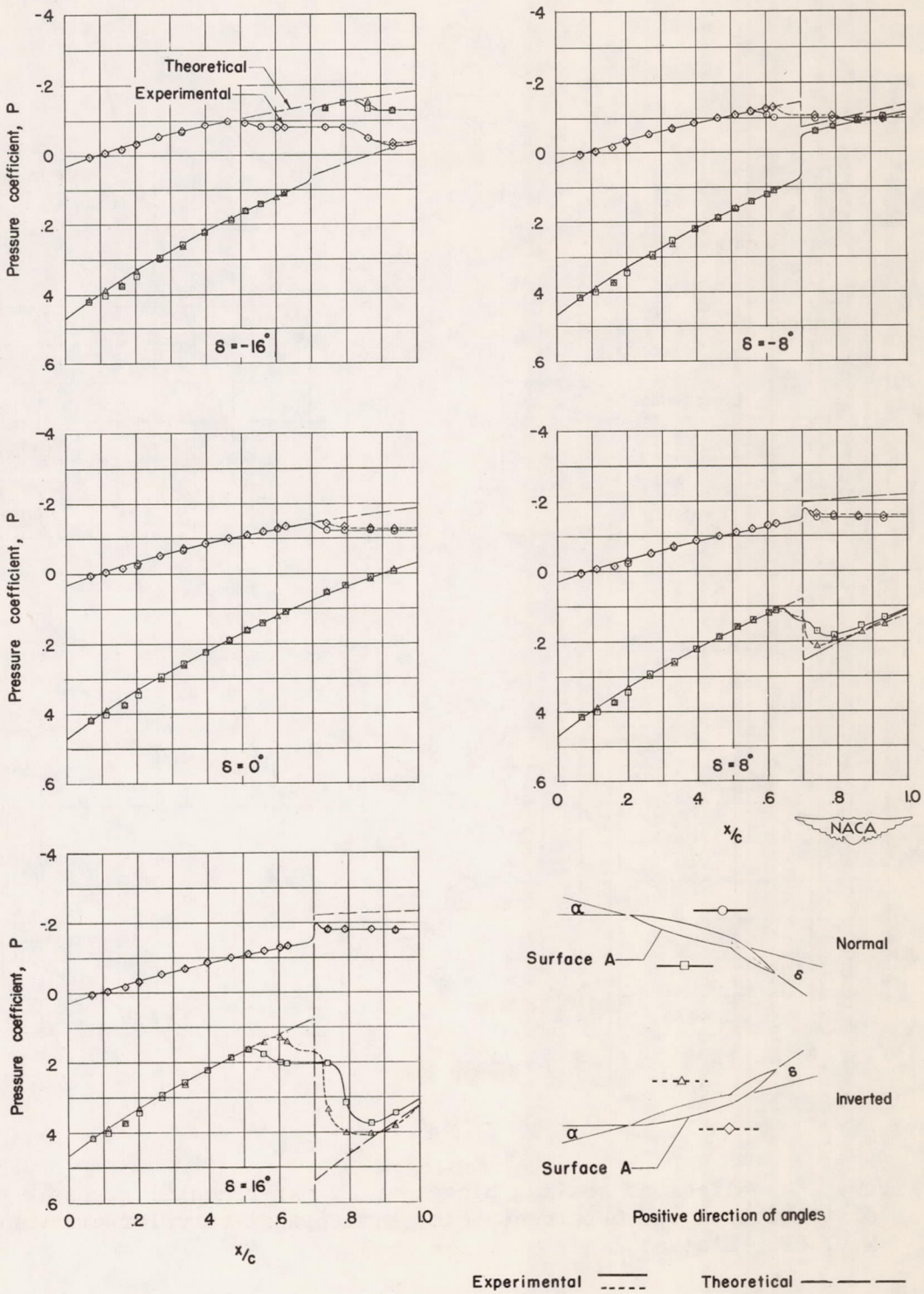

Figure 27.- Comparison of pressure distributions over opposite surfaces of 9-percent-thick symmetrical circular-arc wing. α, 8.35°; M, 2.40. Station 1.

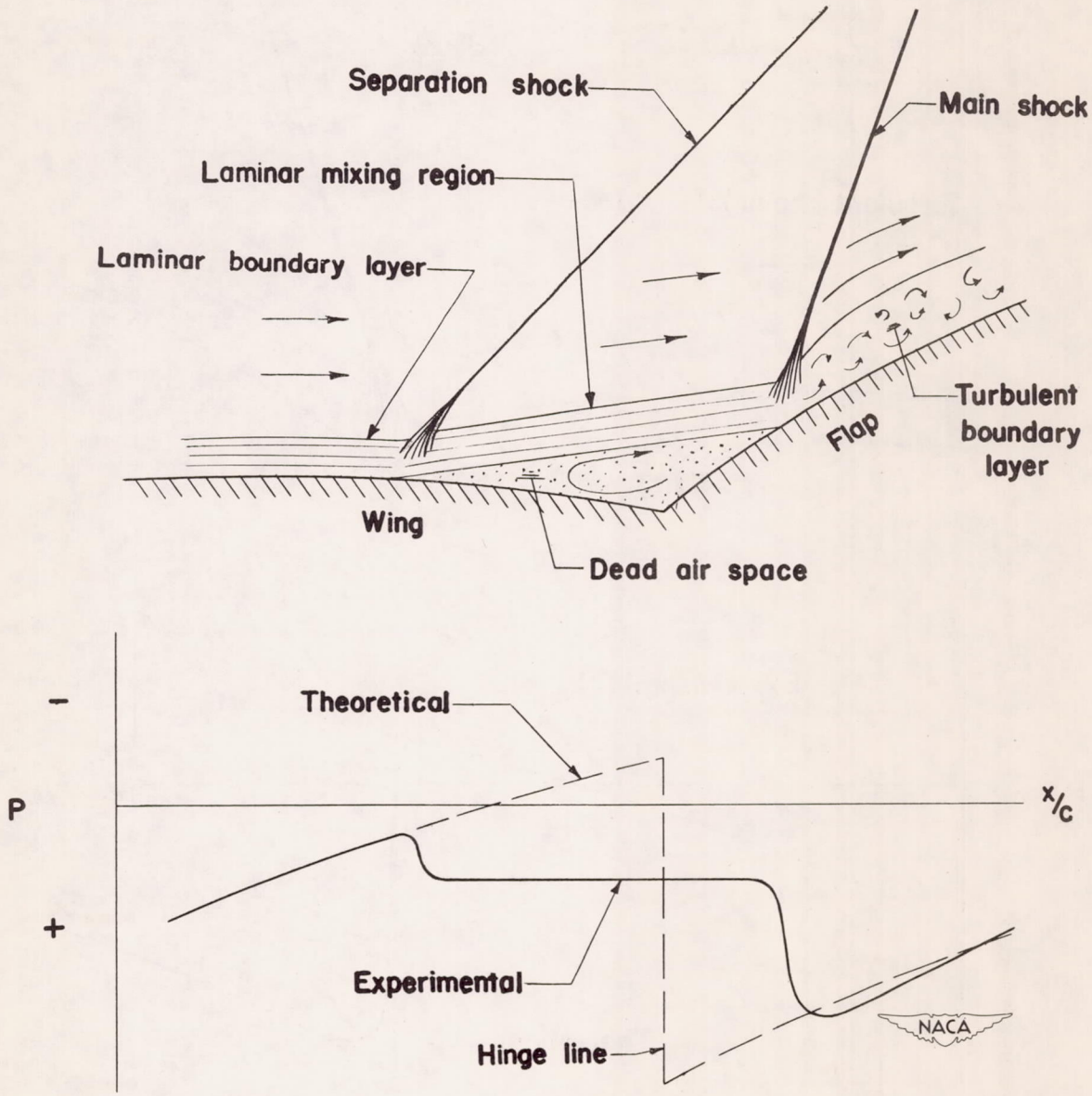

(a) Smooth wing.

Figure 28.- Diagrammatic sketch of shock boundary-layer interaction at hinge line.

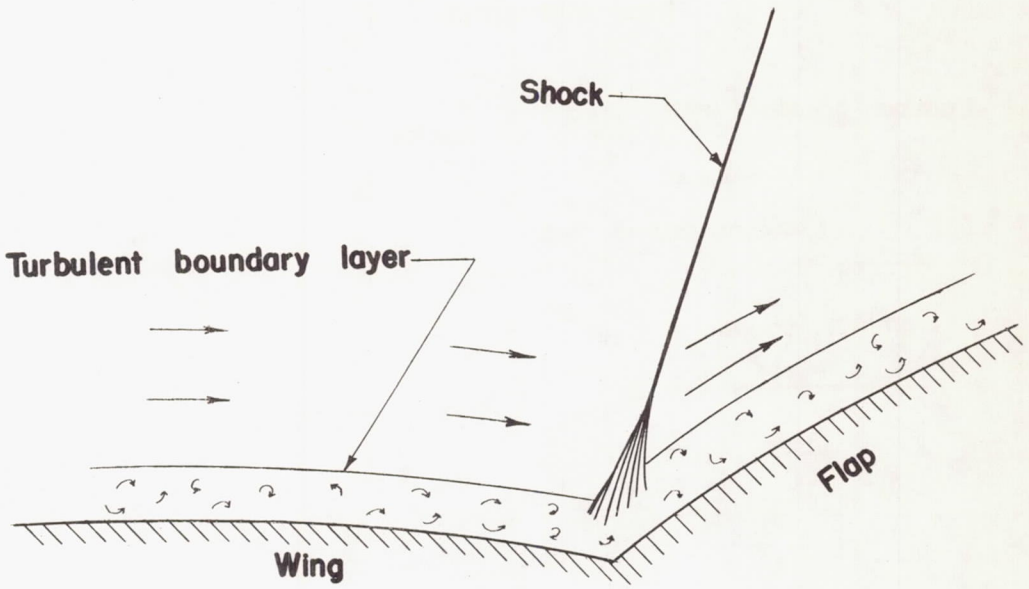

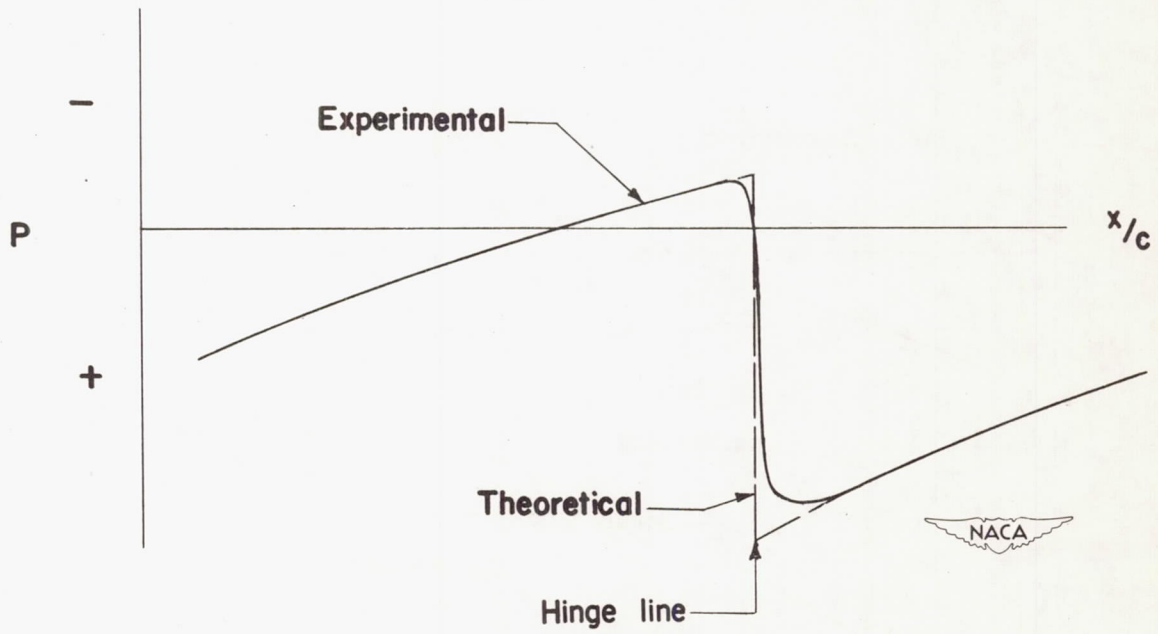

(b) Transition fixed.

Figure 28.- Concluded.

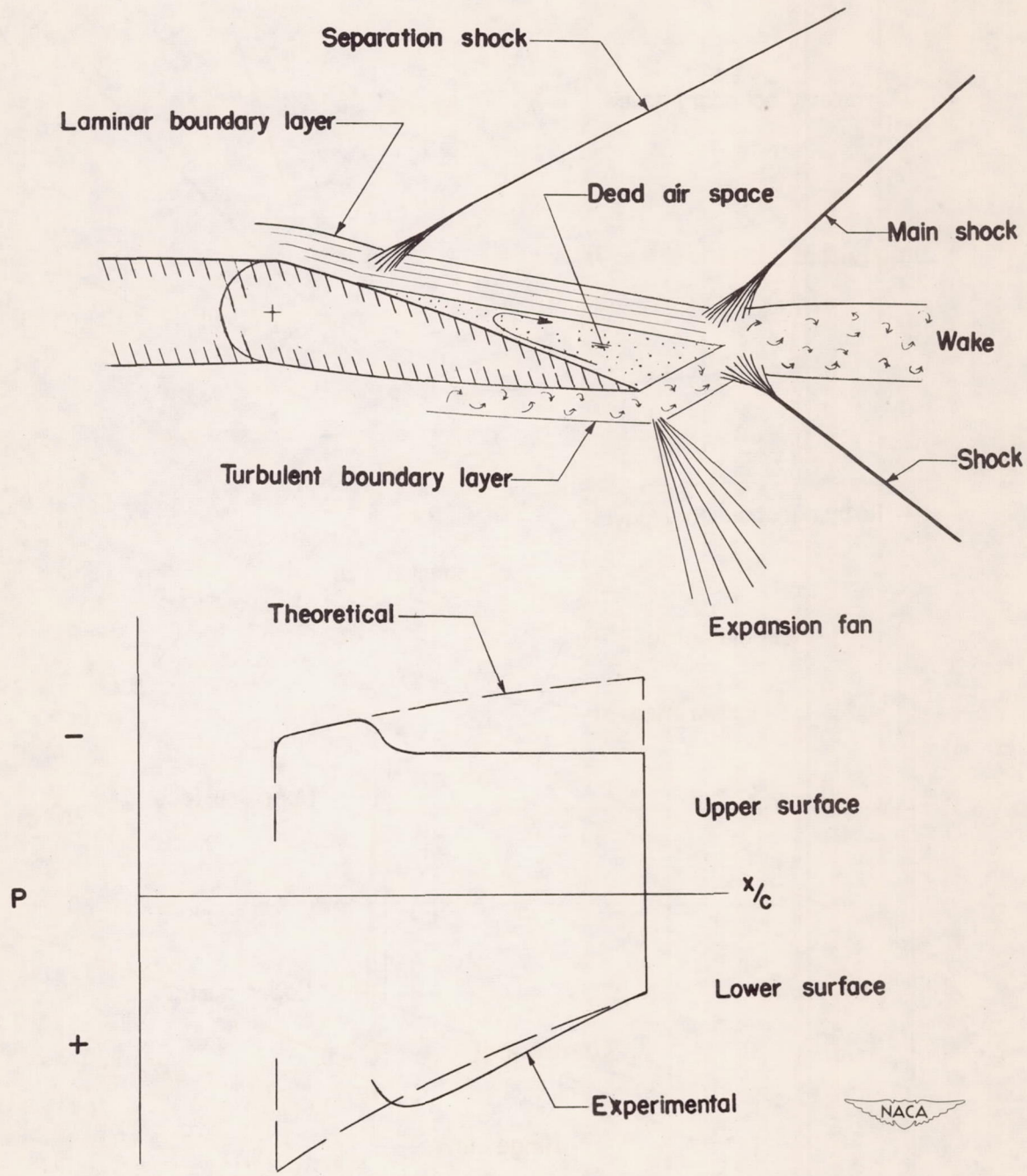

(a) Smooth wing.

Figure 29.- Diagrammatic sketch of shock boundary-layer interaction at flap trailing edge.

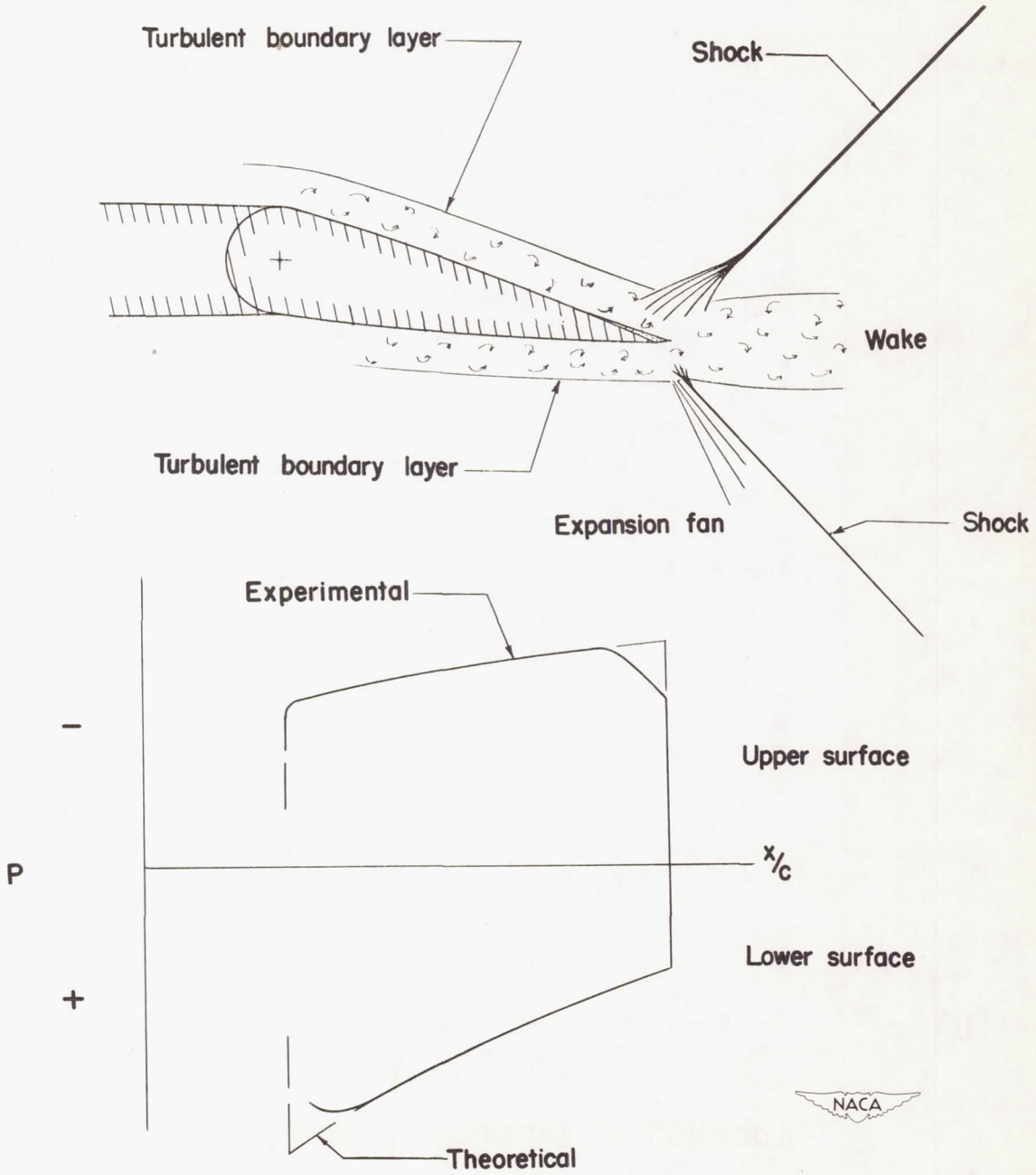

(b) Transition fixed.

Figure 29.- Concluded.

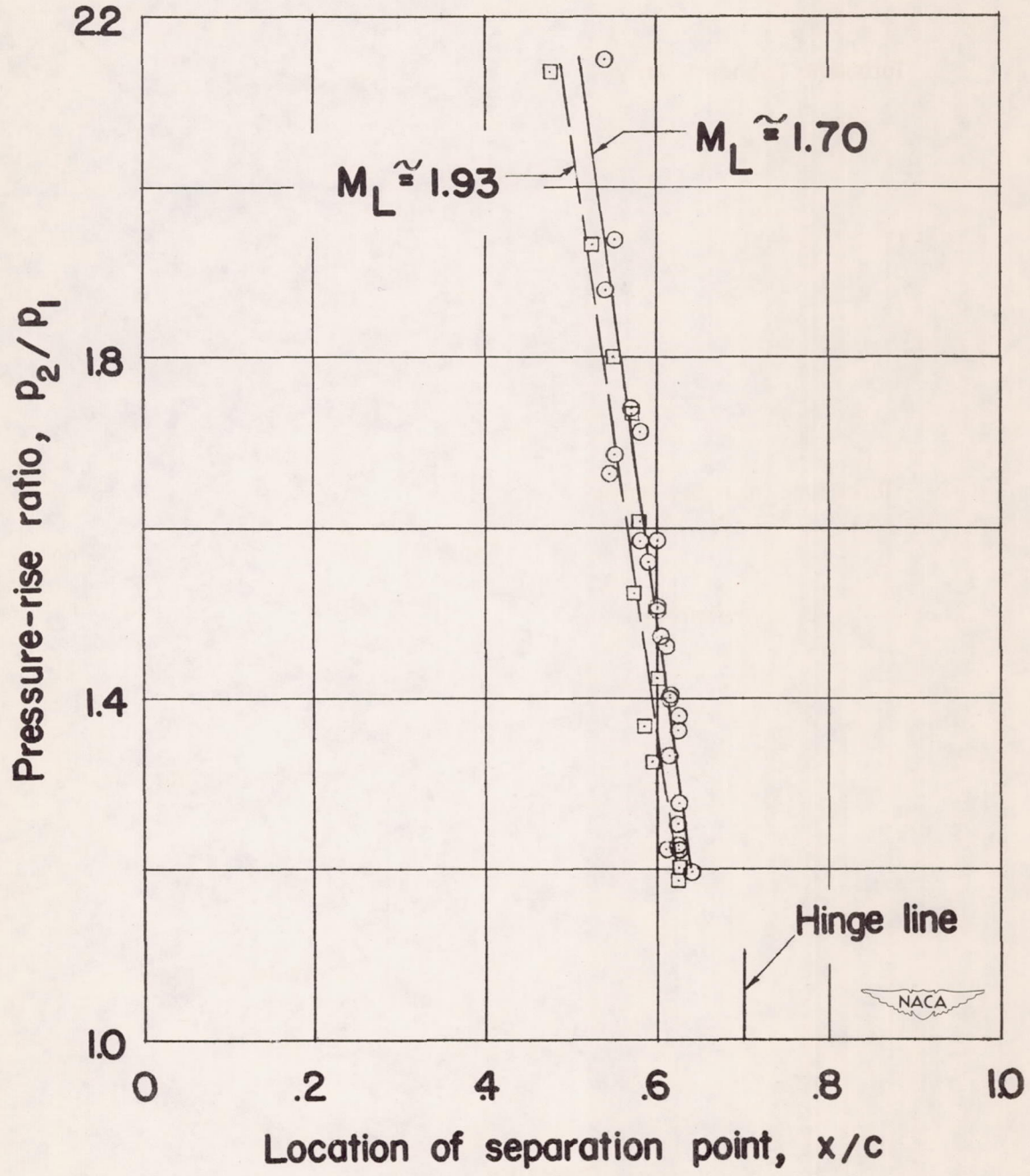

Figure 30.- Typical experimental movement of separation point at hinge line with pressure-rise ratio 9-percent-thick wing; $R = 0.63 \times 10^6$; α from -0.65° to 1.35°.